AD-A055 678 WESTINGHOUSE DEFENSE AND ELECTRONIC SYSTEMS CENTER B--ETC F/G 17/7
CAPTURE EFFECT ARRAY GLIDE SLOPE GUIDANCE STUDY.(U)
MAR 78 J T GODFREY, H F HARTLEY, R A MOORE DOT-FA-74WA-3353
UNCLASSIFIED FAA/RD-78/41 NL

1 OF 1
ADA
055678

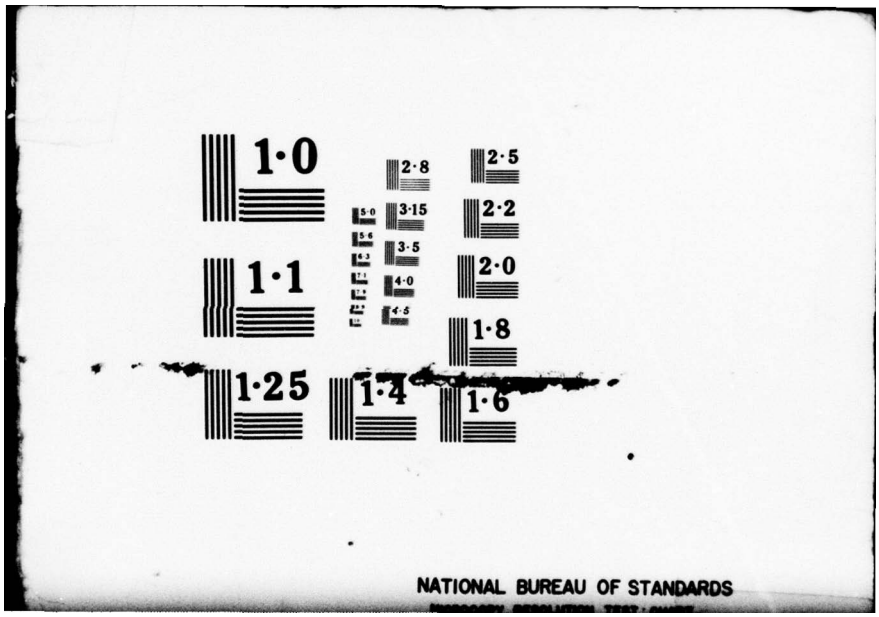
1·0
1·1
1·25
2·8
3·15
3·5
4·0
4·5
5·0
2·5
2·2
2·0
1·8
1·4
1·6
NATIONAL BUREAU OF STANDARDS

FOR FURTHER TRAN...

Report No. FAA-RD-78-41

12

AD A055678

AD No. ____
DDC FILE COPY

CAPTURE EFFECT ARRAY GLIDE SLOPE GUIDANCE STUDY

J. T. Godfrey
H. F. Hartley
R. A. Moore
G. J. Moussally

MARCH 1978

INTERIM REPORT

Prepared for

U.S. DEPARTMENT OF TRANSPORTATION
FEDERAL AVIATION ADMINISTRATION
Systems Research & Development Service
Washington, D.C. 20590

NOTICE

This document is disseminated under the sponsorship of the Department of Transportation in the interest of information exchange. The United States Government assumes no liability for its contents or use thereof.

Technical Report Documentation Page

1. Report No.	2. Government Accession No.	3. Recipient's Catalog No.
FAA-RD-78-41		

4. Title and Subtitle
Capture Effect Array Glide Slope Guidance Study

5. Report Date
March 1978

6. Performing Organization Code

7. Author(s)
J. T. Godfrey, H. F. Hartley, R. A. Moore, G.T. Moussally

8. Performing Organization Report No.

9. Performing Organization Name and Address
Westinghouse Defense and Electronic Systems Center
Aerospace Electronic Systems Division
Baltimore, Maryland 21203

10. Work Unit No. (TRAIS)

11. Contract or Grant No.
DOT-FA74WA-3353

13. Type of Report and Period Covered
Interim Report
Modification #3

12. Sponsoring Agency Name and Address
Federal Aviation Administration
Systems Research & Development Service
Washington, D.C. 20591

14. Sponsoring Agency Code

15. Supplementary Notes

12 46 p.

16. Abstract

This study has examined the performance of the Capture Effect Glide Slope Array as a function of the quality and quantity of required ground plans. Methods of improvement were also investigated: Wherein either a smoothing of the glide path structure or a reduction of the required ground plane was considered an improvement. An extensive computer model was developed and it was used to study the effect on glide path DDM of different position arrangements of elements. It was found that a unique arrangement of elements could be found for any terrain environment which would give a near zero DDM along the entire glide path up to threshold.

18 FAA/RD 19 78/47

17. Key Words	18. Distribution Statement
Instrument Landing Systems Capture Effect Glide Slope Rough & Short Ground Planes	Document is available to the U.S. public through the National Technical Information Service, Springfield, Virginia 22161.

19. Security Classif. (of this report)	20. Security Classif. (of this page)	21. No. of Pages	22. Price
UNCLASSIFIED	UNCLASSIFIED	96	

Form DOT F 1700.7 (8-72) Reproduction of completed page authorized

405 532 slt

METRIC CONVERSION FACTORS

Approximate Conversions to Metric Measures

Symbol	When You Know	Multiply by	To Find	Symbol
	LENGTH			
in	inches	*2.5	centimeters	cm
ft	feet	30	centimeters	cm
yd	yards	0.9	meters	m
mi	miles	1.6	kilometers	km
	AREA			
in^2	square inches	6.5	square centimeters	cm^2
ft^2	square feet	0.09	square meters	m^2
yd^2	square yards	0.8	square meters	m^2
mi^2	square miles	2.6	square kilometers	km^2
	acres	0.4	hectares	ha
	MASS (weight)			
oz	ounces	28	grams	g
lb	pounds	0.45	kilograms	kg
	short tons (2000 lb)	0.9	tonnes	t
	VOLUME			
tsp	teaspoons	5	milliliters	ml
Tbsp	tablespoons	15	milliliters	ml
fl oz	fluid ounces	30	milliliters	ml
c	cups	0.24	liters	l
pt	pints	0.47	liters	l
qt	quarts	0.95	liters	l
gal	gallons	3.8	liters	l
ft^3	cubic feet	0.03	cubic meters	m^3
yd^3	cubic yards	0.76	cubic meters	m^3
	TEMPERATURE (exact)			
°F	Fahrenheit temperature	5/9 (after subtracting 32)	Celsius temperature	°C

*1 in = 2.54 (exactly). For other exact conversions and more detailed tables, see NBS Misc. Publ. 286, Units of Weights and Measures, Price $2.25, SD Catalog No. C13.10:286.

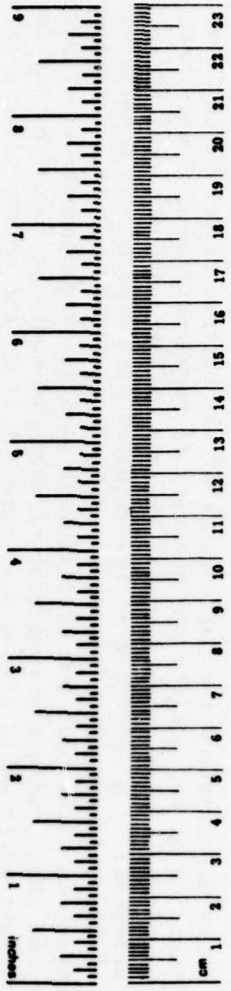

Approximate Conversions from Metric Measures

Symbol	When You Know	Multiply by	To Find	Symbol
	LENGTH			
mm	millimeters	0.04	inches	in
cm	centimeters	0.4	inches	in
m	meters	3.3	feet	ft
m	meters	1.1	yards	yd
km	kilometers	0.6	miles	mi
	AREA			
cm^2	square centimeters	0.16	square inches	in^2
m^2	square meters	1.2	square yards	yd^2
km^2	square kilometers	0.4	square miles	mi^2
ha	hectares (10,000 m^2)	2.5	acres	
	MASS (weight)			
g	grams	0.035	ounces	oz
kg	kilograms	2.2	pounds	lb
t	tonnes (1000 kg)	1.1	short tons	
	VOLUME			
ml	milliliters	0.03	fluid ounces	fl oz
l	liters	2.1	pints	pt
l	liters	1.06	quarts	qt
l	liters	0.26	gallons	gal
m^3	cubic meters	35	cubic feet	ft^3
m^3	cubic meters	1.3	cubic yards	yd^3
	TEMPERATURE (exact)			
°C	Celsius temperature	9/5 (then add 32)	Fahrenheit temperature	°F

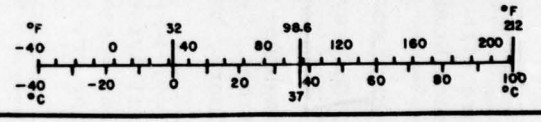

TABLE OF CONTENTS

		Page
1.0	INTRODUCTION -	1
2.0	APPROACH -	1
3.0	CAPTURE EFFECT ARRAY GUIDANCE OVER LONG GROUND PLANES - - -	2
4.0	CAPTURE EFFECT ARRAY GUIDANCE OVER SHORT GROUND PLANES - - -	4
5.0	ADDITIONAL PRESENTATIONS OF PATH DATA - - - - - - - - - - -	7
6.0	FIVE ELEMENT ARRAY WITH DECREASED LOW ANGLE RADIATION - - -	10
7.0	PHASE SENSITIVITY OF THE CAPTURE EFFECT ARRAY - - - - - - -	11
8.0	FOUR AND FIVE ELEMENT VARIATIONS OF THE CAPTURE EFFECT ARRAY HAVING IMPROVED PHASE SENSITIVITY - - - - - - - - - - - - - -	11
9.0	GLIDE PATH FLY-IN STRUCTURE WITH A LATERAL EDGE - - - - - -	12
10.0	CONCLUSIONS, SIGNIFICANT FINDINGS, RECOMMENDATIONS - - - - -	12

APPENDIX A.	IMAGE TYPE GLIDE SLOPE SYSTEMS AND GUIDANCE SIGNAL (DDM) DERIVATION	A-1
APPENDIX B.	MATHEMATICAL MODEL USED TO CALCULATE FIELD OF A HORIZONTALLY POLARIZED ELECTRIC DIPOLE OVER A CONDUCTING HALF PLANE	B-1
APPENDIX C.	CORRELATION OF WESTINGHOUSE HALF PLANE ANALYSIS WITH TRANSPORTATION SYSTEMS CENTER ANALYSIS	C-1
APPENDIX D.	COMPARISON BETWEEN THEORY AND EXPERIMENT FOR THE CAPTURE EFFECT ARRAY OVER A SEMI-INFINITE GROUND PLANE	D-1
APPENDIX E.	ANALYSIS OF A SEMI-INFINITE GROUND PLANE OVER AN INFINITE GROUND PLANE	E-1

LIST OF ILLUSTRATIONS AND TABLES

FIGURE	CAPTION	PAGE
1	CAPTURE EFFECT ARRAY GEOMETRY	16
2	CAPTURE EFFECT ARRAY FLY-IN OVER INFINITE PLANE	17
3	CAPTURE EFFECT ARRAY INFINITE PLANE (VARIABLE FOCUSING)	18
4	CAPTURE EFFECT ARRAY FLY-IN OVER INFINITE PLANE MODIFIED FOCUS	19
5	CAPTURE EFFECT ARRAY FLY-IN OVER INFINITE PLANE (UNFOCUSED, VARIABLE AZIMUTH)	20
6	DITTO (FOCUSED, VARIABLE AZIMUTH)	21
7	CAPTURE EFFECT ARRAY FLY-IN WITH 2000 FT. HALF PLANE (FOCUSED, VARIABLE AZIMUTH)	22
8	CAPTURE EFFECT ARRAY FLY-IN OVER INFINITE PLANE (MODIFIED FOCUS, VARIABLE AZIMUTH)	23
9	CAPTURE EFFECT ARRAY FLY-IN OVER 2000 FT. HALF PLANE (MODIFIED FOCUS, VARIABLE AZIMUTH)	24
10	CAPTURE EFFECT ARRAY WITH HALF PLANE (VARIABLE EDGE)	25
11	CAPTURE EFFECT ARRAY 800 FT. HALF PLANE	26
12	" " " 600 FT. " "	27
13	" " " 400 FT. " "	28
14	" " " 300 FT. " "	29
15	" " " 200 FT. " "	30
16	CAPTURE EFFECT ARRAY FLY-IN WITH 1000 FT. HALF PLANE (FOCUSED)	31
17	DITTO WITH 500 FT. HALF PLANE (FOCUSED)	32
18	CAPTURE EFFECT ARRAY ELEVATION ANGLE DDM (VARIABLE EDGE)	33
19	DITTO (VARIABLE EDGE, HEIGHT AND SIDEBAND LEVEL ADJUSTED)	34
20	CAPTURE EFFECT ARRAY FLY-IN WITH 1000 FT. HALF PLANE (MODIFIED FOCUS)	35
21	DITTO WITH 500 FT. HALF PLANE (MODIFIED FOCUS)	36
22	DITTO (PREFERRED MODIFIED FOCUS)	37
23	CAPTURE EFFECT ARRAY ELEVATION ANGLE DDM - MODIFIED FOCUS	38
24A	ACTUAL PATH ANGLE FOR DDM INDICATIONS (INFINITE GROUND)	39
24B	DITTO (500 FT. GROUND PLANE)	40
25	5 ELEMENT AND CAPTURE EFFECT ARRAY EXCITATION AND HEIGHT	41

List of Illustrations and Tables (cont.)

Figure	Caption	Page
26	5 ELEMENT AND CAPTURE EFFECT RADIATION FIELDS	42
27	5 ELEMENT ARRAY ELEVATION DDM	43
28	5 ELEMENT ARRAY FLY-IN OVER INFINITE PLANE	44
29	SBO RADIATION FIELDS - STANDARD CAPTURE EFFECT ARRAY	45
30	CSB RADIATION FIELDS - STANDARD CAPTURE EFFECT ARRAY	46
31	ELEVATION DDM - STANDARD CAPTURE EFFECT ARRAY	47
32	CAPTURE EFFECT ARRAY (STANDARD AND 4 ELEMENT CONFIGURATIONS)	48
33	SBO RADIATION FIELDS - 4 ELEMENT CAPTURE EFFECT ARRAY	49
34	CSB RADIATION FIELDS - 4 ELEMENT CAPTURE EFFECT ARRAY	50
35	ELEVATION DDM - 4 ELEMENT CAPTURE EFFECT ARRAY	51
36	CAPTURE EFFECT ARRAY (STANDARD AND 5 ELEMENT CONFIGURATIONS)	52
37	ELEVATION DDM - 5 ELEMENT CAPTURE EFFECT ARRAY	53
38	CAPTURE EFFECT LATERAL EDGE (ΔY = -0 TO -40 FT.)	54
39	DITTO (ΔY = -20 TO -700 FT.)	55
B-1	ILLUSTRATING COORDINATES FOR FIELD CALCULATION	B-3
B-2	ILLUSTRATING ϵ COORDINATES	B-4
C-1	NULL REFERENCE ARRAY FLY-IN OVER 5000 FT. HALF PLANE	C-2
C-2	CAPTURE EFFECT ARRAY 1200 FT. HALF PLANE WITH 10, 20 AND 30 FT. DROP OFF	C-3
D-1	GEOMETRY OF LUCAS EXPERIMENTS	D-5
D-2a	CAPTURE EFFECT SBO X_e = 1785' x = 4400'	D-6
D-2b	CAPTURE EFFECT CSB DITTO	D-7
D-2c	CAPTURE EFFECT DDM DITTO	D-8
D-3a	CAPTURE EFFECT SBO X_e = 1200' x = 4400'	D-9
D-3b	CAPTURE EFFECT CSB DITTO	D-10
D-3c	CAPTURE EFFECT DDM DITTO	D-11
D-4a	CAPTURE EFFECT SBO X_e = 600' x = 2600'	D-12
D-4b	CAPTURE EFFECT CSB DITTO	D-13
D-4c	CAPTURE EFFECT DDM DITTO	D-14
D-5a	CAPTURE EFFECT SBO X_e = 450' x = 2600'	D-15
D-5b	CAPTURE EFFECT CSB DITTO	D-16
D-5c	CAPTURE EFFECT DDM DITTO	D-17
D-6	COMPARISON OF CALCULATION AND LUCAS MEASUREMENT	D-18
E.1.	GEOMETRY FOR HALF PLANE OVER INFINITE PLANE	E-3

List of Illustrations and Tables (cont.)

TABLE	Caption	Page
5-1	PATH CHARACTERISTICS FOR VARIOUS GROUND PLANES WITH STANDARD FOCUSED CAPTURE EFFECT ARRAY	8
5-2	PATH CHARACTERISTICS FOR VARIOUS GROUND PLANES WITH MODIFIED FOCUS CAPTURE EFFECT ARRAY	9
10-1	DDM DEROGATION WITH GROUND PLANE LENGTH	15

1.0 INTRODUCTION

The purpose of this study has been to examine the performance of the Capture Effect Glide Slope Array as a function of the quality and quantity of required ground plan. Methods of improvement were also investigated; wherein either a smoothing of the glide path structure or a reduction of the required ground plane was considered an improvement. The study was directed entirely to the structure on glide path. All Capture Effect installations are operated with an additional clearance signal which guarantees sufficient below path fly-up to provide absolute safety. In the conclusions it is shown that some modification of the standard antenna configuration results in a reduction of the phase sensitivity of the glide path structure. This would result in a reduction in the exactness of monitoring presently used on all operational systems. The results of this study have favorably compared to limited experimental data. However, a complete and controlled experimental program would be required to establish the useful range of application of this analysis.

2.0 APPROACH

Standard image type glide slope systems, as described in Appendix A, were computer modeled over the infinite plane as a preliminary to the study of their performance over finite ground planes. It was discovered during this preliminary work that the standard antenna element focusing method used in present Capture Effect array installations can be modified to provide a greatly improved guidance signal in the threshold approach region of the glide path. This improvement is discussed in Section 3.

Prior to the award of this contract Westinghouse engineers were involved in the study of solutions of the field of a horizontal electric dipole over a conducting half-plane. A closed form solution of this problem was evolved, the final result of which is given in Appendix B. This solution was incorporated into the computer programs for the multi-element arrays thus giving computer models to evaluate the performance of image type glide slope arrays over finite ground planes.

Before extensive use of the Westinghouse half-plane computer model in the Capture Effect Array studies, it was desirable to compare analytical and experimental results obtained by other methods with those obtained using the Westinghouse model. The first comparisons were made with analytical results reported by the Transportation Systems Center (TSC). These comparisons are discussed in Appendix C. The next comparisons made were of Westinghouse computer results with experimental results obtained by Lucas[2]. Details of this comparison are given in Appendix D. In the above cases, where valid comparisons could be made, the Westinghouse computer modeling results were found to be 1) identical with results from other theoretical models, and 2) very close to experimental results.

The next step was to use the Westinghouse computer model, as validated by the above comparisons, to calculate fly-in and elevation DDM characteristics of standard and modified Capture Effect Arrays over finite ground planes. The results of these calculations are given in Section 4. This work satisfies objective (1) of Section 1.

To accomplish objective (2), three modifications of the standard Capture Effect Array, involving 4 and 5 elements, were analyzed. In section 6, the results are given of analysis of a 5 element array giving significantly reduced low angle SBO (side band only) radiation. One problem associated with the standard Capture Effect Array is the high sensitivity of low angle DDM to changes in phase of the signal applied to the middle antenna element. Results of calculation of this sensitivity are presented in Section 7. In Section 8, 4 and 5 element variations of the Capture Effect Array are analyzed which offer some reduction of phase sensitivity.

Objective (3) is satisifed in the presentation of the results of the various cases analyzed.

The final element of work presented in this report is the result of fly-in calculations with the standard capture Effect array over a lateral edge (half-plane with edge parallel to the runway). This work is summarized in Section 8.

3.0 CAPTURE EFFECT ARRAY GUIDANCE OVER LONG GROUND PLANES

A Fortran computer program model of the Capture Effect guidance system in three dimensions was developed for the purpose of studying the effects of antenna

element position on fly-in DDM. The objective of the study was to improve the Capture Effect fly-in characteristics over both long and short ground planes. A prerequisite to the efficient conduct of this study was the development of a closed form mathematical solution involving Fresnel integrals for the field diffracted by the edge of the ground plane. The total field of the aircraft, in this idealized model, is the sum of direct, specular ground reflected, and edge diffracted fields from all three transmitting antenna elements. The mathematical model for the total field for one element is delineated in Appendix B.

Figure 1 shows the array element co-ordinates and runway position used to designate element positions for the fly-ins described below. The elements are indicated as focused on the runway touchdown point, i.e., all elements are equidistant from the touchdown point and lie in the Y-Z plane.

Figure 2 shows results of fly-in DDM with antenna heights adjusted for 2.86° glide slope, both focused and unfocused, over an infinite plane. An offset (YRW in Figure 1) of 300 feet was assumed. End of runway, or threshold, is about 1100 feet from touchdown in this case. Element positions for the focused case can be obtained from Figure 3 where dimensions are given in meters unless otherwise indicated. In the unfocused case, the elements lie in a vertical straight line above the co-ordinate origin O in Figure 1.

In Figure 2 DDM points were computed at 100 foot increments. The change of DDM polarity with and without focus suggests that an intermediate adjustment of element position could improve the guidance signal. This was indeed found to be the case as indicated by the line of boxes DDM characteristic in Figure 3. Here the guidance would be essentially perfect down to about 1000 feet from touchdown.

Figure 4 shows the DDM fly-in over the infinite plane with the modified focus as given by the box (⊡) co-ordinates in Figure 3 (dimensions of meters). Note that, in Figure 4, distance is from threshold, whereas, in Figure 3 distance is from touchdown.

Additional fly-ins were computed for a 3° glide path and 400 foot antenna offset. Also the effect of $\pm 8^{\circ}$ azimuth approach angle was evaluated. Figure 5 shows fly-ins for unfocused elements (elements in straight line). On the glide path (3°) at zero azimuth approach angle, increasing fly-down DDM is obtained

as threshold is approached. A qualitative explanation of the far field DDM variation with azimuth angle in the outer ranges is as follows. At a given distance from threshold at 3° elevation and 0° azimuth the DDM is zero microamps, indicating that the receiving antenna is on the SBO radiation pattern null. At the same range from threshold, a large transverse movement of the receiving antenna causes it to move under the null, thus given a fly-up (positive) DDM signal. The signal is assymetrical with respect to zero DDM because of the antenna offset from the runway.

Figure 6 shows fly-ins over an infinite plane with the antennas focused on the runway as indicated in Figure 1. Now the on-path signal is increasingly fly-up (negative) as the threshold is approached, and the azimuth approach angle variation causes relative fly-down signals. It is also observed that sensitivity to azimuth angle increases as the elevation angle of fly-in is decreased. Figure 7 shows fly-ins over a half-plane whose edge extends 2000 feet in front of the antenna array with standard focusing. It is noted that the results are very nearly the same as those with the infinite plane, indicating that about 2000 feet of flat foreground is the upper limit on grading requirements for the Capture Effect Array. The small oscillations near threshold are due to interference between the edge diffracted fields (edge about 1000 feet from threshold) and the direct and reflected fields.

Figure 8 shows fly-ins over an infinite plane with a modified focus giving the ideal zero DDM signal over the entire glide slope path of 3° elevation and 0° azimuth. Figure 9 shows fly-in results over the 2000 feet half-plane using the same modified focus. Again almost ideal DDM is obtained on the glide path. Figures 8 and 9 show also that the modified focus gives much smaller, DDM azimuth sensitivity than does the standard focusing method of Figures 6 and 7.

4.0 CAPTURE EFFECT ARRAY GUIDANCE OVER SHORT GROUND PLANES

In this section the results of calculations of fly-ins over limited ground planes are presented. These are of special interest because they show that it is possible to obtain very good guidance over very short ground planes if proper adjustments are made to the antenna element positions.

Figure 10 shows fly-in results with fixed array element positions and various ground plane lengths. Elements are standard focused and at proper height for

2.86^{o} glide slope angle over infinite ground plane. As the ground plane is shortened fly-down signal increases. This is a result of the decreasing of the sideband pattern null angle by the edge diffraction field. The antennas can be lowered to raise the carrier and sideband beams for proper guidance on the desired glide slope path. Figures 11 through 15 illustrates fly-ins obtained for ground planes of 800 through 200 feet. Distances are measured from touchdown. The indicated distance for antenna lowering applies to the first (lowest) element of the array and is relative to the position for proper guidance over an infinite plane. The second and third elements are lowered by 2 and 3 times the indicated amount. Only the top element position was adjusted in offset to achieve the illustrated DDM fly-ins, and it was adjusted in both X and Y to obtain a near flat characteristic over almost the entire range of fly-in. Note that the X offsets for the top element correspond to a small movement away from the edge and vary from 15 cm down to 1 cm for the 200 foot edge.

The short range characteristics of the fly-ins could be further improved by adjustment of the y offset of the lowest element as was done in Figure 3. The 200 foot ground plane guidance is not a practical implementation because the first false sideband null angle is only a fraction of a degree from the desired null.

In Figures 16 and 17 fly-ins over 1000 feet and 500 feet ground planes are shown for the standard method of antenna adjustment as used by the FAA. This method consists of reducing the height of the array to bring the SBO pattern null up to the glide path and focusing the antenna elements on the runway certerline. For the 1000 feet ground plane, the first element is lowered 1.5 cm., the second, 3 cm., and the third, 4.5 cm. Also the y offsets of elements 1 and 3 for focusing are indicated (see Figure 1). The SBO requires an amplitude amplification of 1.13 times relative to the infinite plane SBO to achieve the sensitivity of 150 microamps for

0.7° pathwidth. On path, the increasing fly-up signal (negative DDM) as threshold is approached is observed. Similar, but more pronounced, conditions occur for the 500 feet ground plane. The first element is now lowered by 29 cm and the SBO amplification is 1.37 times. The azimuth approach angle DDM spread has become large as the fly-in elevation angle decreases and the fly-up signal with threshold approach has increased.

Figures 18 and 19 show elevation angle DDM at 30,000 feet slant range for ground planes of 2000, 1000 and 500 feet. In Figure 18 the antenna element heights and focus coordinates are for 3° glide path with 400 feet runway offset over an infinite plane (see Figure 6 for dimensions). It is seen that, as the ground plane is shortened, there is a loss of sensitivity and a decrease in the null angle. Also, as the ground plane is shortened, the low angle DDM minimum increases but the DDM does not cross zero again. In Figure 19, the array height, focus and SBO amplification are adjusted as in Figures 7, 16 and 17 to give essentially identical elevation DDM characteristics, at 30,000 feet range, which are equivalent to the infinite plane elevation DDM.

Figures 20 and 21 show fly-ins over 1000 feet and 500 feet ground planes with modified focus and height relative to the standard method, as used in Figures 16 and 17. The objective here is, to obtain the near zero DDM over the entire glide path. To obtain this effect element heights were further decreased, y offsets were modified, and the top element was given a backset (parallel to runway, away from threshold). This method of obtaining the ideal on-path DDM is unfavorable because it results in a large spread of DDM with azimuth approach angle and greater loss of elevation DDM sensitivity (requiring greater SBO amplification). Figure 22

illustrates the preferred method of obtaining the ideal characteristic. In this case the standard method of height adjustment is used, i.e., the elements are lowered to zero the DDM on the desired glide path angle in the far glide slope region, as in Figure 17. Then the transverse (y-direction) coordinates of the first and third antenna elements are adjusted to bring the on-path DDM to zero in the threshold approach region. This procedure produces the near ideal on-path DDM as shown in Figure 22, with no additional loss of path width sensitivity, and less spread of DDM with azimuth approach angle.

Figure 23 shows the elevation angle DDM for the various cases of half-planes with modified focus as delineated in Figures 9, 20, 21 and 22. The curve indicated by 500' (XA3 = 0) corresponds to the preferred method of obtaining the ideal DDM as illustrated in Figure 22.

5.0 ADDITIONAL PRESENTATIONS OF PATH DATA

The fly-in data of sections 3.0 and 4.0 gave DDM values for an aircraft flying on-path and at the path width limits ($\pm.35^{\circ}$). It is also of interest to know what the actual path angle is when the pilot is flying according to 0 and $\pm$75 µa DDM indication. This information has been computed by linear interpolation from fly-in data above over long and short ground planes and for standard and non-standard focus conditions. The results are presented in Figures 24A and 24B. Both figures show path angle versus azimuth approach angle for 0 µa, 75 µa FLYUP, and 75 µa FLYDOWN at 30,000 feet range. Figure 24A is for infinite ground (2,000 feet or more is equivalent) and shows variations with the antenna elements unfocused (in line), standard focus (on runway centerline), and modified focus (for near zero DDM into the threshold). Modified focusing generally causes less path angle and width variation when the azimuth approach angle departs from zero than does standard focusing. Figure 24B shows results for a 500 feet ground plane with standard and modified focus. Here the antenna-side azimuth approach has considerable lowered path angles for 0 and 75 µa FLYUP with standard focusing. Modified focusing offers only slight improvement in path angle variation with azimuth. The important feature of modified focus is the planar fly-in to threshold obtained.

Data on path characteristics is summarized numerically in Tables 5-1 and 5-2. Path angle is the angle an aircraft would fly for zero DDM indication.

Table 5-1

PATH CHARACTERISTICS FOR VARIOUS GROUND PLANES WITH STANDARD FOCUSED CAPTURE EFFECT ARRAY

		Infinite Plane		Comments
Azimuth Angle (°)	-8	0	+8	
Path Angle (°)	2.94	3.00	2.95	Data from Figure 6
Path Widht (°)	.78	.70	.79	
Flare (ha) RWTH	0	43 FU	53FU	
Flare (ha) 1000 FEET	16 FD	12 FU	14 FU	
		2000 Feet Halfplane		
Azimuth Angle	-8	0	+8	
Path Angle	2.94	3.01	2.95	
Path Width	.75	.69	.79	Data from Figure 7
Flare RWTH	0	44 FU	53 FU	
Flare 1000 feet	16 FD	12 FU	15 FU	
		500 Feet Halfplane		
Azimuth Angle	-8	0	+8	
Path Angle	2.91	3.00	2.99	
Path Width	.91	.70	.65	Data from Figure 17
Flare RWTH	56 FU	104 FU	119 FU	
Flare 1000 feet	11 FU	43 FU	52 FU	

TABLE 5-2

PATH CHARACTERISTICS FOR VARIOUS GROUND PLANES WITH MODIFIED FOCUS CAPTURE EFFECT ARRAY

		Infinite Plane		Comments
Azimuth Angle	-8	0	8	
Path Angle (°)	3.00	3.00	3.03	
Path Width (°)	.70	.70	.74	Data from Figure 8
Flare (μa) RWTH	49 FD	0	52FU	
1000 feet	26 FD	0	30 FU	
		2000 Feet Halfplane		
Azimuth Angle	-8	0	8	
Path Angle	3.01	3.01	3.04	
Path Width	.73	.69	.72	Data from Figure 9
Flare RWTH	48 FD	1 FU	52 FU	
1000 feet	25 FD	0	30 FU	
		500 Feet Halfplane		
Azimuth Angle	-8	0	8	
Path Angle	3.07	2.99	2.96	
Path Width	.69	.71	.78	Data from Figure 22
Flare RWTH	36 FD	2 FU	42 FU	
1000 feet	6 FD	0	14 FU	

Pathwidth is the degree width between angles flown for $\pm 75\mu$a DDM. Path angle and pathwidth data are also shown in Figures 24A and 24B. Flare is the DDM departure from zero as the threshold is approached when the aircraft is flying on the design glide path angle. The data following RWTH is the flare at runway threshold. The next line of data is the flare at 1000 feet from threshold. FU is fly-up and FD is fly-down. Inspection of Table 5-1 for the standard focused array shows that for zero azimuth approach angle fly-up flare exists for all ground planes and flare increases as length of ground plane decreases. Table 5-2 shows the same data with modified focus aimed at minimizing the DDM along the entire glide path. Very small DDM values for zero azimuth angle were obtained for all ground planes.

6.0 FIVE ELEMENT ARRAY WITH DECREASED LOW ANGLE RADIATION

Objective (2) of Section 1 called for investigation of improvements to be obtained by adding up to three additional antenna elements to the Capture Effect Array. One desirable improvement would be to further reduce the low angle radiation. Figures 25 through 28 give the characteristics of one example of an arrangement in which the SBO field at 1° elevation angle is 10.5 dB below the corresponding field for the standard Capture Effect Array. Figure 25 gives the height and excitation of the standard Capture Effect array and the five element array. The CSB levels shown are less than FAA standard; however, this is corrected for in the calculations by a path width sensitivity calibration. The five element array was formed by adding elements 4 and 5 to the Capture Effect array. The SBO on 4 and 5 were chosen to have a null at 3° and simultaneously cancel a large part of the standard SBO low angle radiation. The particular excitation indicated for the five element array in Figure 25 was chosen to 1) give 10.5 dB less radiation at 1°, 2) to linearize the DDM versus elevation in the 3° region and 3) to obtain a low angle DDM which does not cross zero.

Figure 26 shows the relative amplitude at 30,000 feet range of the CSB and SBO fields for both arrays. The SBO amplification factor of 2.559 (to obtain normal pathwidth sensitivity) is included in the five element SBO field. Figure 27 shows the elevation DDM characteristic for both arrays. Figure 28 shows fly-ins over an infinite plane with unfocused antenna elements. These are similar to those obtained with the standard Capture Effect array as shown in Figure 5 but the flare in the threshold approach region is greater.

7.0 PHASE SENSITIVITY OF THE CAPTURE EFFECT ARRAY

The low angle radiation of the Capture Effect array is quite sensitive to phase shifts of the excitation on the second antenna element. Such phase shift may occur in field installations of this array due to circuit mistunings caused by changing environmental conditions. Figure 29 shows the SBO field amplitude sensitivity to $\pm 15^{\circ}$ of phase shift on the middle element. Figure 30 shows sensitivity for the CSB field. In both cases, since the normal excitations are designed to suppress low angle radiation by partial cancellation, dephasing causes an increase in low angle amplitude. Figure 31 shows the derogation of DDM due to the phase shift. It is observed that a strong fly-down signal is obtained at 1° with only $\pm 15^{\circ}$ of phase shift, whereas the normal condition is a strong fly-up at this angle.

8.0 FOUR AND FIVE ELEMENT VARIATIONS OF THE CAPTURE EFFECT ARRAY HAVING IMPROVED PHASE SENSITIVITY

Two variations of the Capture Effect array were studied which have somewhat improved phase sensitivity. The first was the four element array indicated on the right side of Figure 32. The second element of the standard version is replaced by elements 4 and 5 in the four element version. The height of element 4 is designed to give an SBO null at 3.5°, and element 5 to null at 2.5°. The SBO excitations on 4 and 5 were derived by imposing on the far field equation the conditions that the null of the sum of SBO from elements 4 and 5 be zero at 3° and the amplitude at 1.5° be the same that as that of the standard version. The CSB excitations on 4 and 5 were designed to give the same total CSB amplitude at 1.5° as the standard version. Figures 33 and 34 show the resulting SBO and CSB field amplitudes and their variation with 15° of phase shift on the individual elements, one at a time. Figure 35 shows the resulting elevation DDM variations with phase. Comparison of this figure with Figure 31 for the standard Capture Effect shows that there is some improvement in performance. The low angle DDM zero crossings for the four element version occur at 1° or less whereas, for the standard version, a zero crossing occurs as high as 1.35° for the same phase shift. An undesirable characteristic of the four element array is that, even with no phase shift, there is an erroneous zero crossing at about 0.4° elevation angle.

A five element modification of the Capture Effect array was devised which has somewhat less phase sensitivity than the four element array above. The configuration is shown on the right side of Figure 36. Here, element 2 of the standard Capture Effect is added to the four element array above. The SBO excitation is identical to the standard, but the CSB excitation is split between elements 4 and 5 as in the four element version of Figure 32. The elevation DDM characteristics of the resulting five element array are shown in Figure 37. With no phase shift on any element there is no false zero crossing at low angle. With phase shift, there is one false zero crossing at 0.9° ($+15^{\circ}$ on element 2), and others falling at 0.7° or less.

9.0 GLIDE PATH FLY-IN STRUCTURE WITH A LATERAL EDGE

During the Westinghouse studies of edge diffraction of EM waves, a closed form solution was developed for wave diffraction by an edge perpendicular to the axis of a horizontal electric dipole. This solution is in addition to the solution for the edge parallel to the dipole axis (Appendix B) which has been used in all of the limited ground plane analysis results reported prior to this section. The perpendicular edge is also referred to as a lateral edge in that it is parallel to the side of the runway. Thus the lateral edge refers to a half-plane or limited ground plane whose edge is parallel to the runway, as opposed to perpendicular to the runway as in the previous studies.

The lateral edge solution equations were incorporated into the Capture Effect guidance computer model and fly-in runs were made with results shown in Figures 38 and 39. These runs were made for a 2.86° glide path, 300 feet antenna offset, standard element focusing, and with standard infinite plane pathwidth sensitivity. The parameter ΔY is the distance between the array and the lateral edge. When the edge is just under the array ($\Delta Y = 0$), it is interrupting large ground currents and the effect on DDM is large as shown by the $\Delta Y = 0$ curve of Figure 38. To obtain reasonable amplitude of oscillation (less than 10 microamps) the edge must be moved about 40 feet beyond the antenna. Figure 39 is an expanded scale run showing that an edge 200 feet from the antenna has small oscillations and that a 700 feet edge is essentially equivalent to an infinite plane.

10.0 CONCLUSIONS, SIGNIFICANT FINDINGS, RECOMMENDATIONS

An efficient computer model of image type glide slope systems operating

over both long and short ground planes has been developed and used extensively in this study. DDM fly-in results for a Null Reference array over a 5000 feet ground plane obtained with this model were compared with results obtained by the Transportation Systems Center (TSC) personnel and found to be identical. The Westinghouse computer model incorporates a closed form solution for edge diffraction of EM waves and requires an order of magnitude less computer time than the TSC method which requires numerical summation of EM fields arising from ground current strips. Calculations were also made for a Capture Effect array over a limited ground plane which was, in turn, over an infinite ground plane corresponding to the experimental conditions of Lucas. A high degree of correlation was obtained between the calculations and the experimental data taken by Lucas.

The computer model was then used to study the effect on fly-in DDM of different position arrangements of the Capture Effect array elements. It was discovered that a unique arrangement of elements could be found for any given system environment which would give a near zero DDM along the entire glide path up to the runway threshold. This improved fly-in characteristic can be obtained for both long and short ground planes.

Another goal of the study was to consider what improvements could be made to the Capture Effect array performance by adding a maximum of three antenna elements. One five element array was devised which has 10.5 dB less SBO field radiation at 1^{o} elevation angle than does the standard Capture Effect array; however, this array is higher than the standard array height. Two other configurations were studied, one four element and one five element, which gave decreased DDM sensitivity to phase changes of antenna current.

The final effort of the study involved calculations of fly-in DDM with Capture Effect array, over a half-plane with a lateral edge. The results show that if the edge is at least 40 feet beyond the array the peak variations of DDM are less than 10 μa.

The thrust of this study has been to improve the glide path structure for operation with reduced ground planes. Only a small range of angles about the glide path have been examined. It is assumed that a separate clearance signal will be required to provide sufficient below path fly-up. The results indicate that systems could be installed where presently CAT-II structure cannot be met, but does not imply that present systems are unsafe.

Table 10-1 shows the derogation of the average DDM in the threshold approach region (Point B to threshold) for standard adjustment. Since Cat. II tolerance allows an average deviation of 37.5 μa at Point B (3500 ft. from threshold), 48.75 μa at Point C (858 ft. from threshold) and 75 μa at threshold, it is clear that both Cat. I and Cat. II tolerances are met for zero azimuth approach with a ground plane as short as 500 ft. With modified focusing, as in Figure 22, the average derogation for ground planes as short as 500 ft. is virtually zero and in addition the fly-up flare is eliminated, thus providing a planar guidance over the entire glide path.

It is recommended that the FAA arrange for field tests to verify that modified focusing as discussed herein will provide a planar glide path guidance average signal. A near field probe system should be devised to permit the establishment of the planar guidance far fields without repeated trial and error fly-ins.

TABLE 10-1

DDM DEROGATION WITH GROUND PLANE LENGTH

Ground Plane Edge Distance

DISTANCE FROM THRESHOLD (FT)	∞ FT.	2000 FT.	DEROGATION	1000 FT.	DEROGATION	500 FT.	DEROGATION
0	- 43 μa	- 43.5 μa	- 0.5 μa	- 51 μa	- 8 μa	- 104 μa	- 61 μa
1000	- 12	- 12	0	- 19	- 7	- 43	- 31
2000	- 6	- 7	- 1	- 13	- 7	- 26	- 20
3000	- 4	- 4.5	- 0.5	- 10	- 6	- 18	- 14
4000	- 2.5	- 3	- 0.5	- 8	- 5.5	- 13.5	- 11

CONDITIONS:

(1) Standard focus and height adjustment as in Figures 6, 7, 16 and 17.

(2) Zero azimuth approach angle.

FIGURE 1 CAPTURE EFFECT ARRAY GEOMETRY

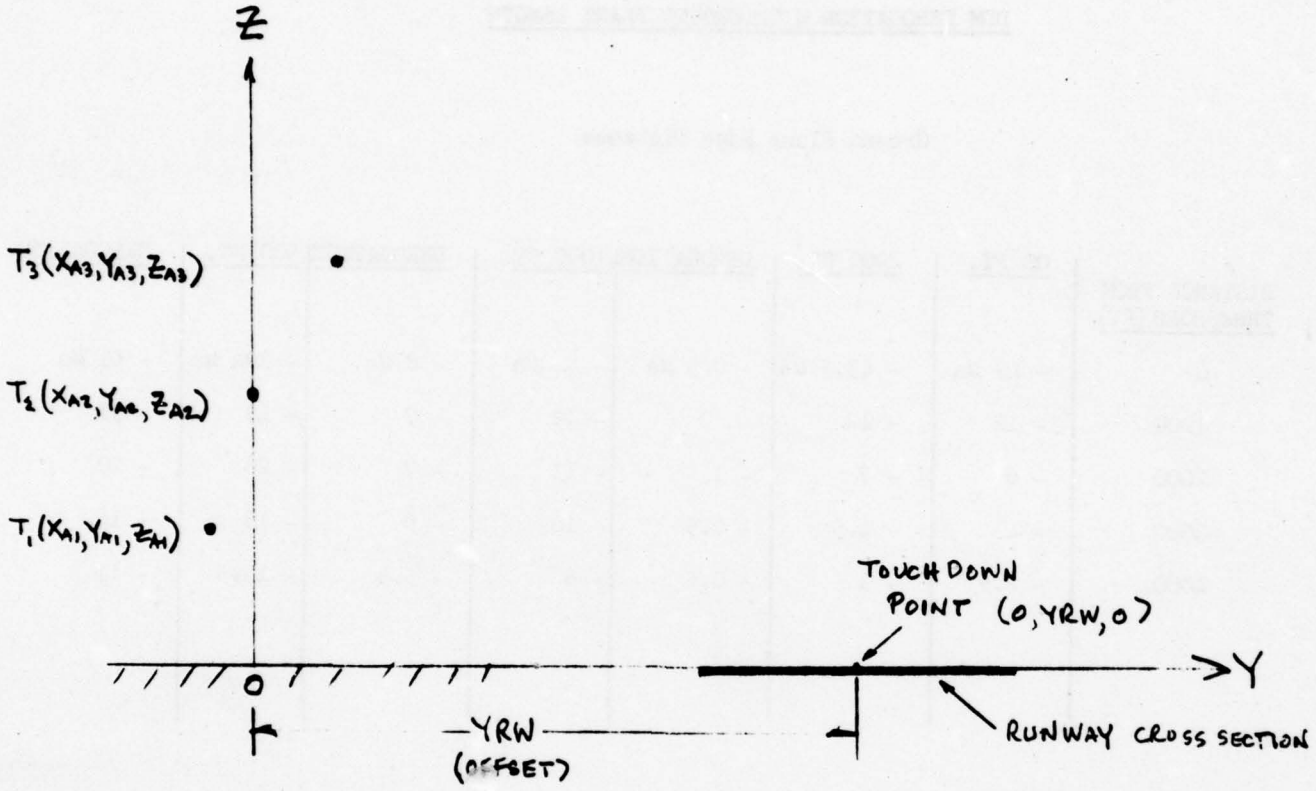

(1) POSITIVE X AXIS TOWARD OBSERVER
(2) ELEMENTS INDICATED AS FOCUSED ON TOUCHDOWN POINT
(3) RUNWAY IS PARALLEL TO X AXIS

FIGURE 2 CAPTURE EFFECT ARRAY FLY IN OVER INFINITE PLANE

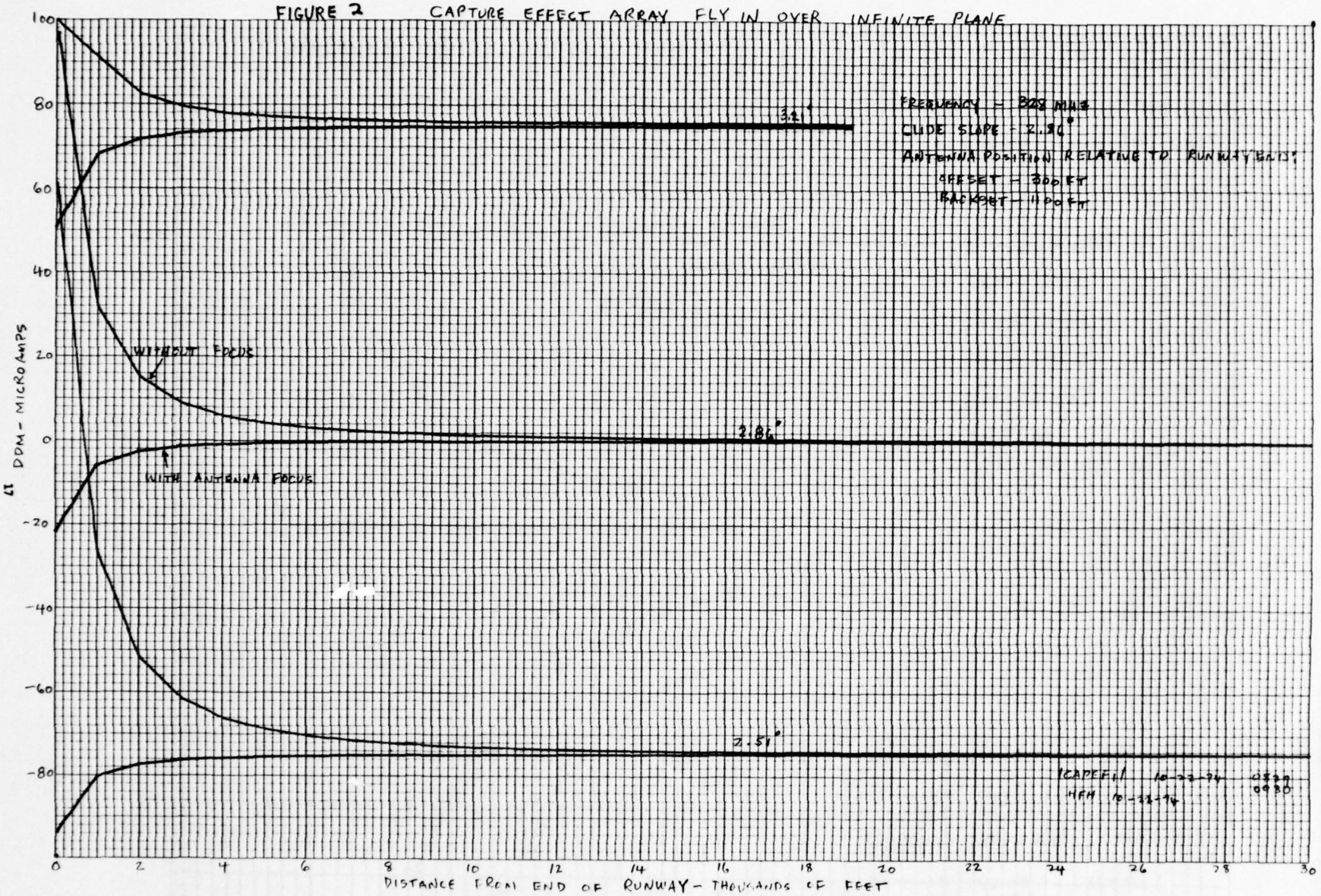

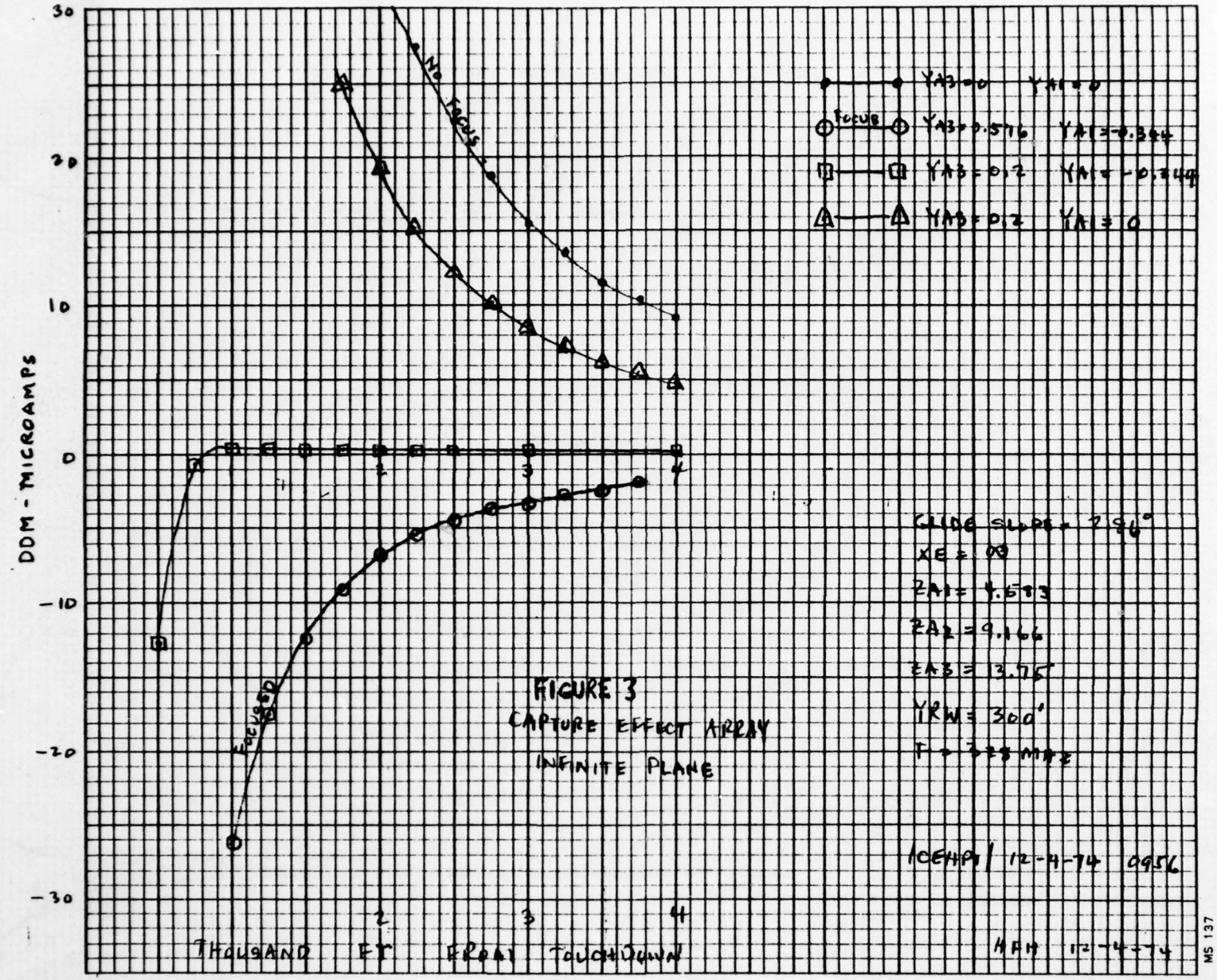

FIGURE 3
CAPTURE EFFECT ARRAY
INFINITE PLANE

FIGURE 4 CAPTURE EFFECT ARRAY FLY IN OVER INFINITE PLANE

MODIFIED FOCUS

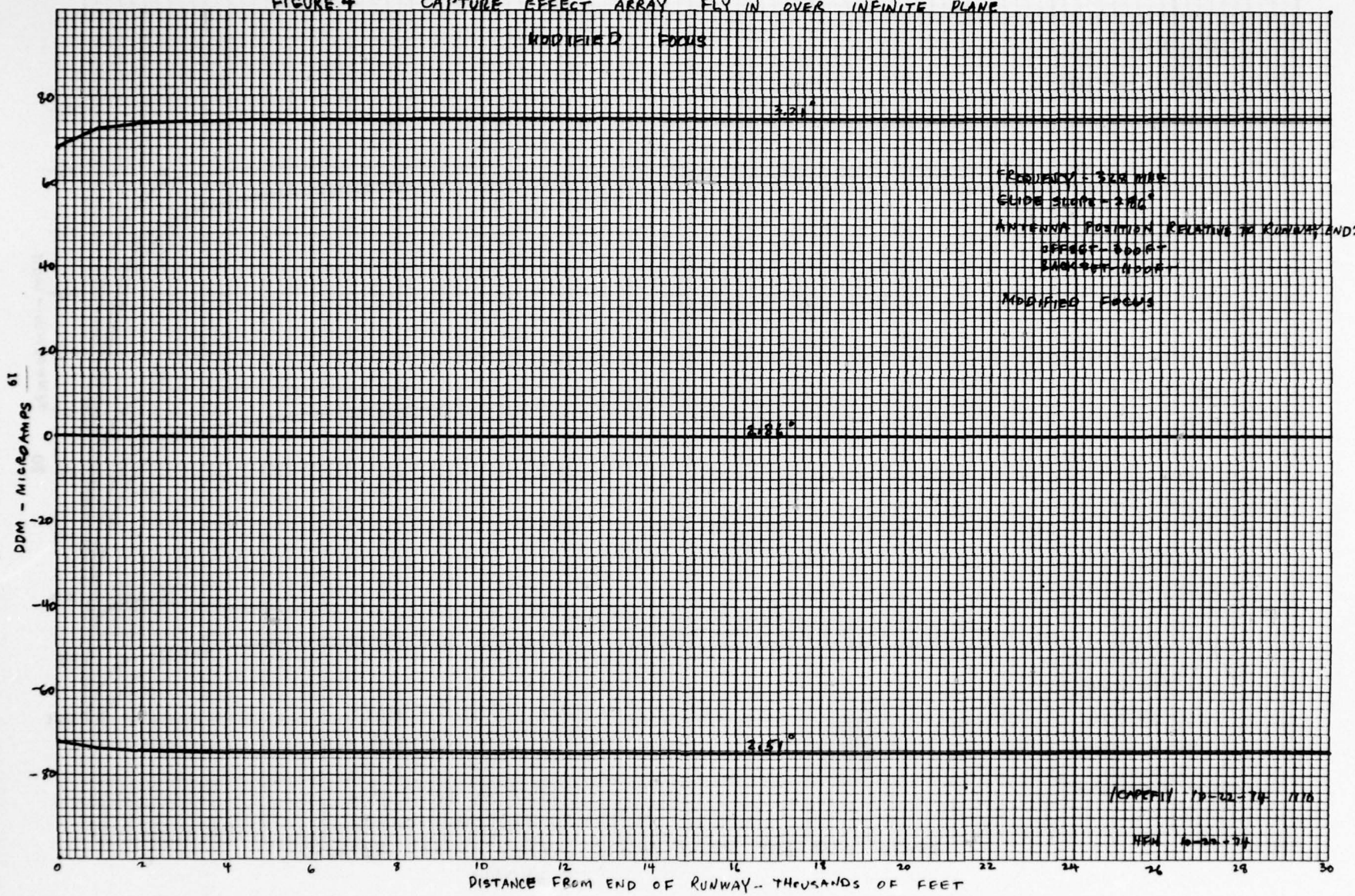

FIGURE 5

CAPTURE EFFECT ARRAY FLYIN OVER INFINITE PLANE

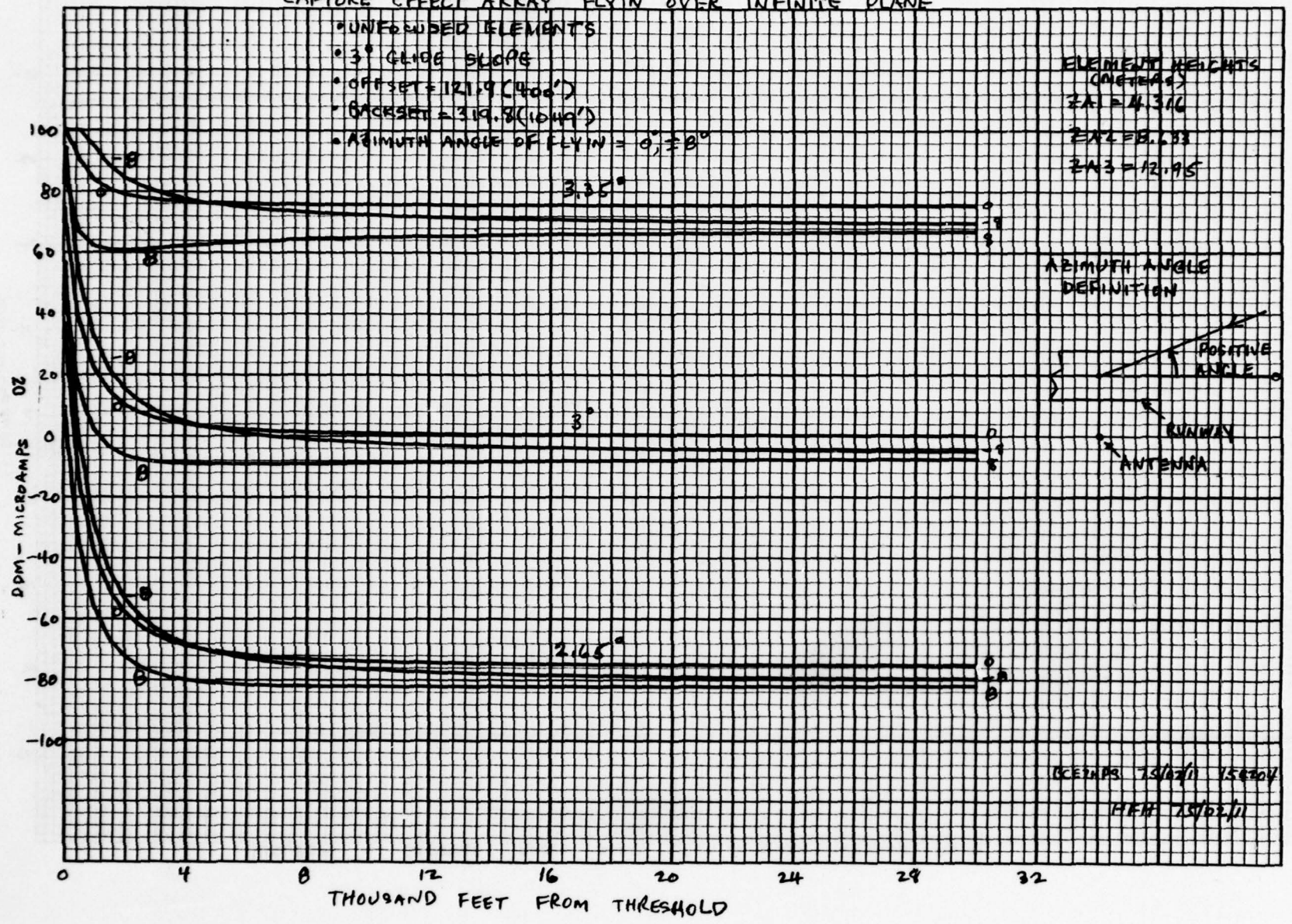

FIGURE 6

CAPTURE EFFECT ARRAY FLYIN OVER INFINITE PLANE

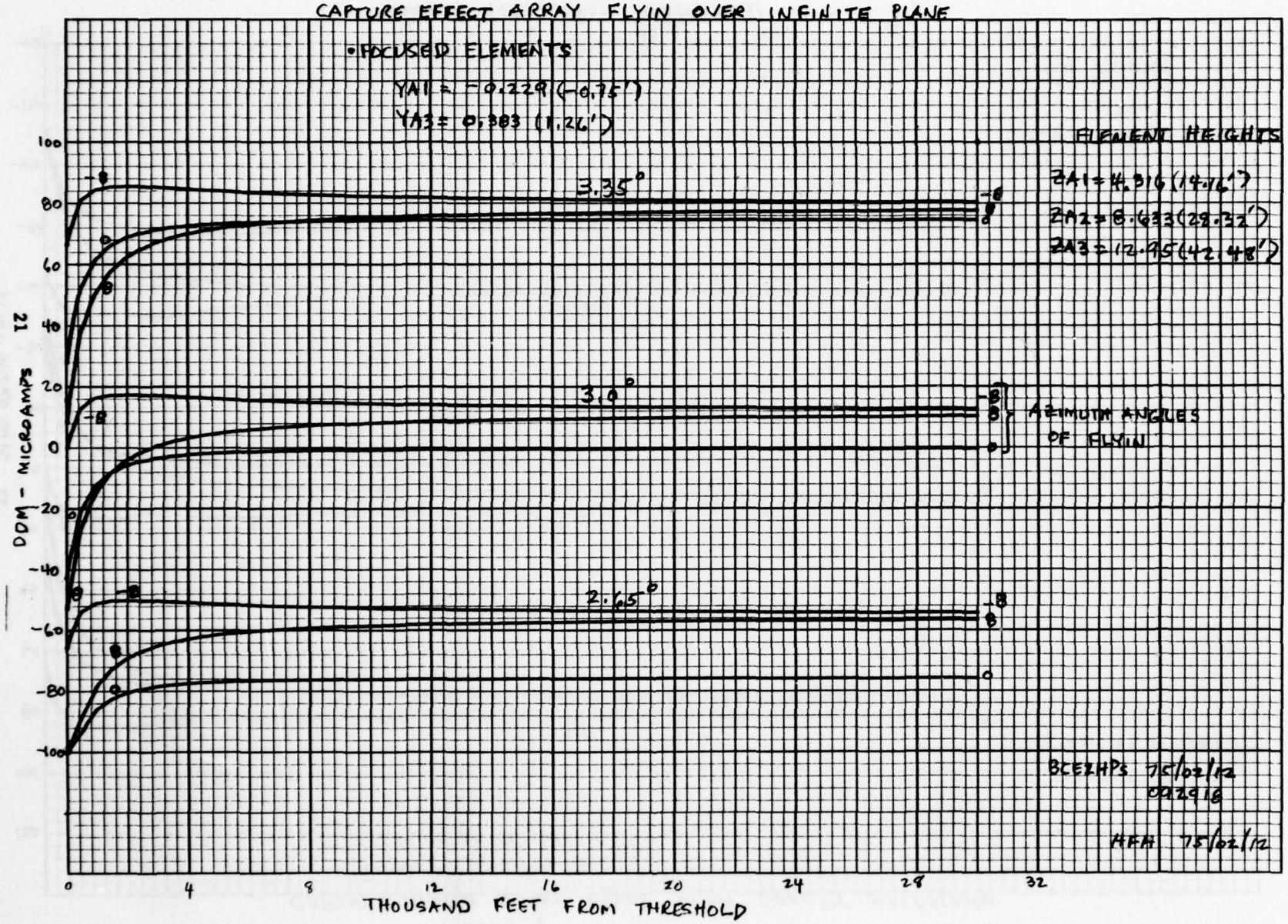

FIGURE 7

CAPTURE EFFECT ARRAY FLYIN WITH 2000 FT HALFPLANE

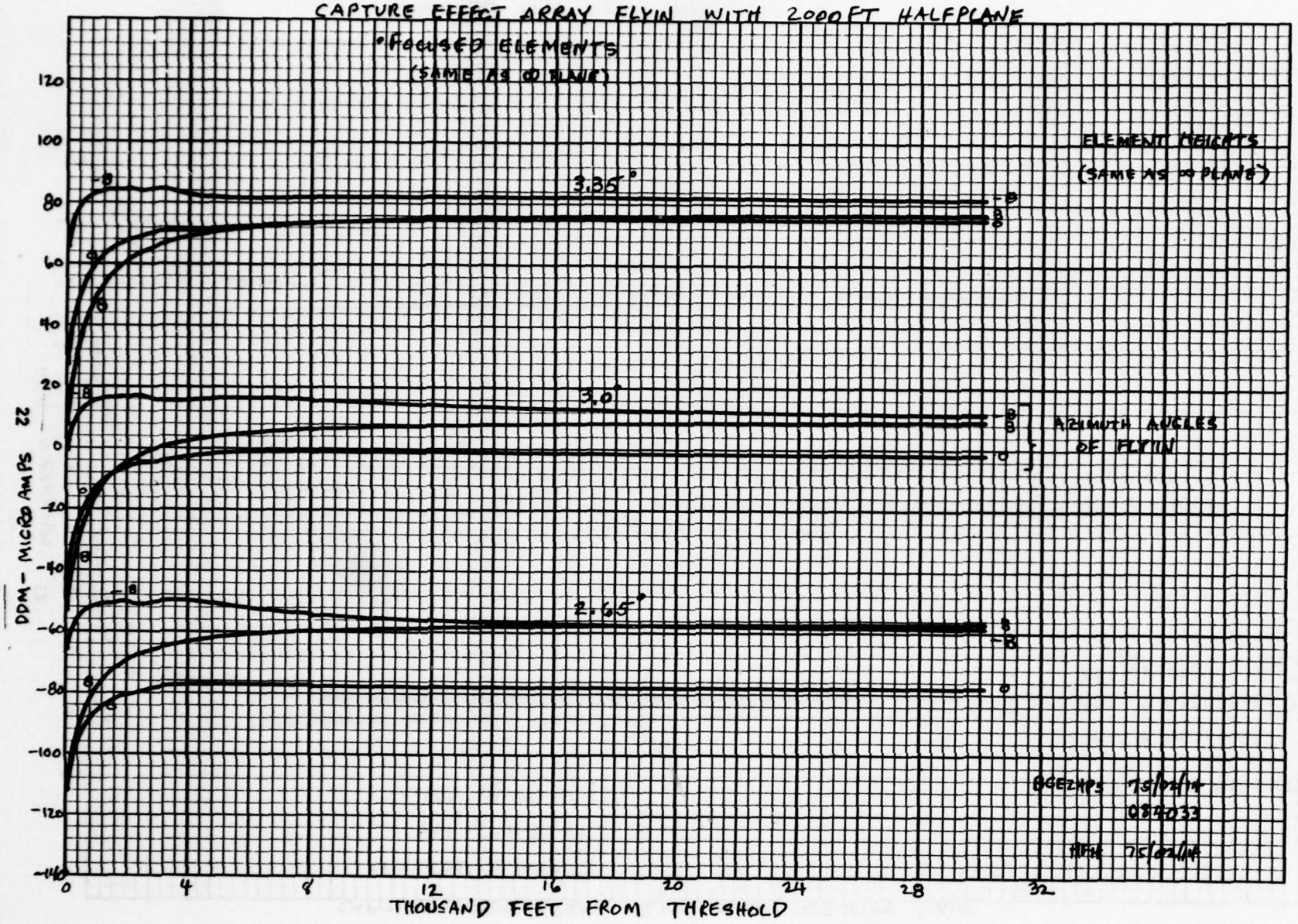

FIGURE 8

CAPTURE EFFECT ARRAY FLYIN OVER INFINITE PLANE

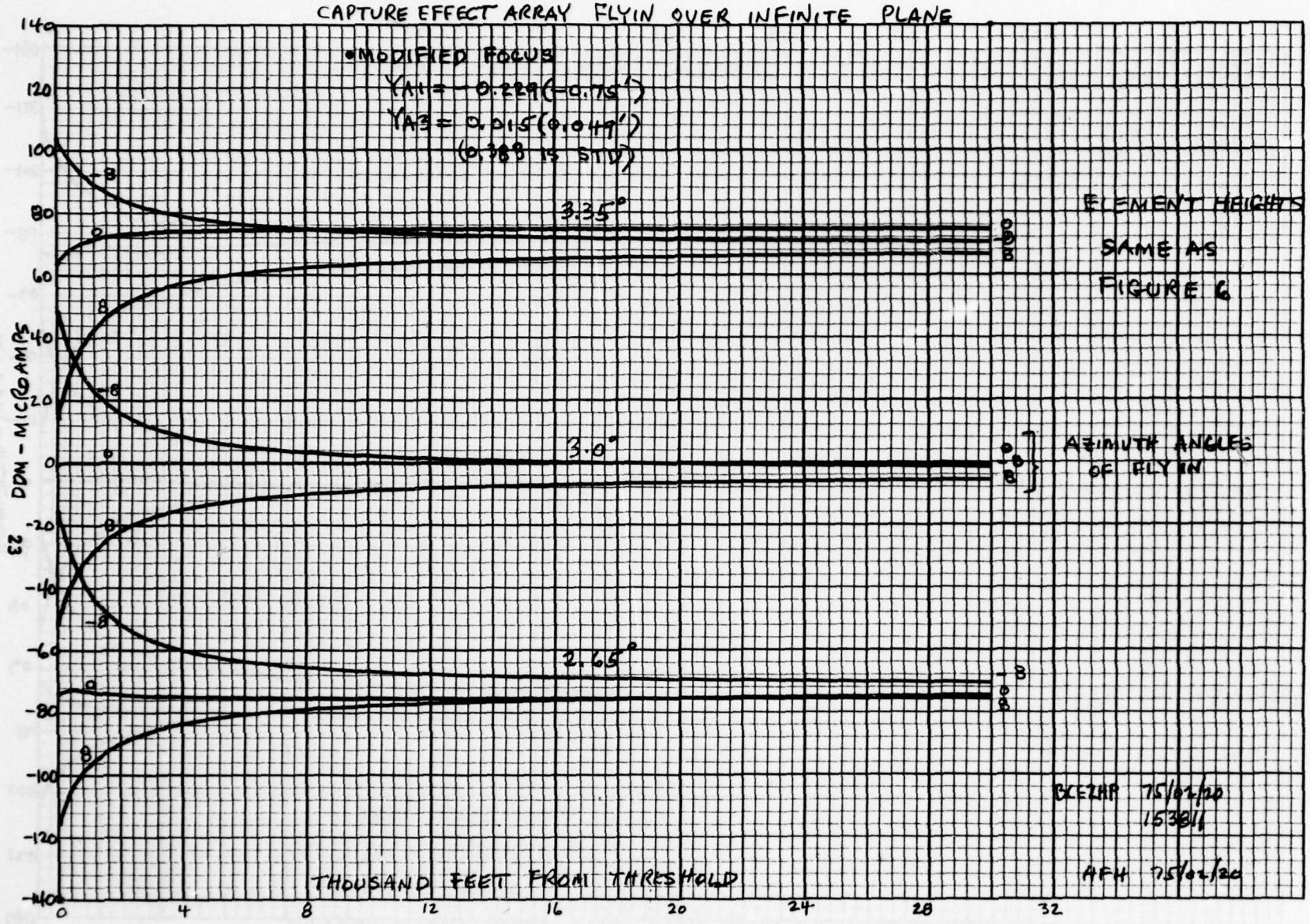

GCEZAP 75/02/20
153811

AFH 75/02/20

FIGURE 9

CAPTURE EFFECT ARRAY FLYIN OVER 2000 FT HALFPLANE

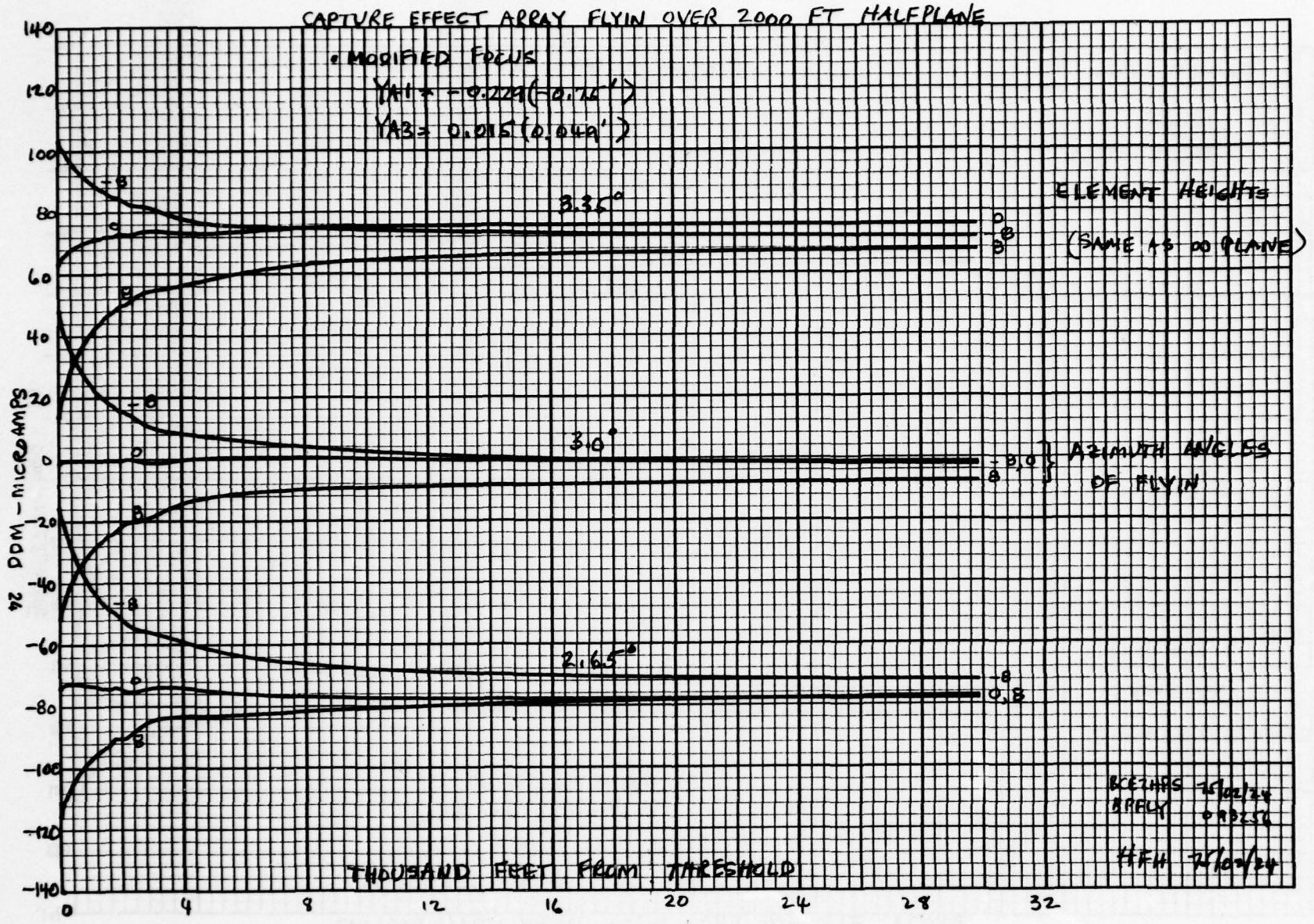

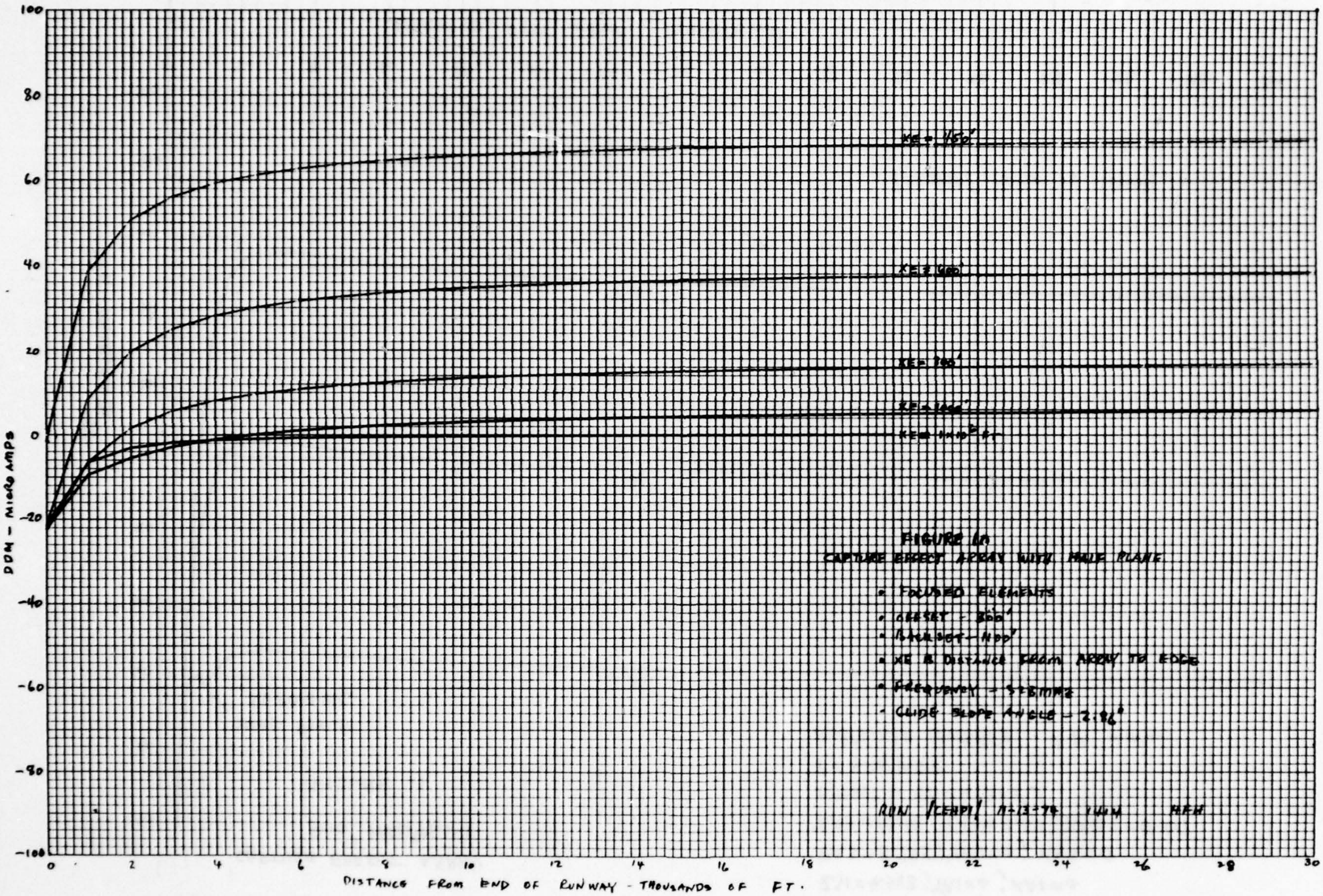
FIGURE 6A
CAPTURE EFFECT ARRAY WITH HALF PLANE
• FOCUSED ELEMENTS
• OFFSET - 300'
• BACKSET - 400'
• XE = DISTANCE FROM ARRAY TO EDGE
• FREQUENCY - 335 MHZ
• GLIDE SLOPE ANGLE - 2.86°
RUN /CEHPI/ 11-13-74 1444 MFH
XE = 1150'
XE = 900'
XE = 700'
XE = 1400'
XE = 1×10⁶ FT
DDM - MICROAMPS
100
80
60
40
20
0
-20
-40
-60
-80
-100
0
2
4
6
8
10
12
14
16
18
20
22
24
26
28
30
DISTANCE FROM END OF RUNWAY - THOUSANDS OF FT.

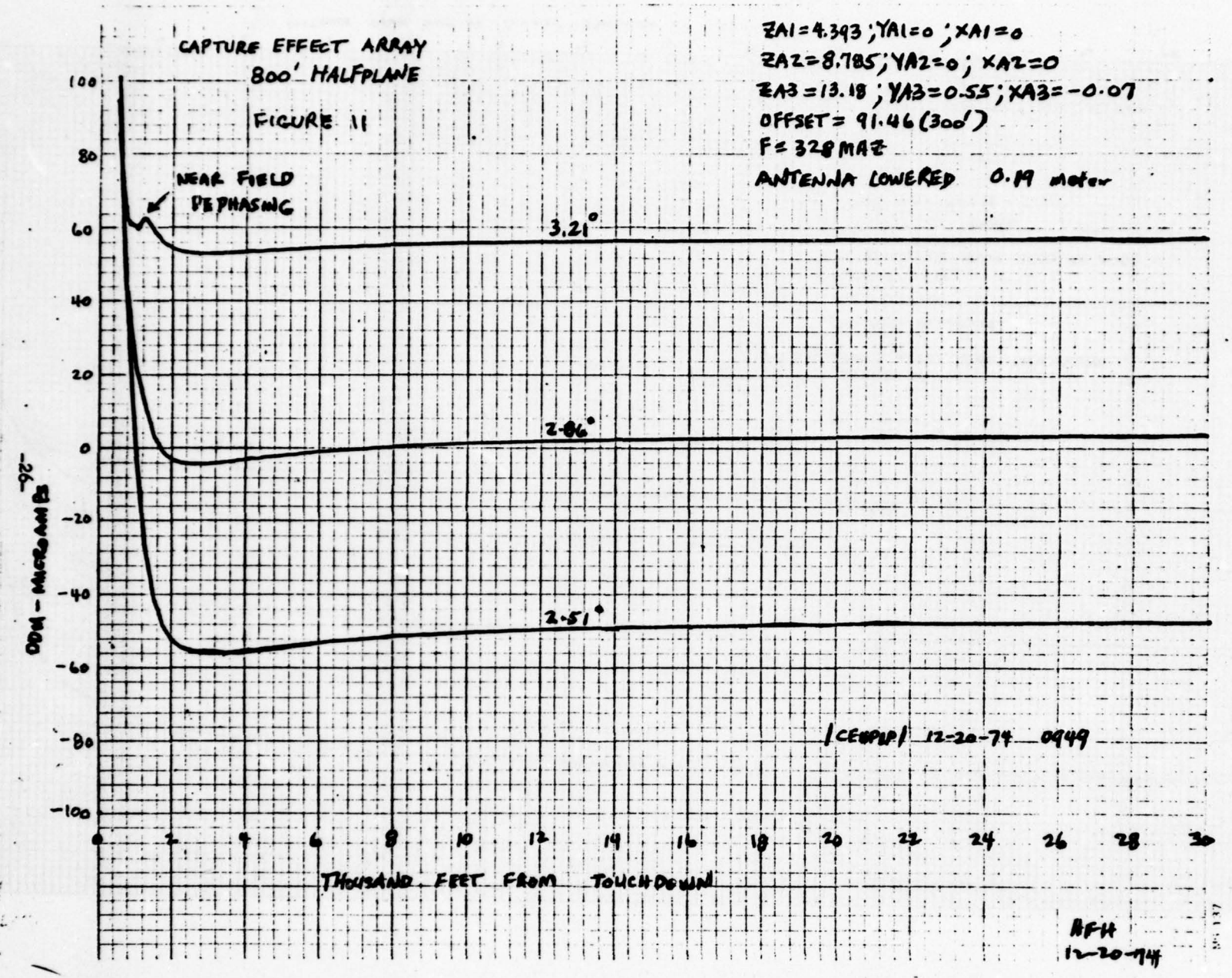
CAPTURE EFFECT ARRAY
800' HALFPLANE
FIGURE 11
ZA1=4.393; YA1=0; XA1=0
ZA2=8.785; YA2=0; XA2=0
ZA3=13.18; YA3=0.55; XA3=-0.07
OFFSET = 91.46 (300')
F = 328 MHZ
ANTENNA LOWERED 0.19 meter
NEAR FIELD DEPHASING
3.21°
2.86°
2.51°
100
80
60
40
20
0
-20
-40
-60
-80
-100
DDM - MICROAMPS
0
2
4
6
8
10
12
14
16
18
20
22
24
26
28
30
THOUSAND FEET FROM TOUCHDOWN
/CEDP1P/ 12-20-74 0949
AFH
12-20-74

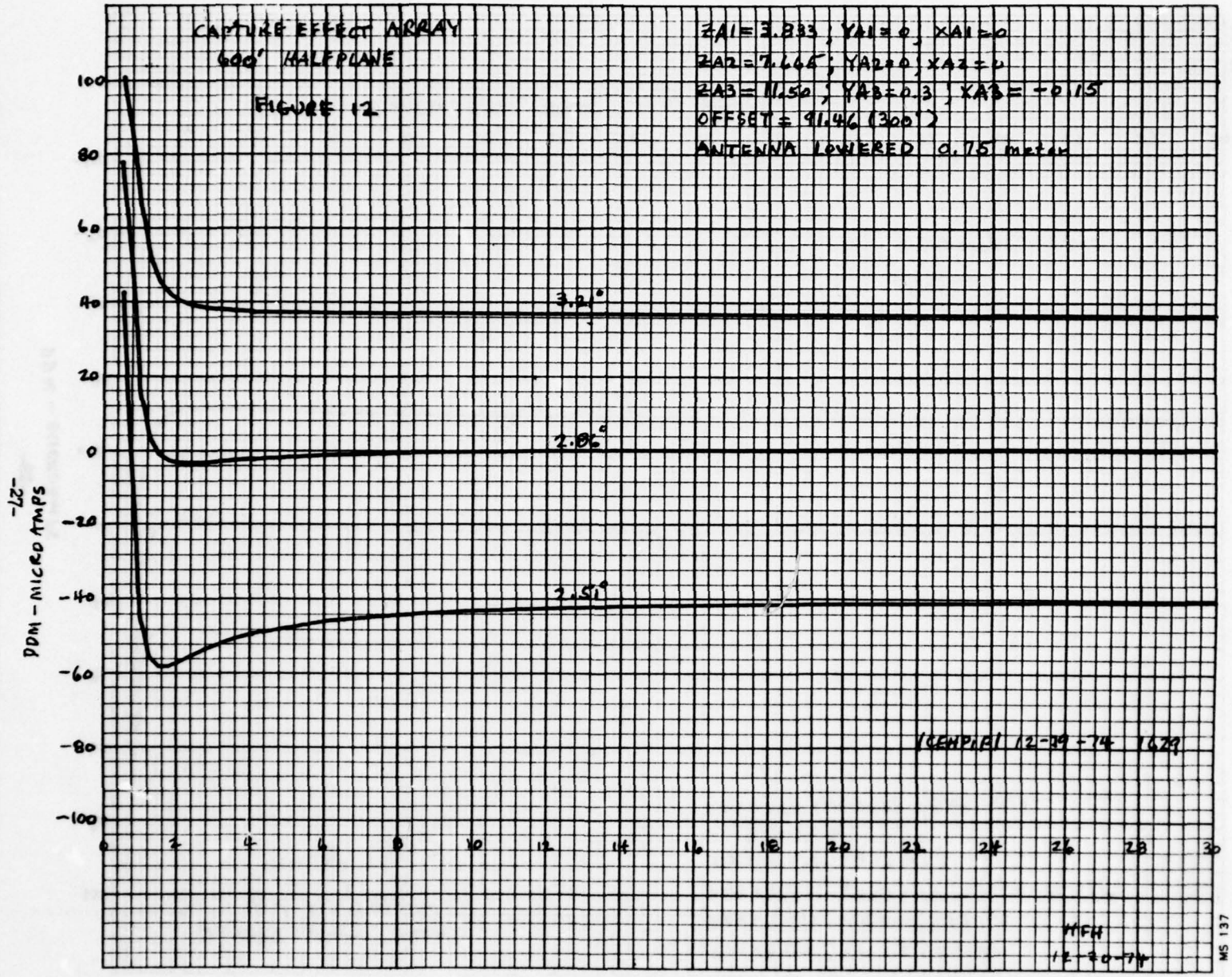
CAPTURE EFFECT ARRAY
600' HALFPLANE
FIGURE 12
ZA1 = 3.833 ; YA1 = 0 ; XA1 = 0
ZA2 = 7.666 ; YA2 = 0 ; XA2 = 0
ZA3 = 11.50 ; YA3 = 0.3 ; XA3 = +0.15
OFFSET = 91.46 (300')
ANTENNA LOWERED 0.75 meter
3.2°
2.8°
3.5°
DDM - MICRO AMPS
-27-
100
80
60
40
20
0
-20
-40
-60
-80
-100
0
2
4
6
8
10
12
14
16
18
20
22
24
26
28
30
WFH
12-20-74
MS 137

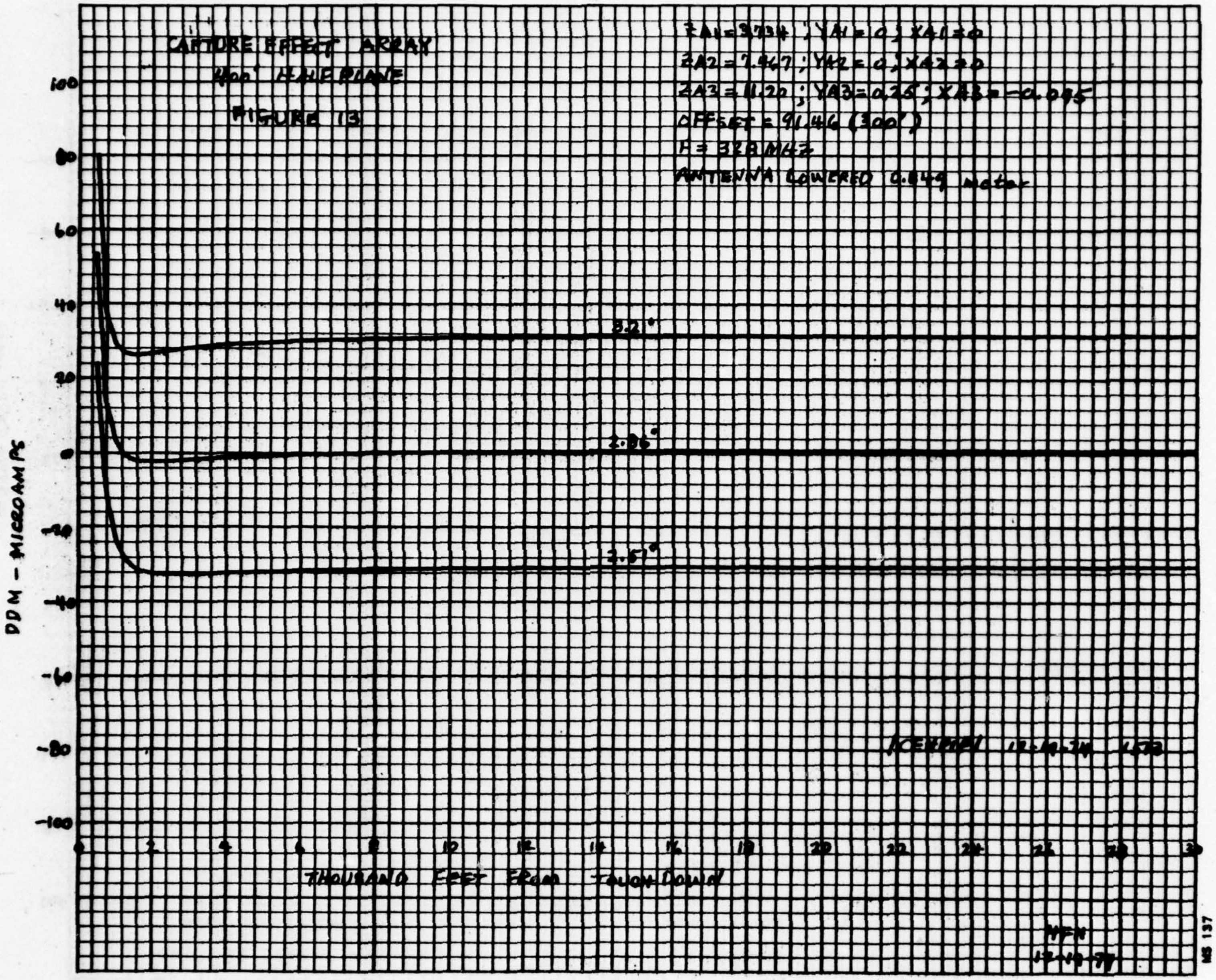
CAPTURE EFFECT ARRAY
400' HALF PLANE
FIGURE 13
ZA1=3.734; YA1=0; XA1=0
ZA2=7.467; YA2=0; XA2=0
ZA3=11.20; YA3=0.25; XA3=-0.085
OFFSET = 91.46 (300')
F = 328 MHZ
ANTENNA LOWERED 0.849 meter
3.2°
2.86°
2.57°
DDM - MICROAMPS
THOUSAND FEET FROM TOUCHDOWN
100
80
60
40
20
0
-20
-40
-60
-80
-100
0
2
4
6
8
10
12
14
16
18
20
22
24
26
28
30
MS 137

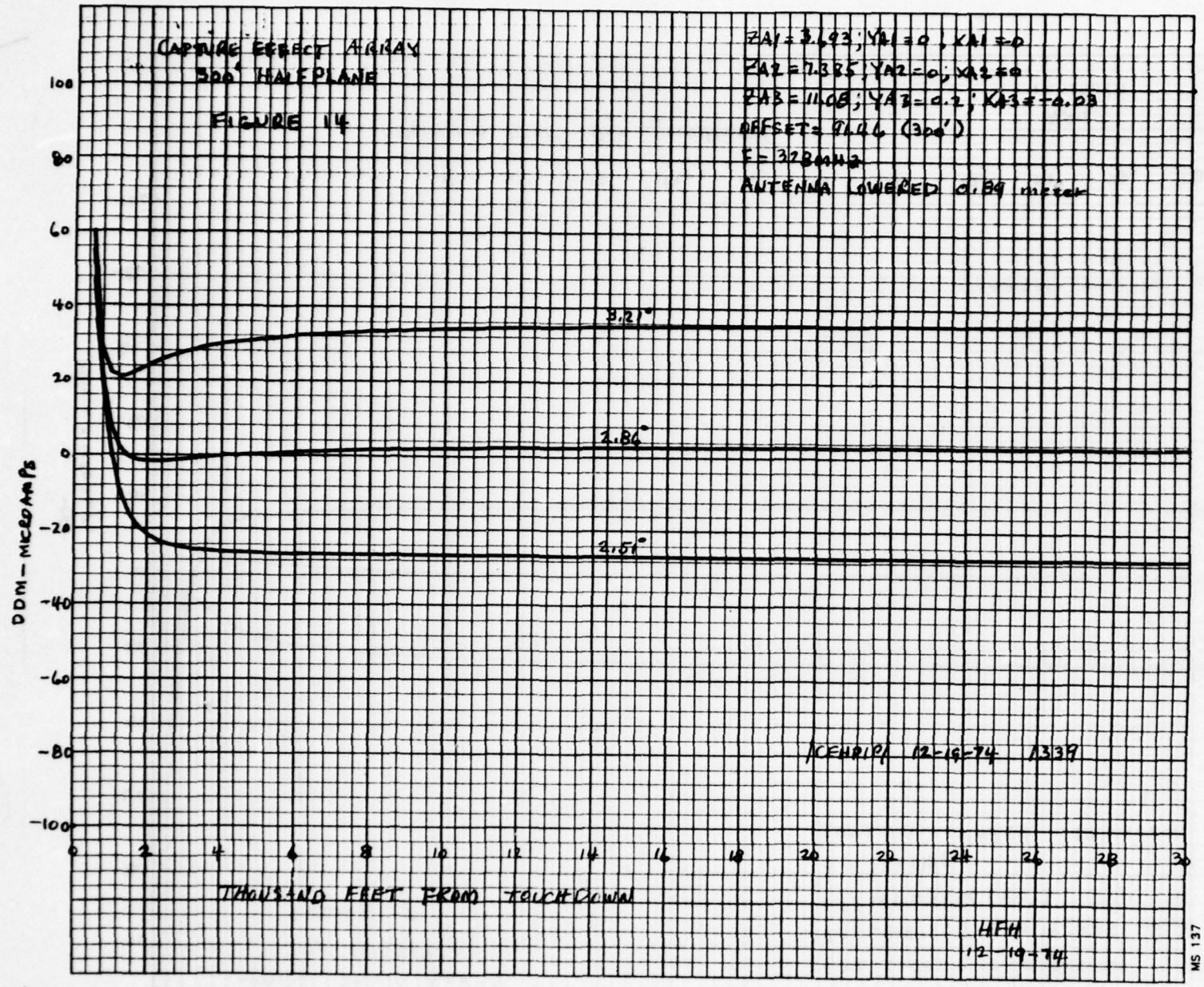
CAPTURE EFFECT ARRAY
300' HALF PLANE
FIGURE 14
ZA1 = 3.693; YA1 = 0, XA1 = 0
ZA2 = 7.385; YA2 = 0; XA2 = 0
ZA3 = 11.08; YA3 = 0.2; XA3 = +0.03
OFFSET = 9.04 (30d')
F = 328MHz
ANTENNA LOWERED 0.89 meter
3.21°
2.84°
2.51°
DDM - MICROAMPS
100
80
60
40
20
0
-20
-40
-60
-80
-100
0
2
4
6
8
10
12
14
16
18
20
22
24
26
28
30
THOUSAND FEET FROM TOUCHDOWN
ACEHRIPI 12-16-74 1339
HFH
12-19-74
MS 137

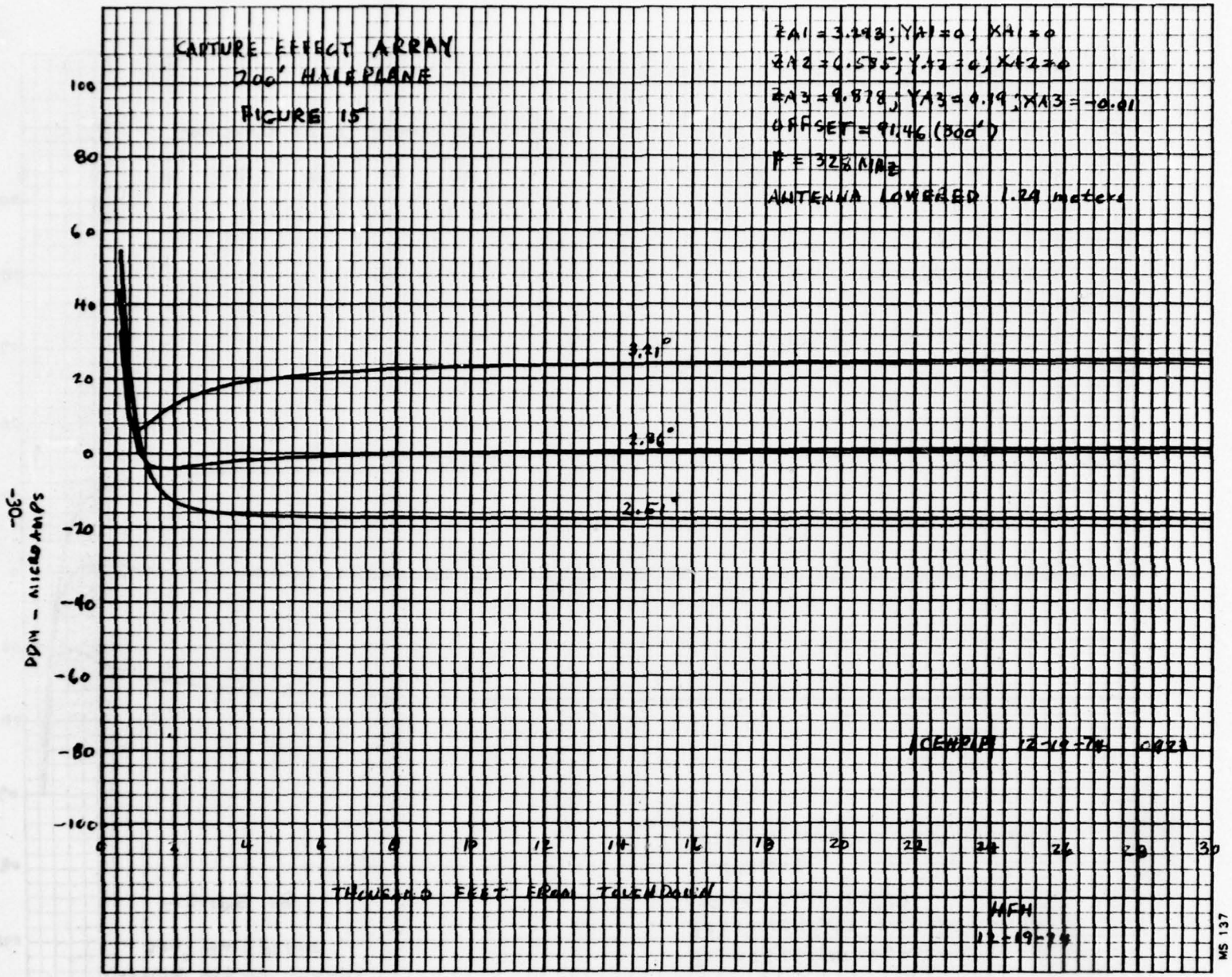
CAPTURE EFFECT ARRAY
300' HALF PLANE
FIGURE 15
ZA1 = 3.293; YA1 = 0; XA1 = 0
ZA2 = 0.585; YA2 = 0; XA2 = 0
ZA3 = 9.878; YA3 = 0.19; XA3 = -0.01
OFFSET = 91.46 (300')
F = 328 MHz
ANTENNA LOWERED 1.29 meters
3.71°
2.96°
2.51°
DBM - NORMALIZED
100
80
60
40
20
0
-20
-40
-60
-80
-100
0
2
4
6
8
10
12
14
16
18
20
22
24
26
28
30
THEORETICAL EFFECT FROM TOUCHDOWN
MFH
12-19-74
MS 137

FIGURE 16

CAPTURE EFFECT ARRAY FLYIN WITH 1000 FT HALFPLANE

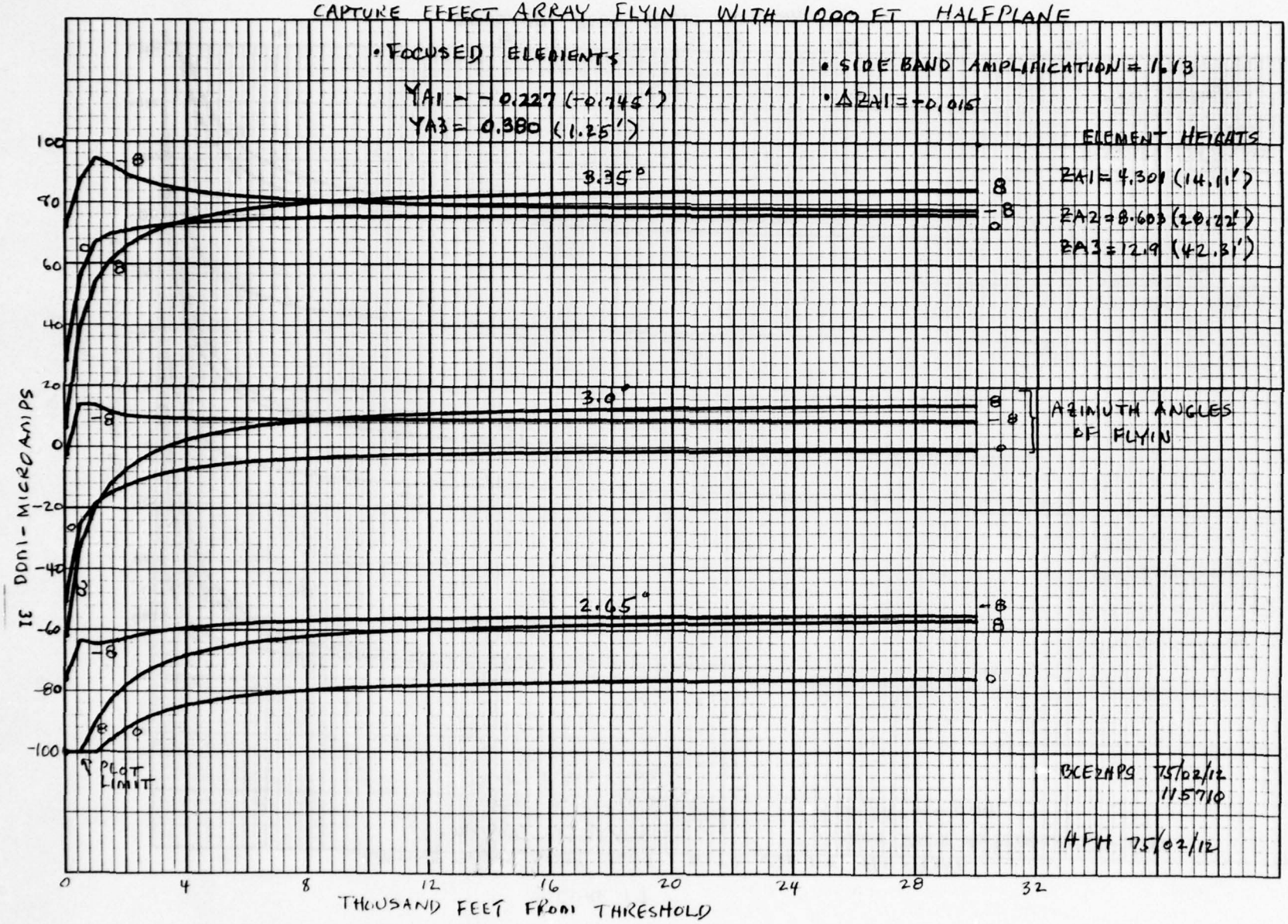

FIGURE 17

CAPTURE EFFECT ARRAY FLYIN WITH 500 FT HALFPLANE

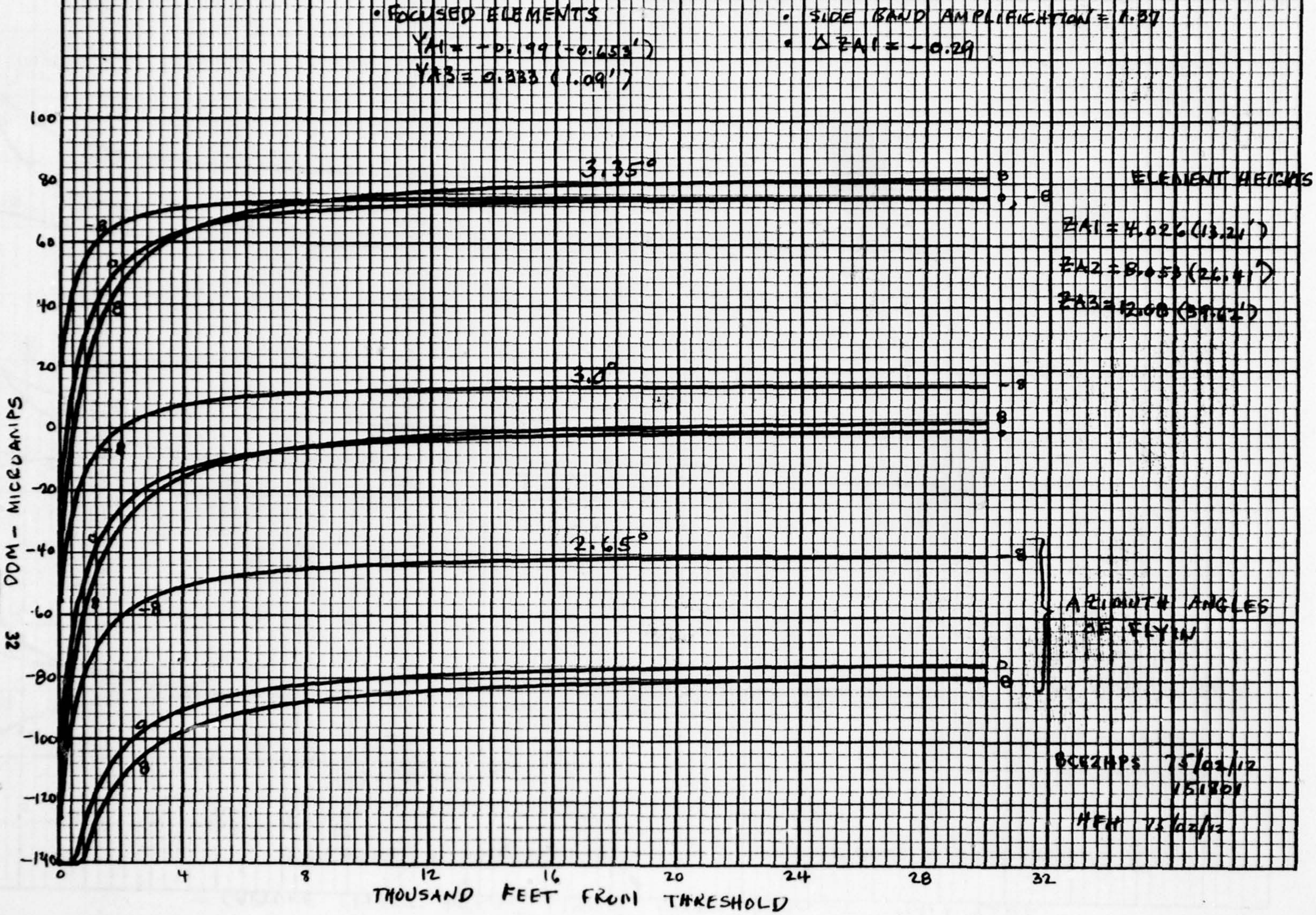

FIGURE 18

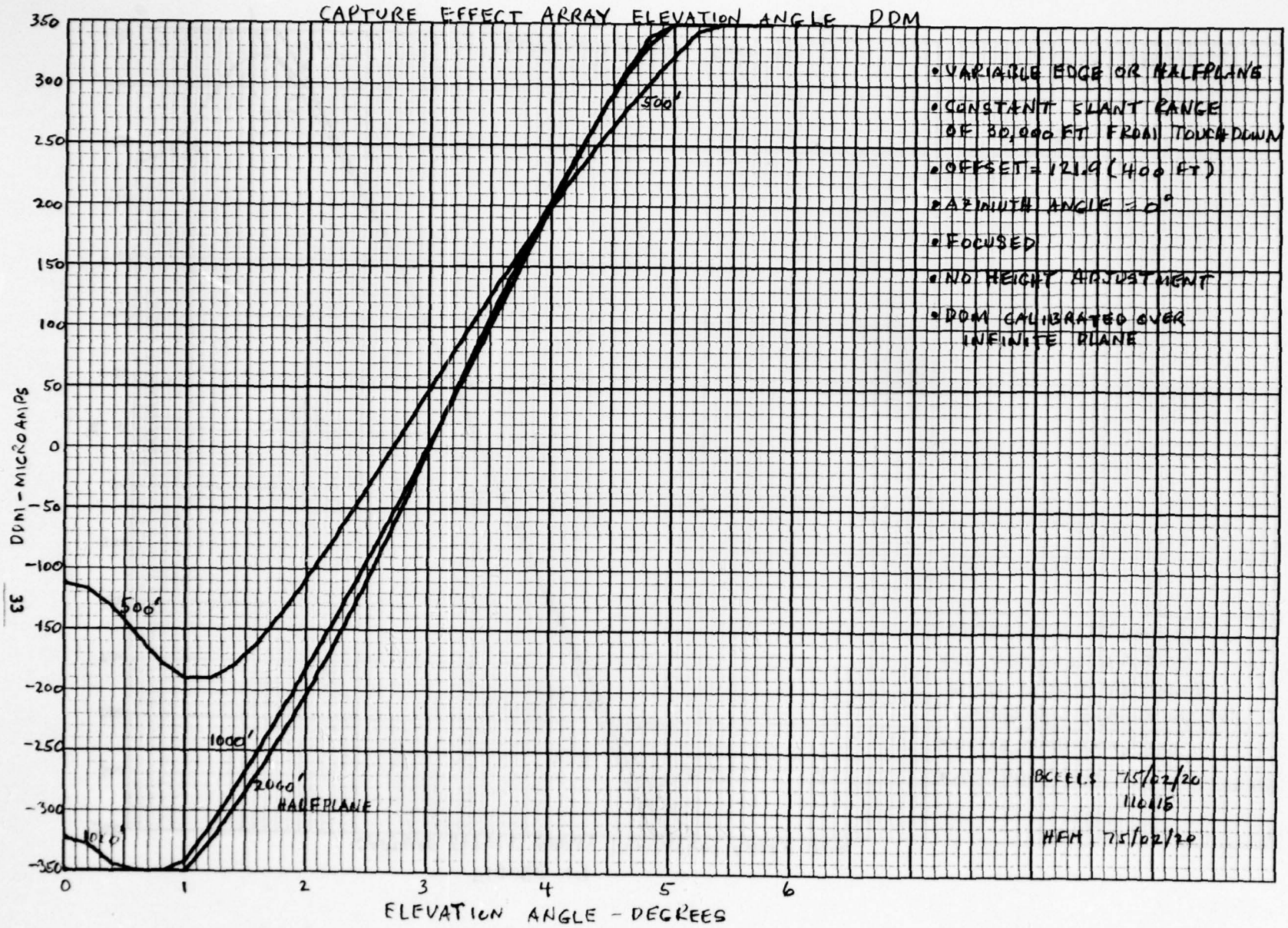
CAPTURE EFFECT ARRAY ELEVATION ANGLE DDM
DDM - MICROAMPS
350
300
250
200
150
100
50
0
-50
-100
150
-200
-250
-300
-350
0
1
2
3
4
5
6
ELEVATION ANGLE - DEGREES
500'
1000'
2000'
HALFPLANE
500'
101.0'
• VARIABLE EDGE OR HALFPLANE
• CONSTANT SLANT RANGE OF 30,000 FT FROM TOUCHDOWN
• OFFSET = 121.9 (400 FT)
• AZIMUTH ANGLE = 0°
• FOCUSED
• NO HEIGHT ADJUSTMENT
• DDM CALIBRATED OVER INFINITE PLANE
BCEELS 75/02/20
110415
HFM 75/02/20

FIGURE 19

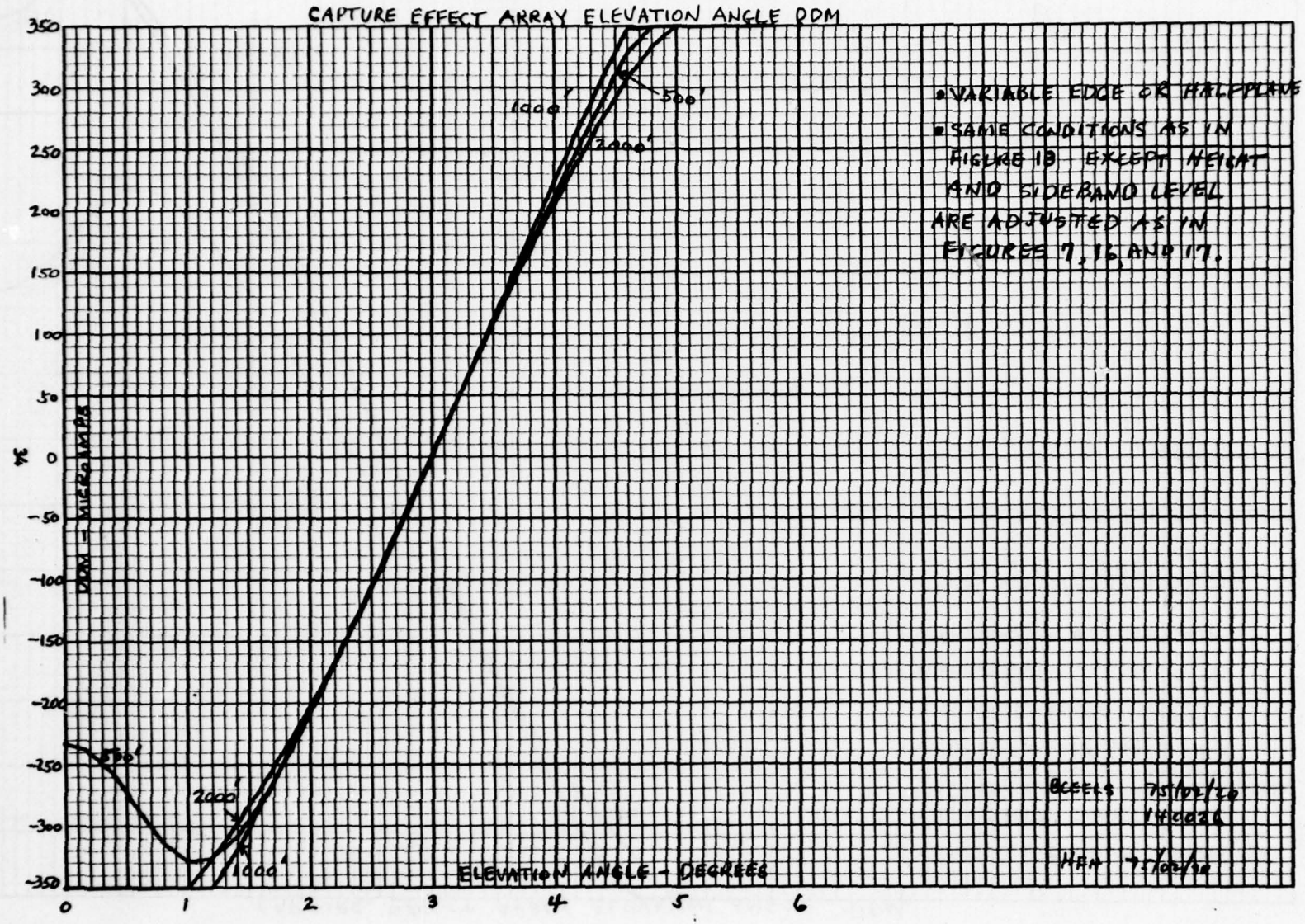
CAPTURE EFFECT ARRAY ELEVATION ANGLE DDM
DDM — MICROAMPS
ELEVATION ANGLE — DEGREES
350
300
250
200
150
100
50
0
-50
-100
-150
-200
-250
-300
-350
0
1
2
3
4
5
6
500'
1000'
2000'
500'
2000'
1000'
• VARIABLE EDGE OR HALFPLANE
• SAME CONDITIONS AS IN FIGURE 18 EXCEPT HEIGHT AND SIDEBAND LEVEL ARE ADJUSTED AS IN FIGURES 7, 16, AND 17.

FIGURE 20

CAPTURE EFFECT ARRAY FLYIN WITH 1000 FT HALFPLANE.

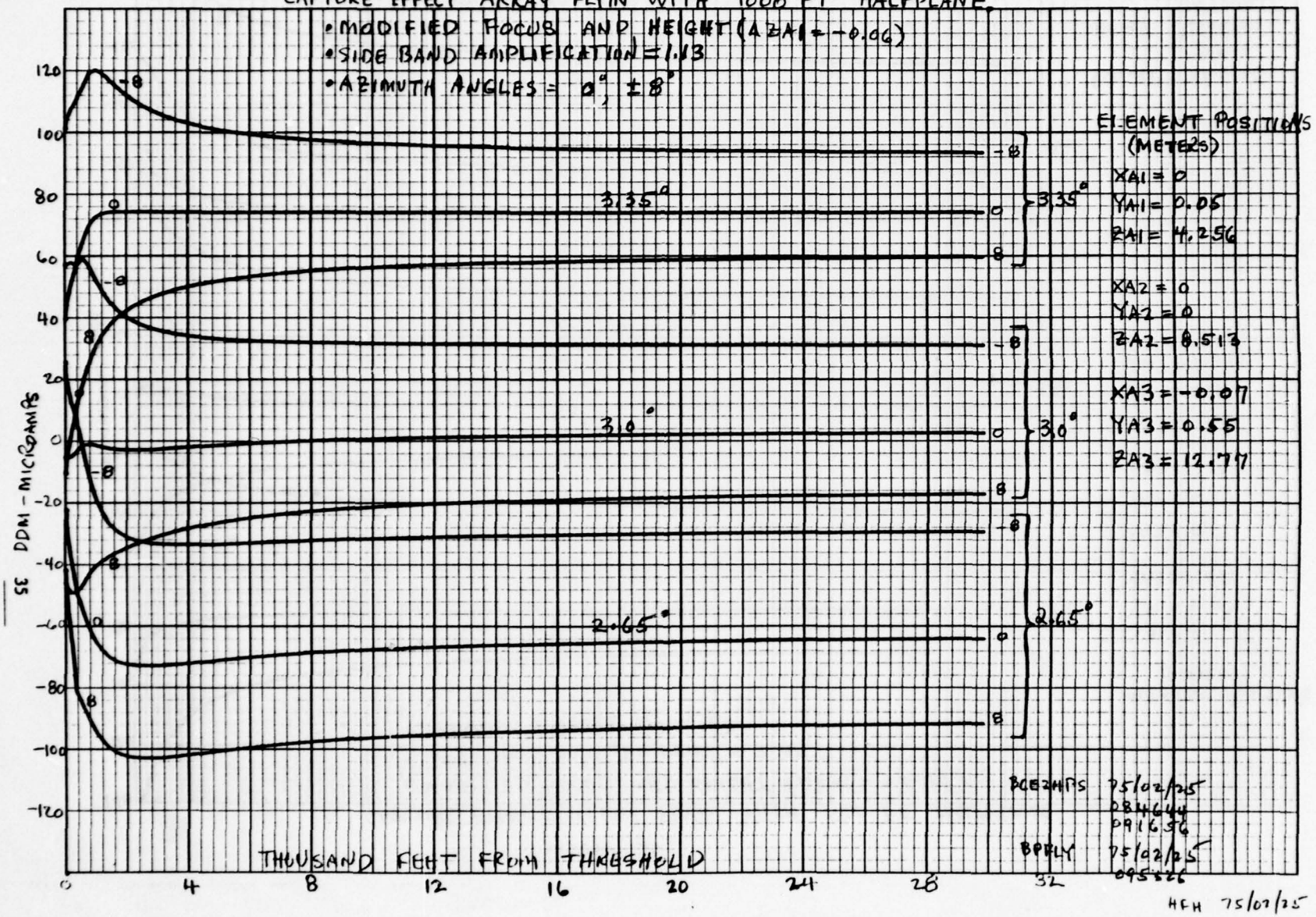

FIGURE 21

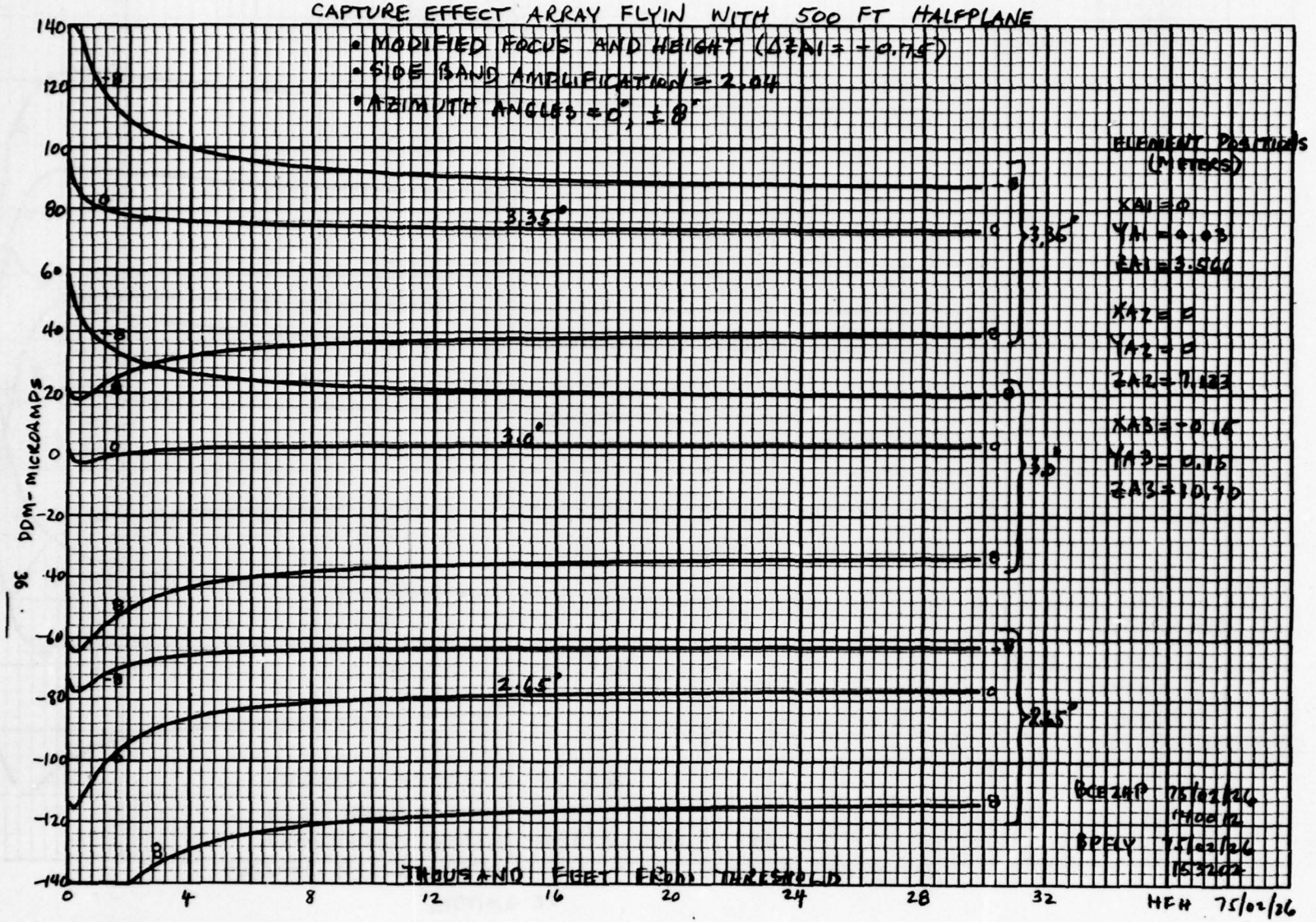
CAPTURE EFFECT ARRAY FLYIN WITH 500 FT HALFPLANE
• MODIFIED FOCUS AND HEIGHT (ΔZA1 = +0.75')
• SIDE BAND AMPLIFICATION = 2.04
• AZIMUTH ANGLES = 0°, ±8°
ELEMENT POSITIONS (METERS)
XA1 = 0
YA1 = 0.03
ZA1 = 3.900
XA2 = 0
YA2 = 0
ZA2 = 7.123
XA3 = +0.16
YA3 = 0.15
ZA3 = 10.70
3.35°
3.0°
2.65°
3.36°
3.0°
2.25°
DDM - MICROAMPS
THOUSAND FEET FROM THRESHOLD
HFH 75/02/26
BCE2AP 75/02/26
BPCLV 75/02/26

FIGURE 22

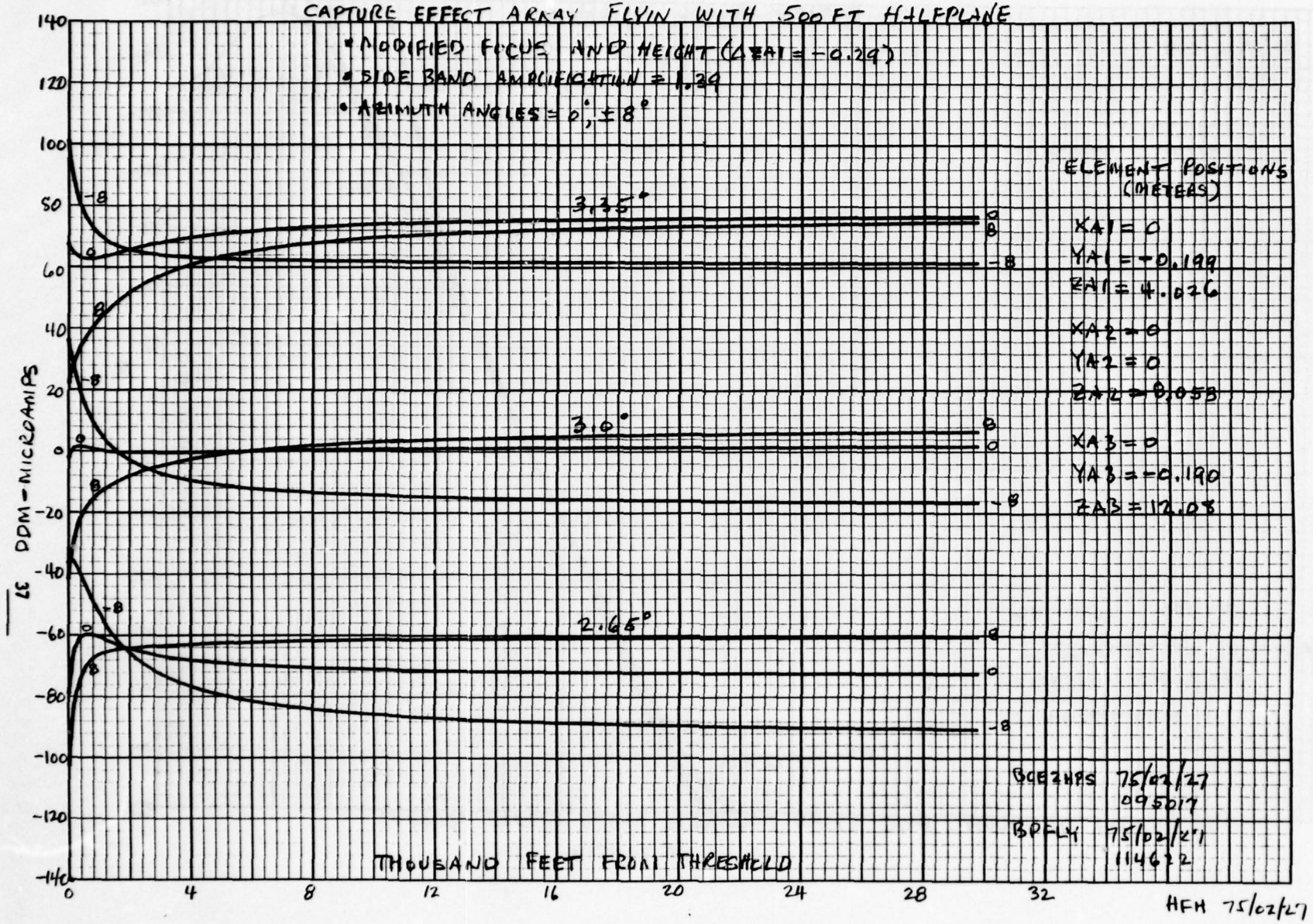

SCEZHPS 75/02/27 095017

BPFLY 75/02/27 114622

HFH 75/02/27

FIGURE 23

CAPTURE EFFECT ARRAY ELEVATION ANGLE DDM - MODIFIED FOCUS

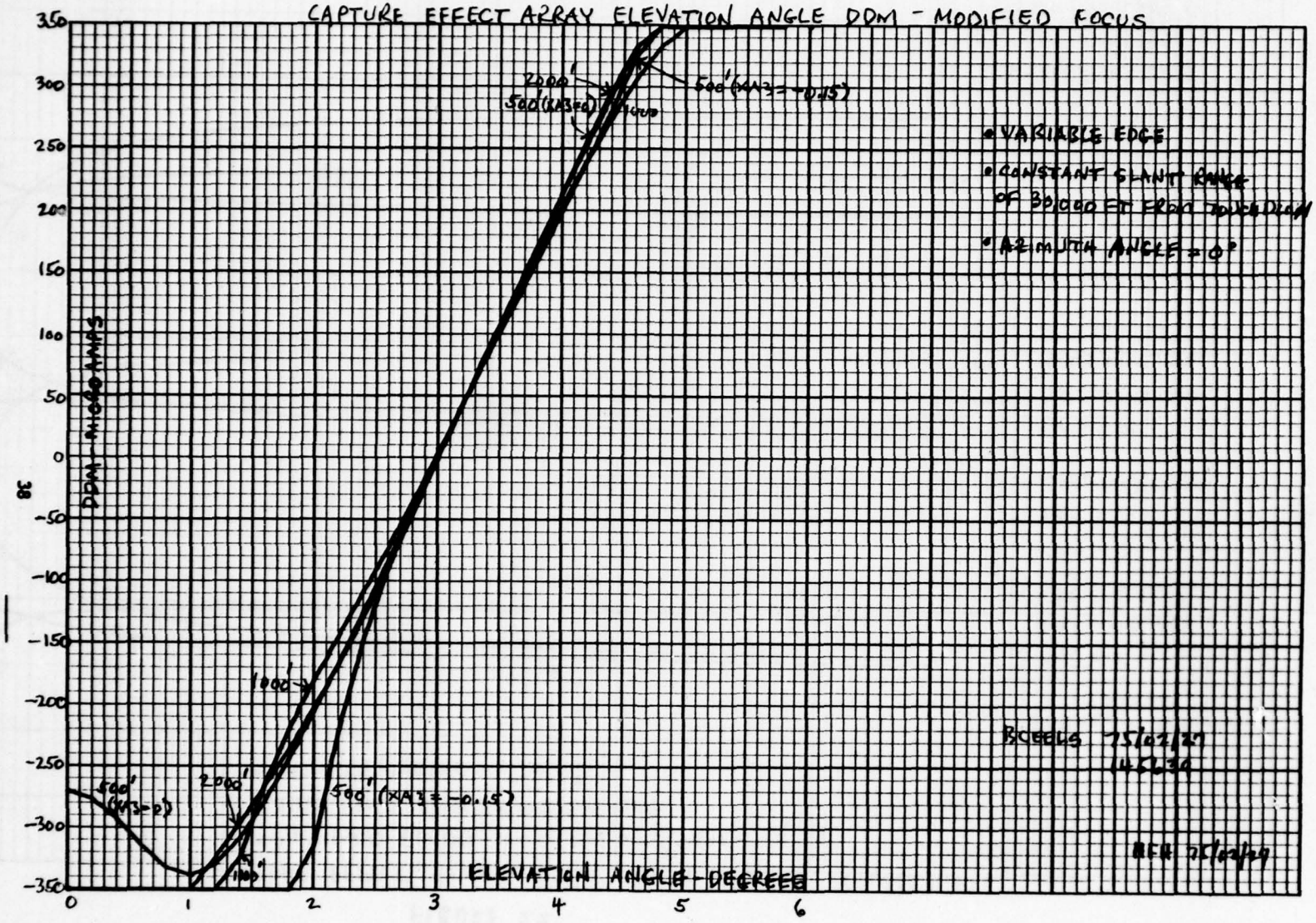

SKETCH SHEET
FORM BA 5635

WESTINGHOUSE ELECTRIC CORPORATION

FIGURE 24A ACTUAL PATH ANGLE FOR DDM INDICATIONS

- INFINITE GROUND
- 30,000 FT RANGE

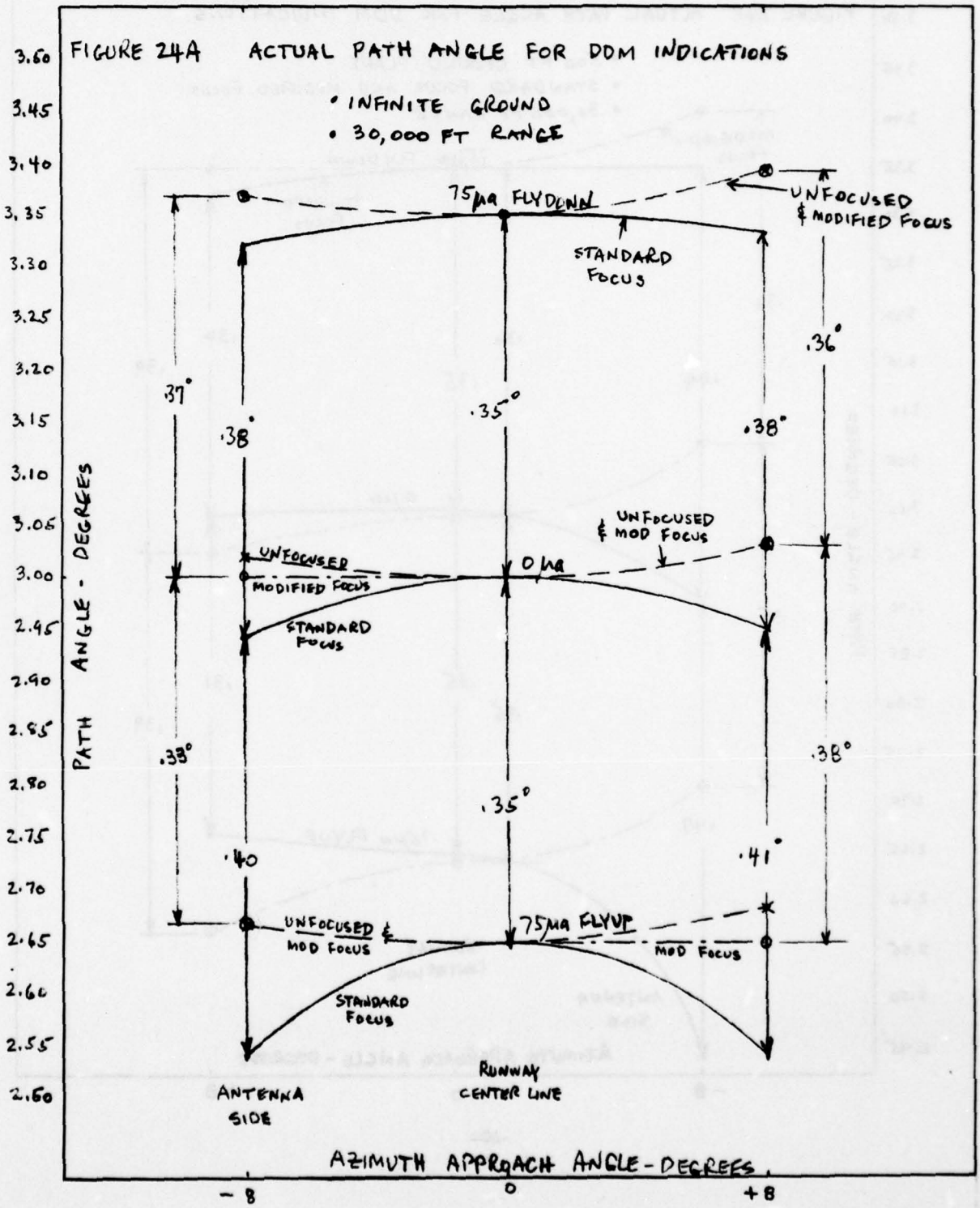

SKETCH SHEET
FORM BA 5635

WESTINGHOUSE ELECTRIC CORPORATION

FIGURE 24B ACTUAL PATH ANGLE FOR DDM INDICATIONS

- 500 FT GROUND PLANE
- STANDARD FOCUS AND MODIFIED FOCUS
- 30,000 FT RANGE

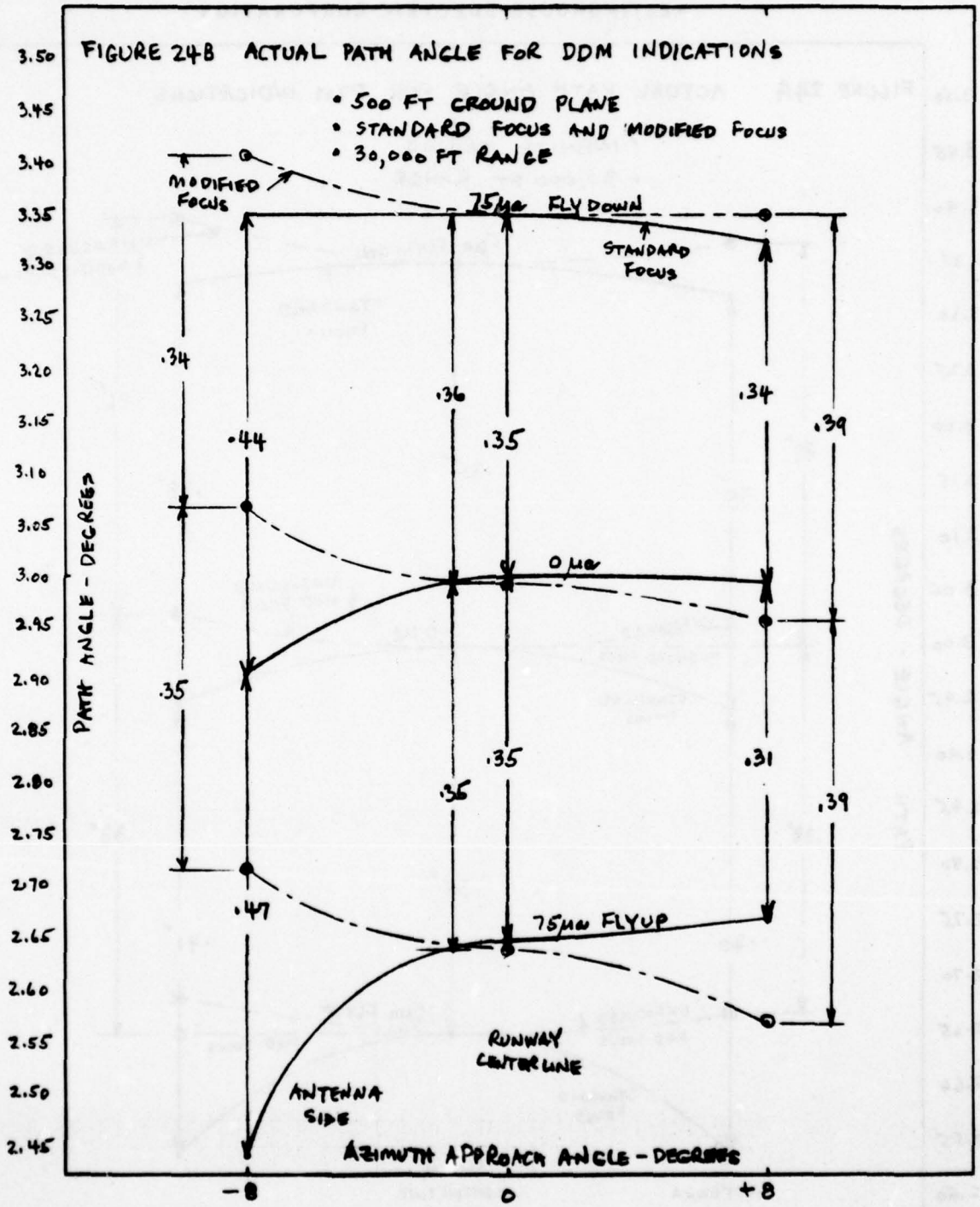

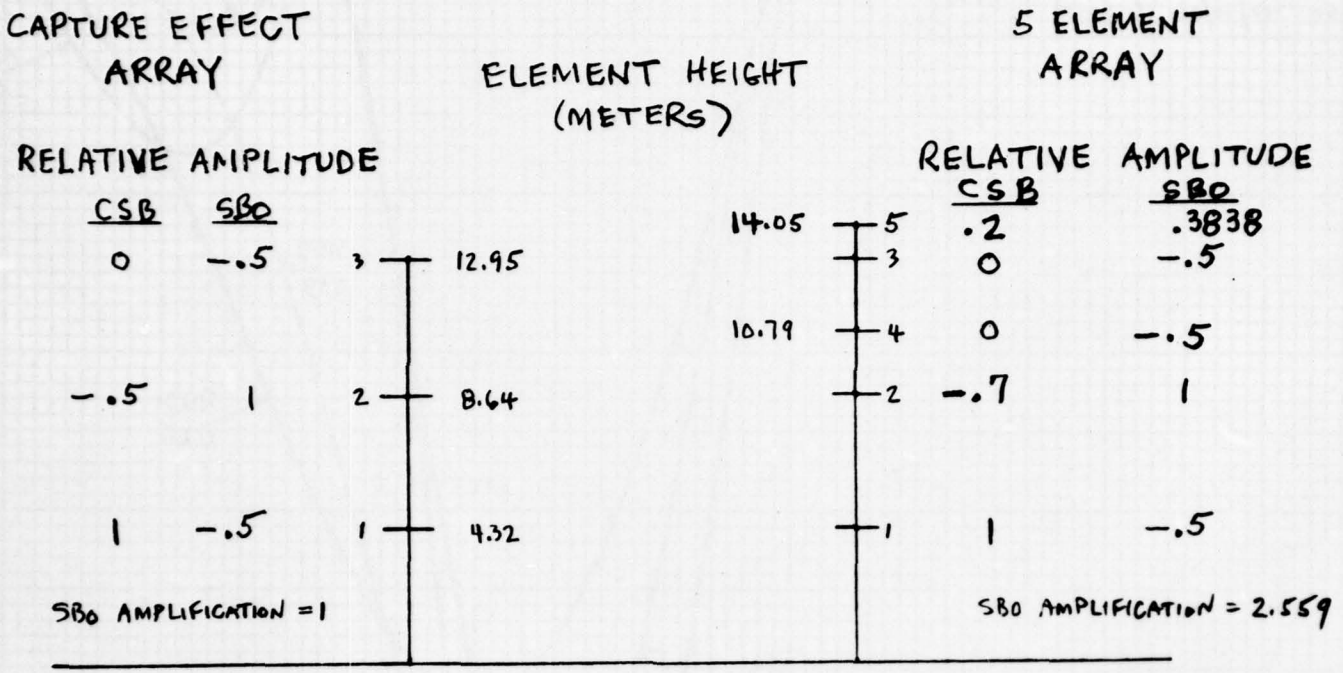

5 ELEMENT AND CAPTURE EFFECT ARRAY EXCITATION AND HEIGHT

FIGURE 25

FIGURE 26

5 ELEMENT AND CAPTURE EFFECT RADIATION FIELDS

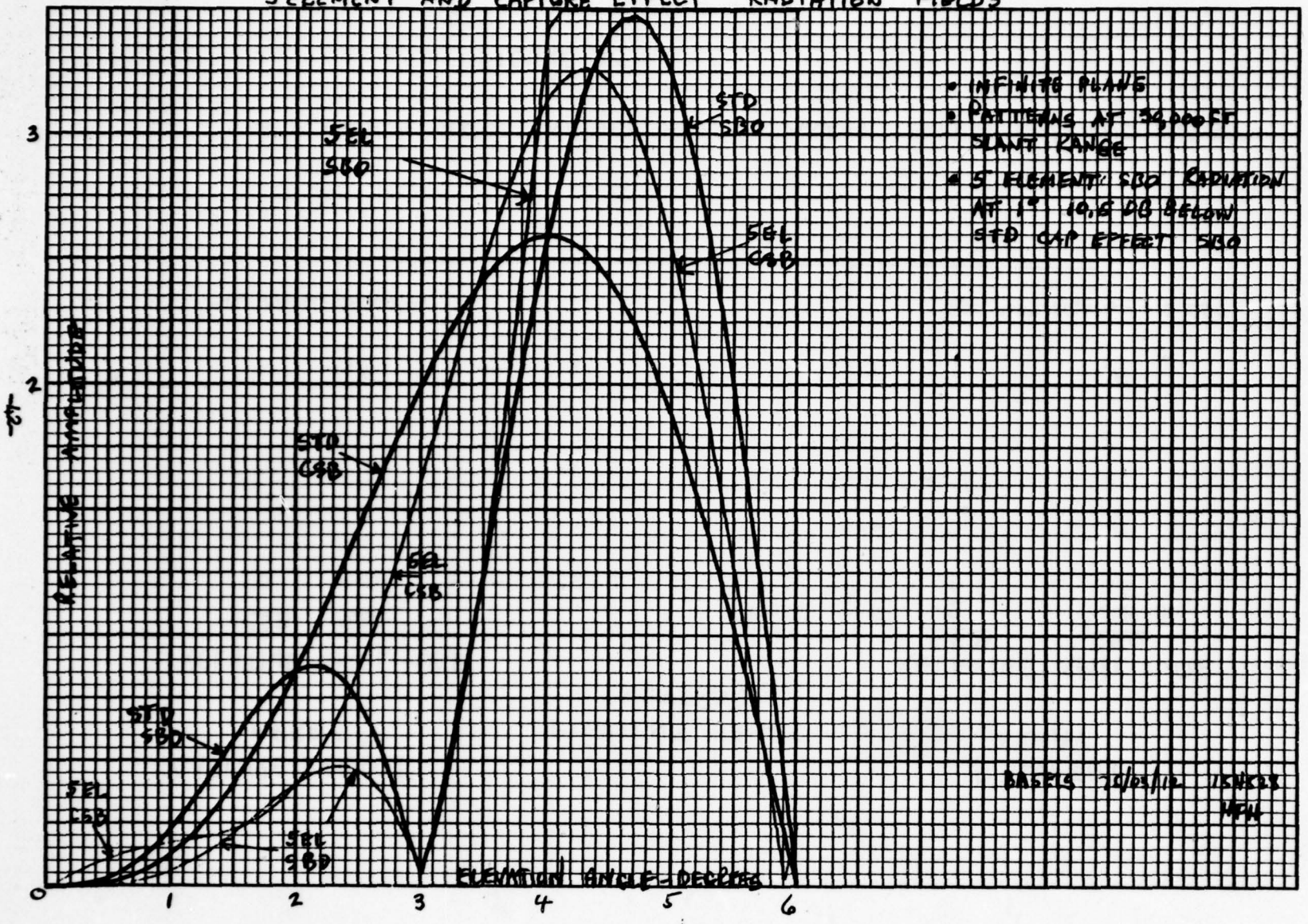

FIGURE 27

5 ELEMENT ARRAY ELEVATION DOM

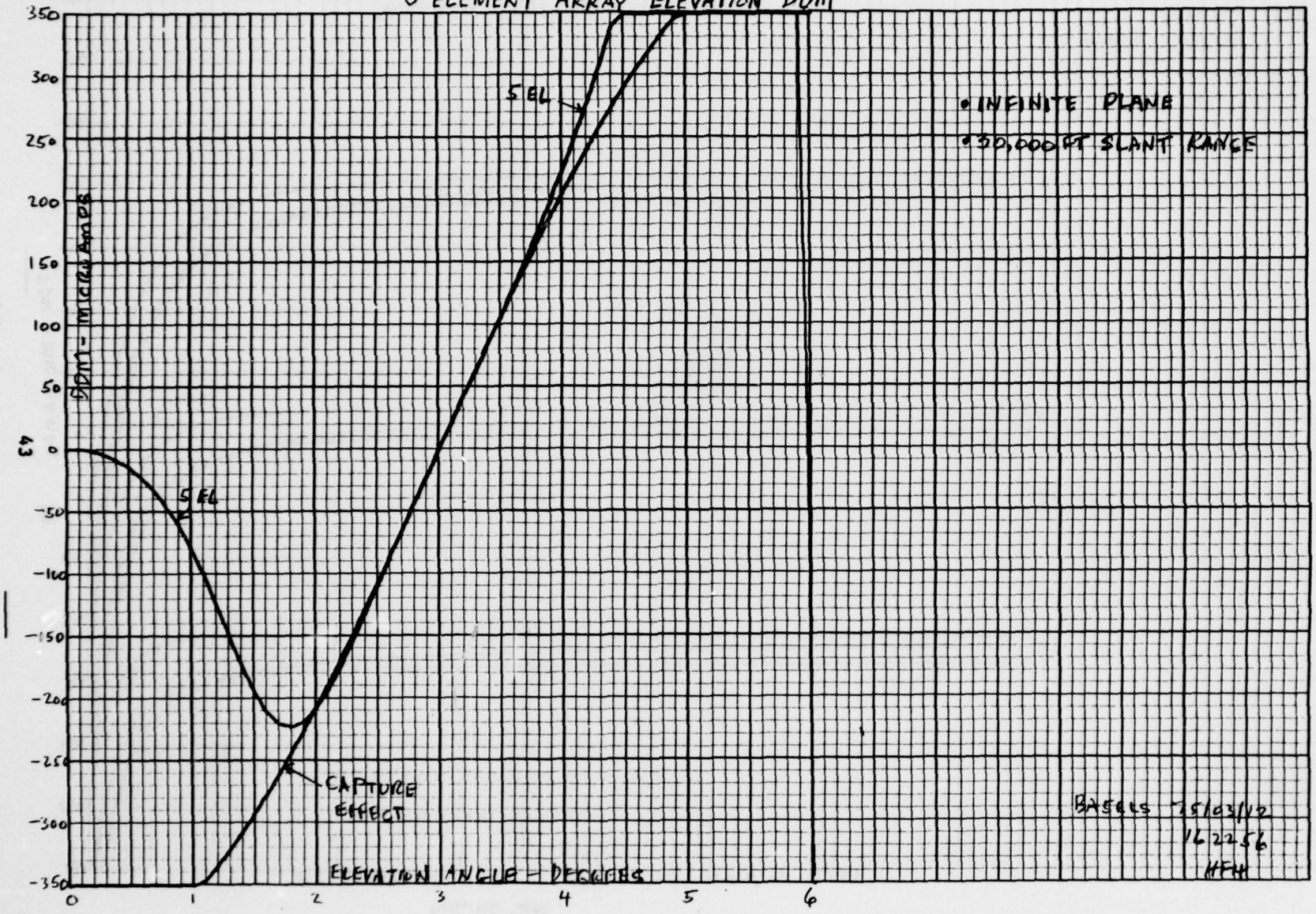

FIGURE 28

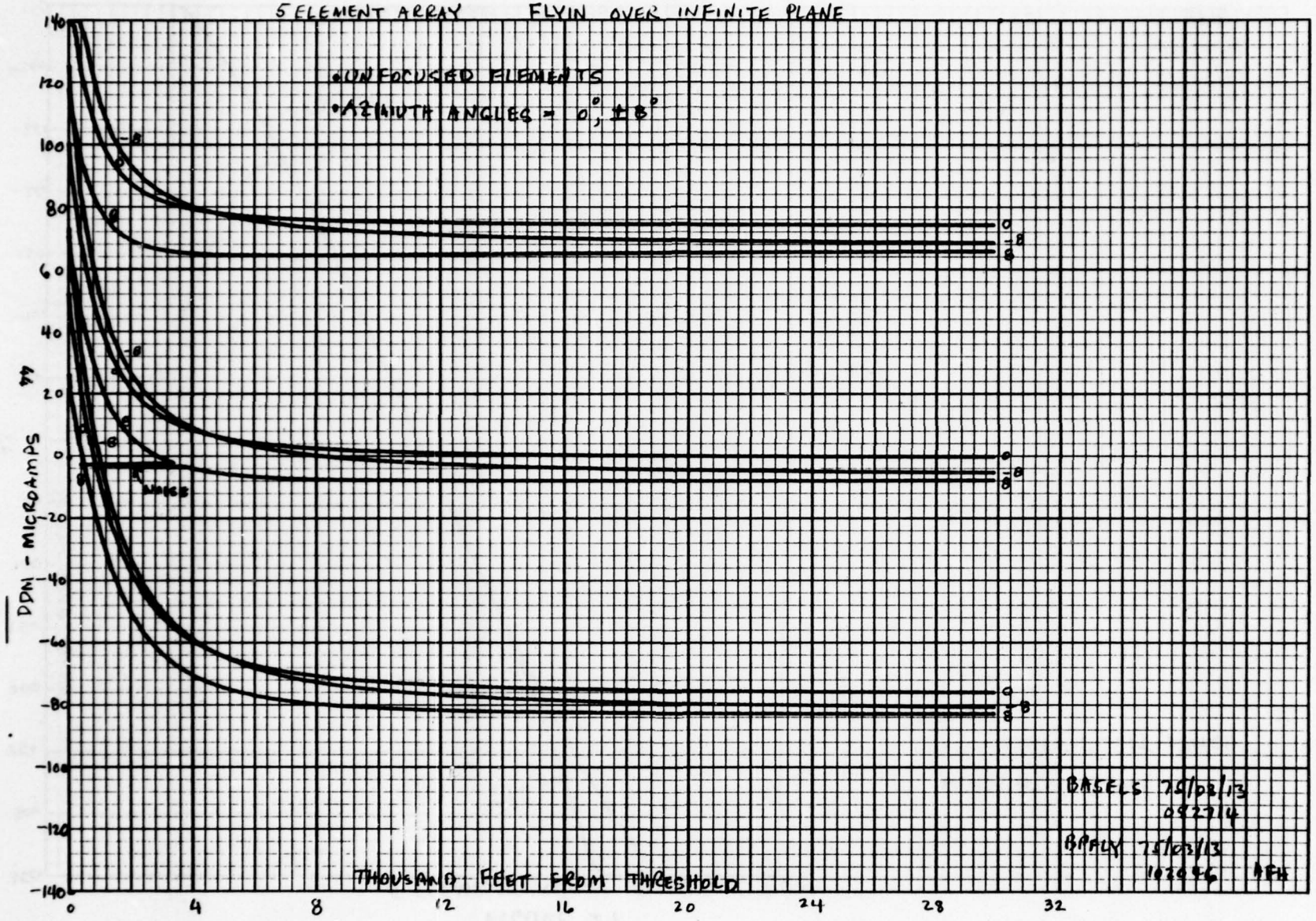
5 ELEMENT ARRAY FLYIN OVER INFINITE PLANE
• UNFOCUSED ELEMENTS
• AZIMUTH ANGLES = 0°, ±8°
DDM - MICROAMPS
THOUSAND FEET FROM THRESHOLD
BASELS 75/03/13 092714
BPFLY 75/03/13 102956 AFH

FIGURE 29 SBO RADIATION FIELDS - STANDARD CAPTURE EFFECT ARRAY

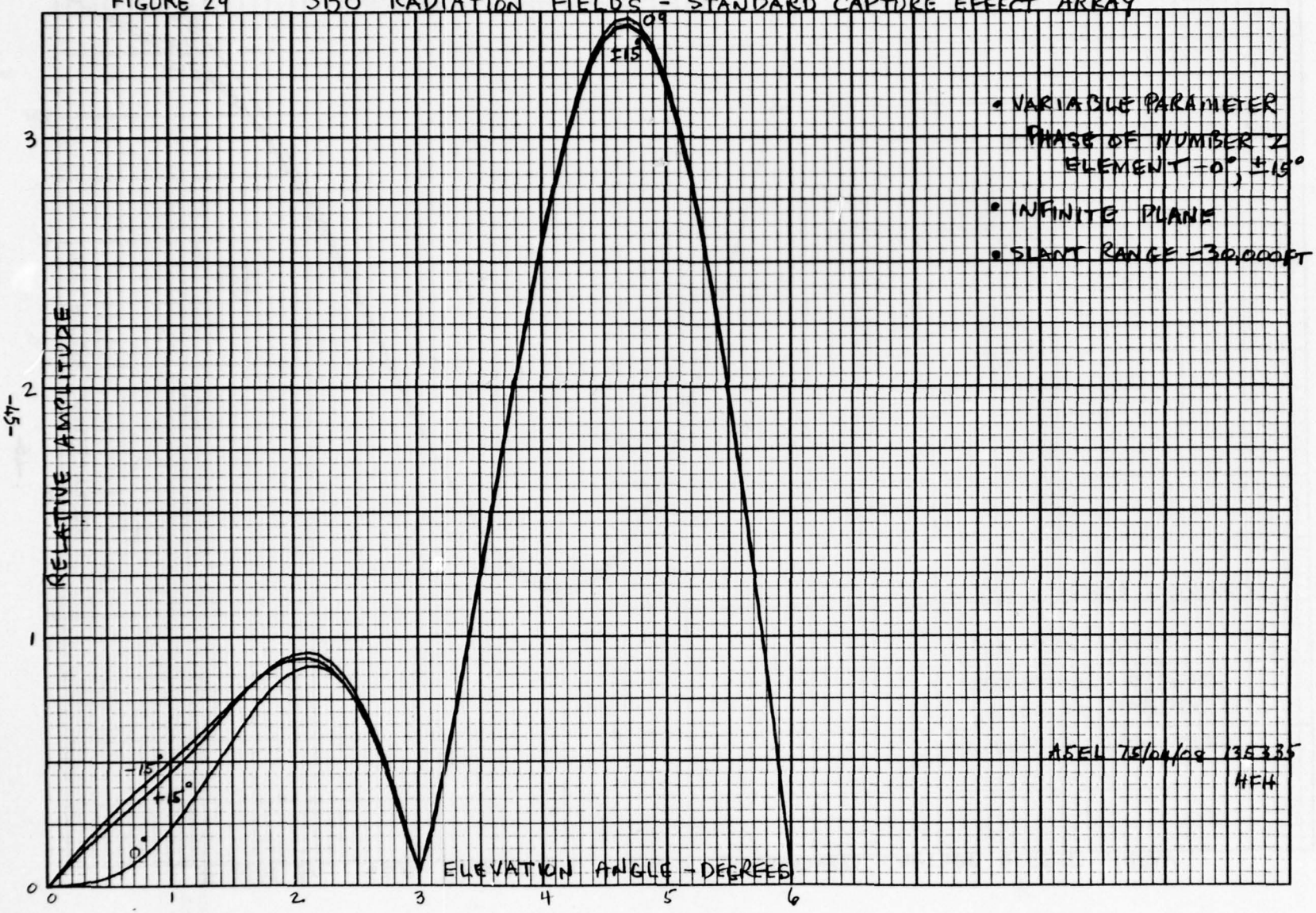

FIGURE 30 CSB RADIATION FIELDS - STANDARD CAPTURE EFFECT ARRAY

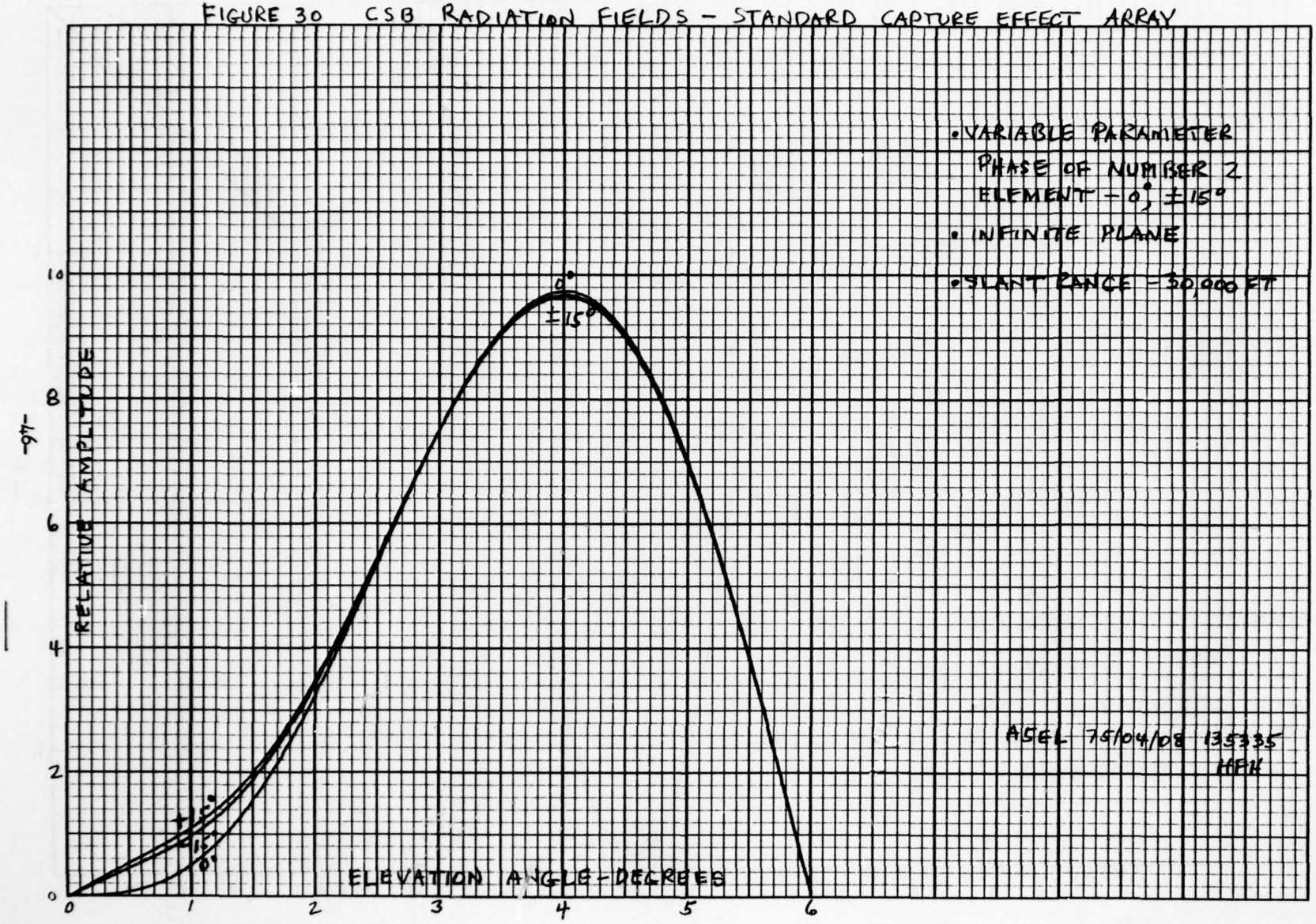

FIGURE 31 ELEVATION DDM – STANDARD CAPTURE EFFECT ARRAY

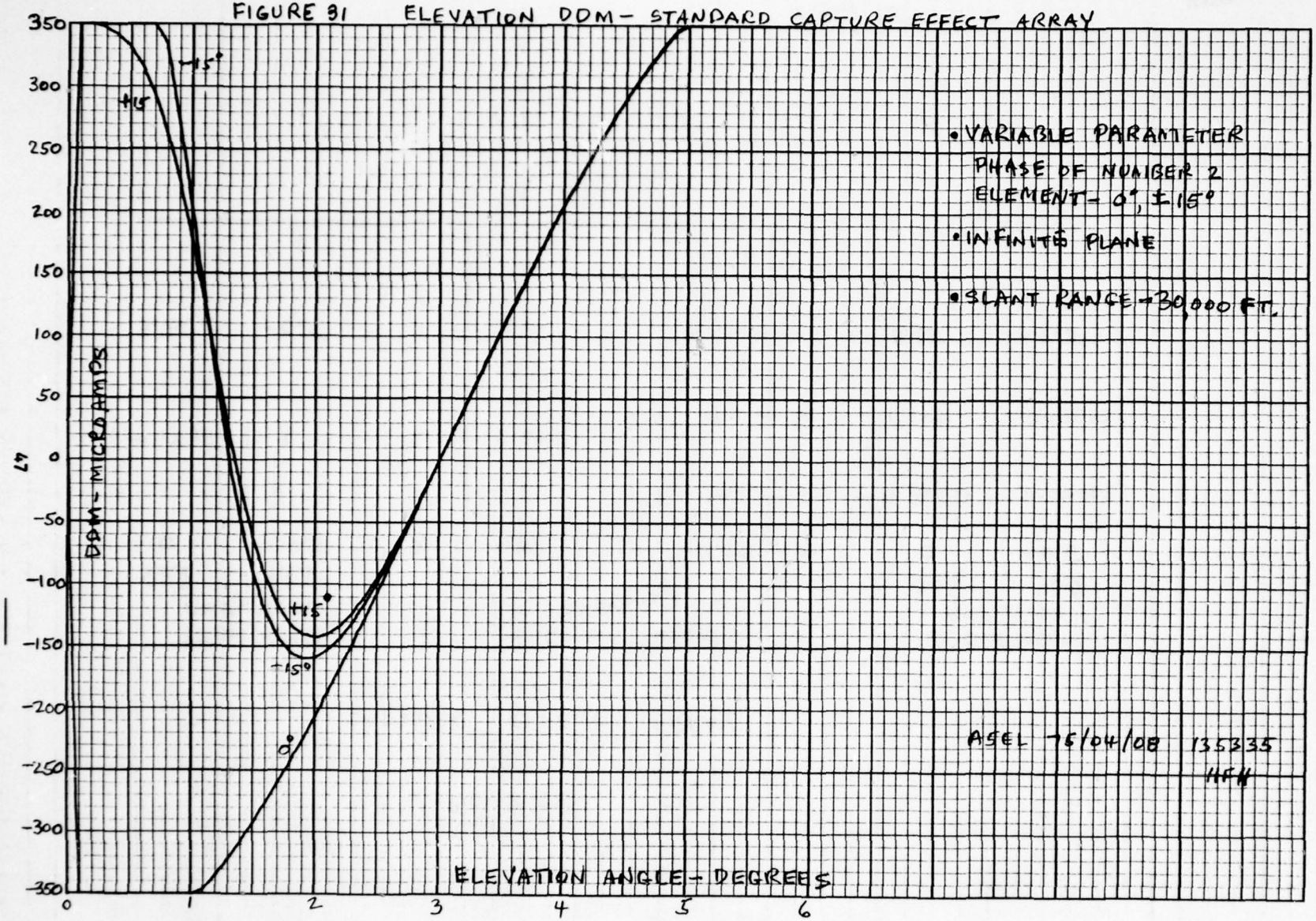

FIGURE 32

CAPTURE EFFECT ARRAY

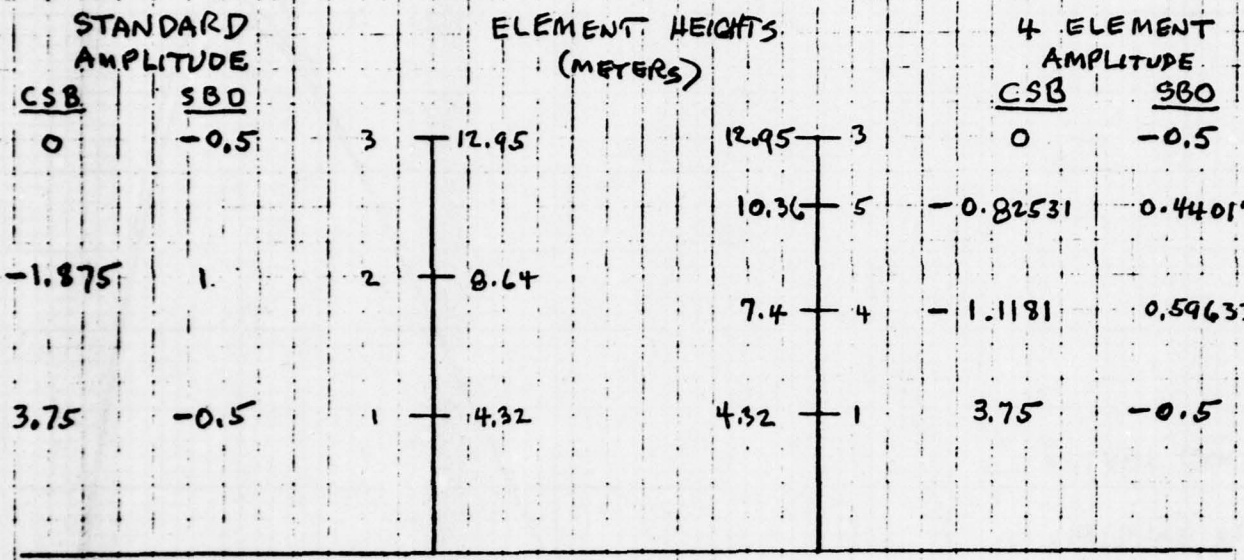

HFH
4-9-75

FIGURE 33 SBO RADIATION FIELDS - 4 ELEMENT CAPTURE EFFECT ARRAY

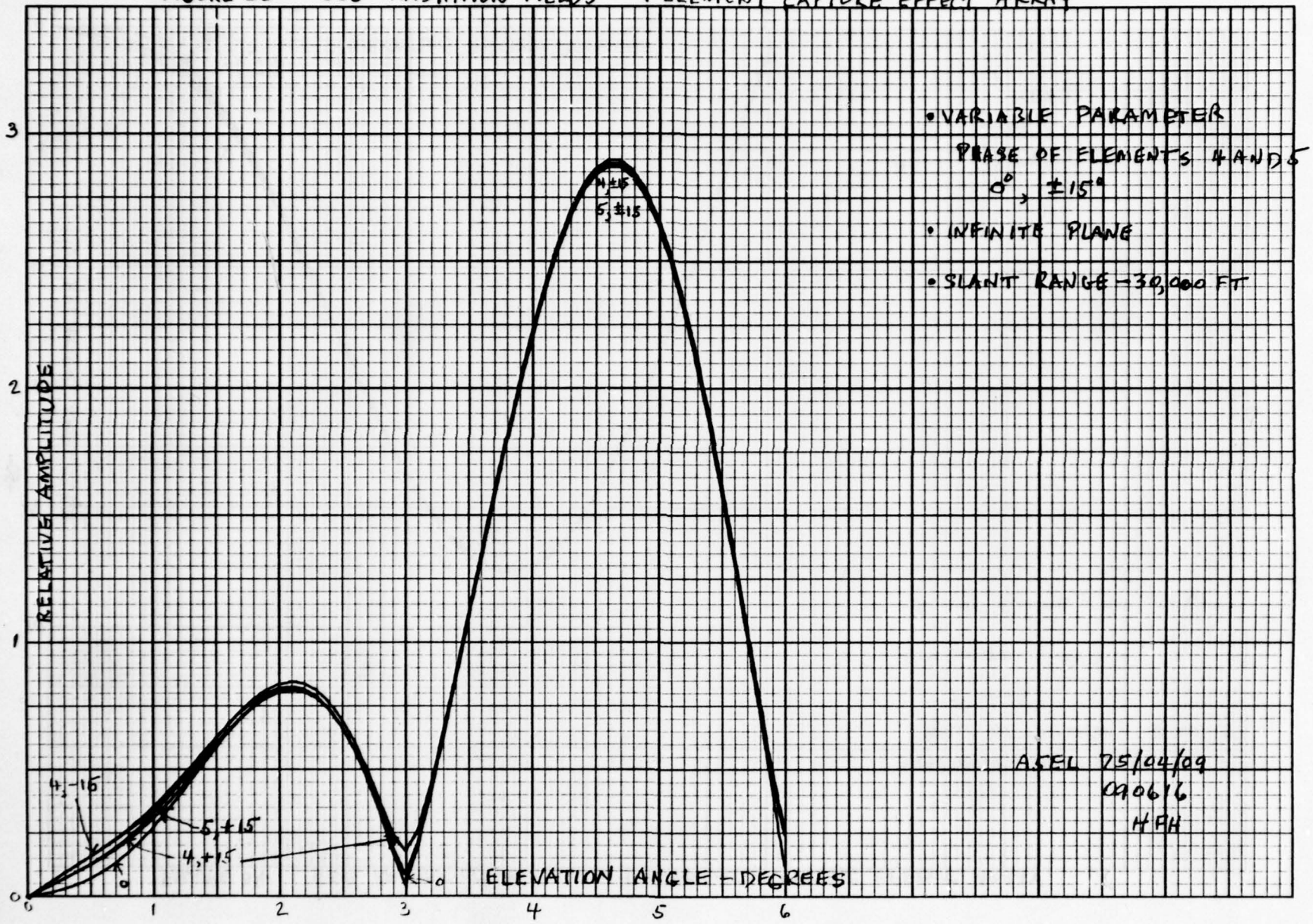

FIGURE 34 CSB RADIATION FIELDS - 4 ELEMENT CAPTURE EFFECT ARRAY

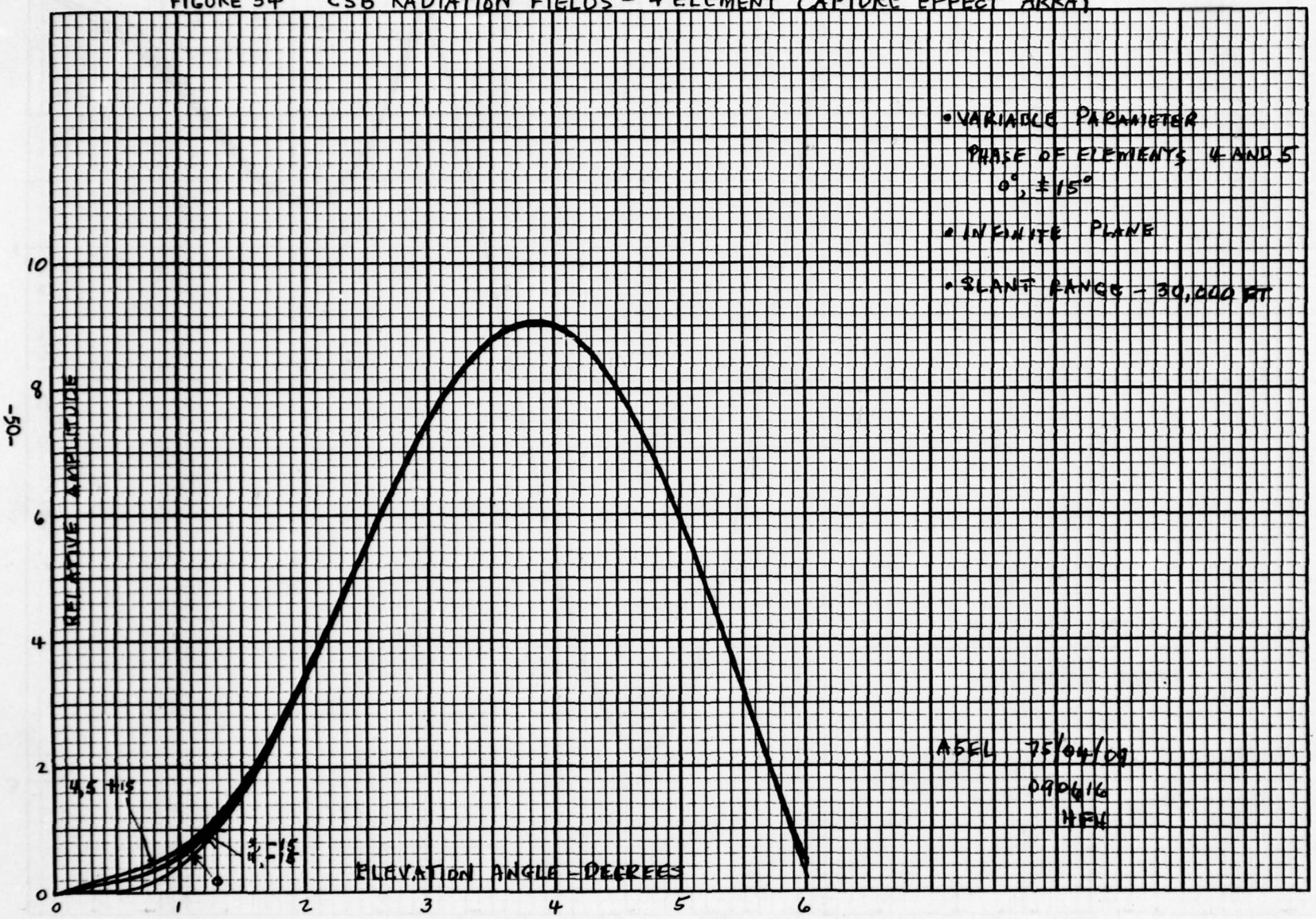

FIGURE 35. ELEVATION DDM – 4 ELEMENT CAPTURE EFFECT ARRAY

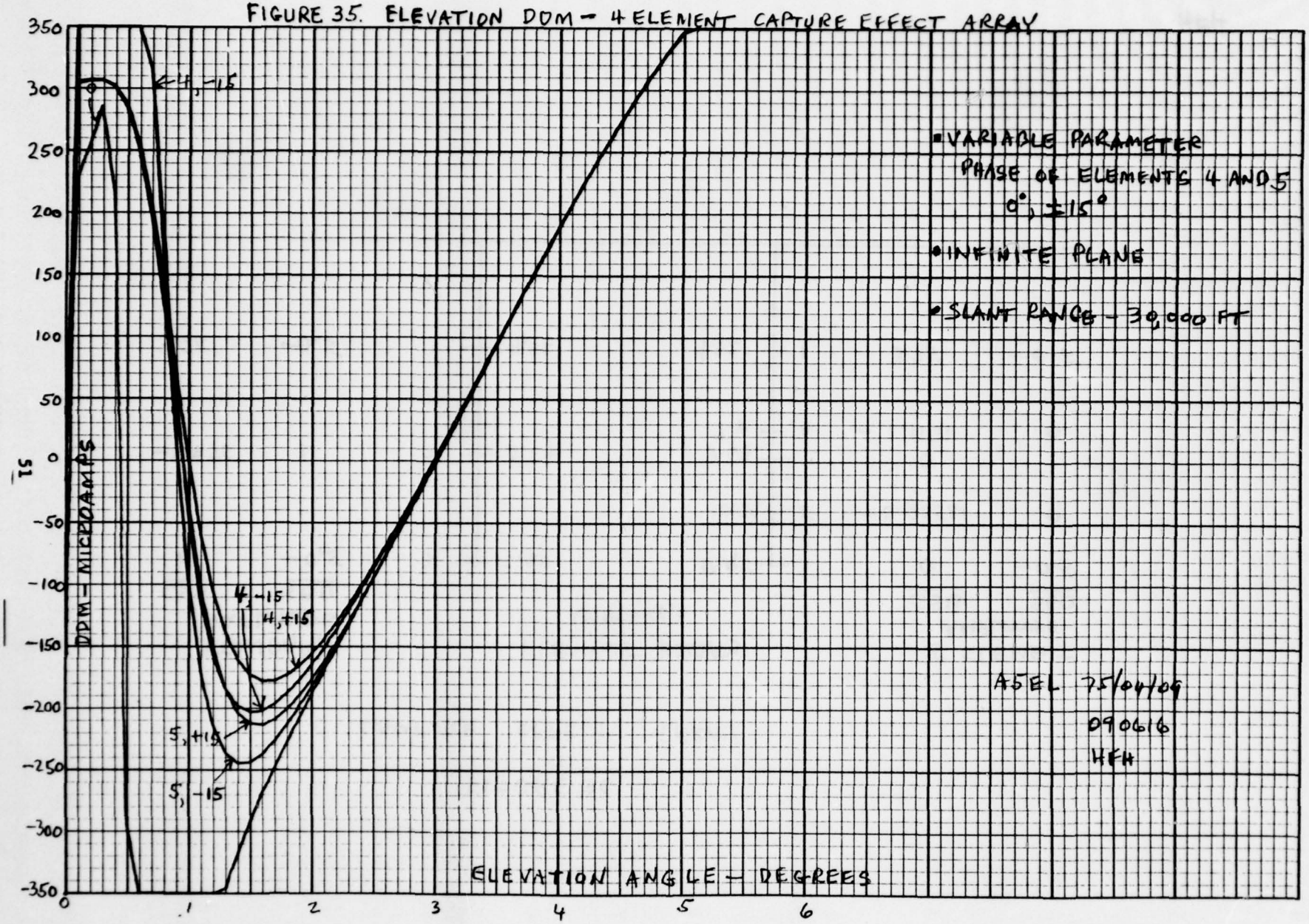

FIGURE 36

CAPTURE EFFECT ARRAY

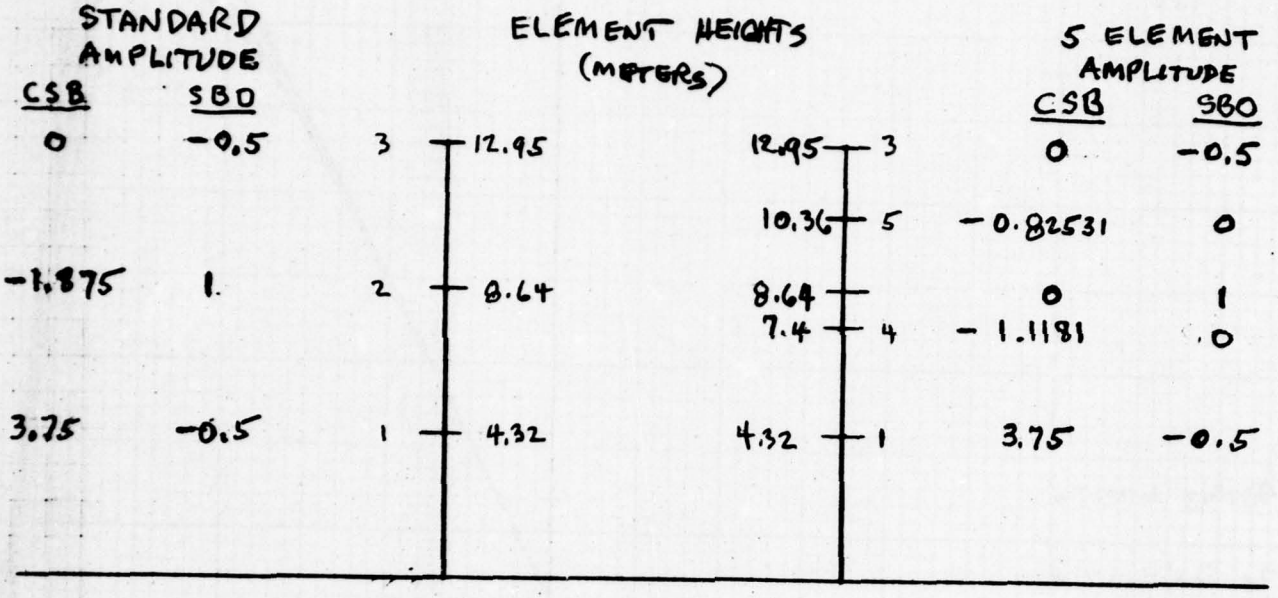

HFH
4-9-75

FIGURE 37 ELEVATION DDM - 5 ELEMENT CAPTURE EFFECT ARRAY

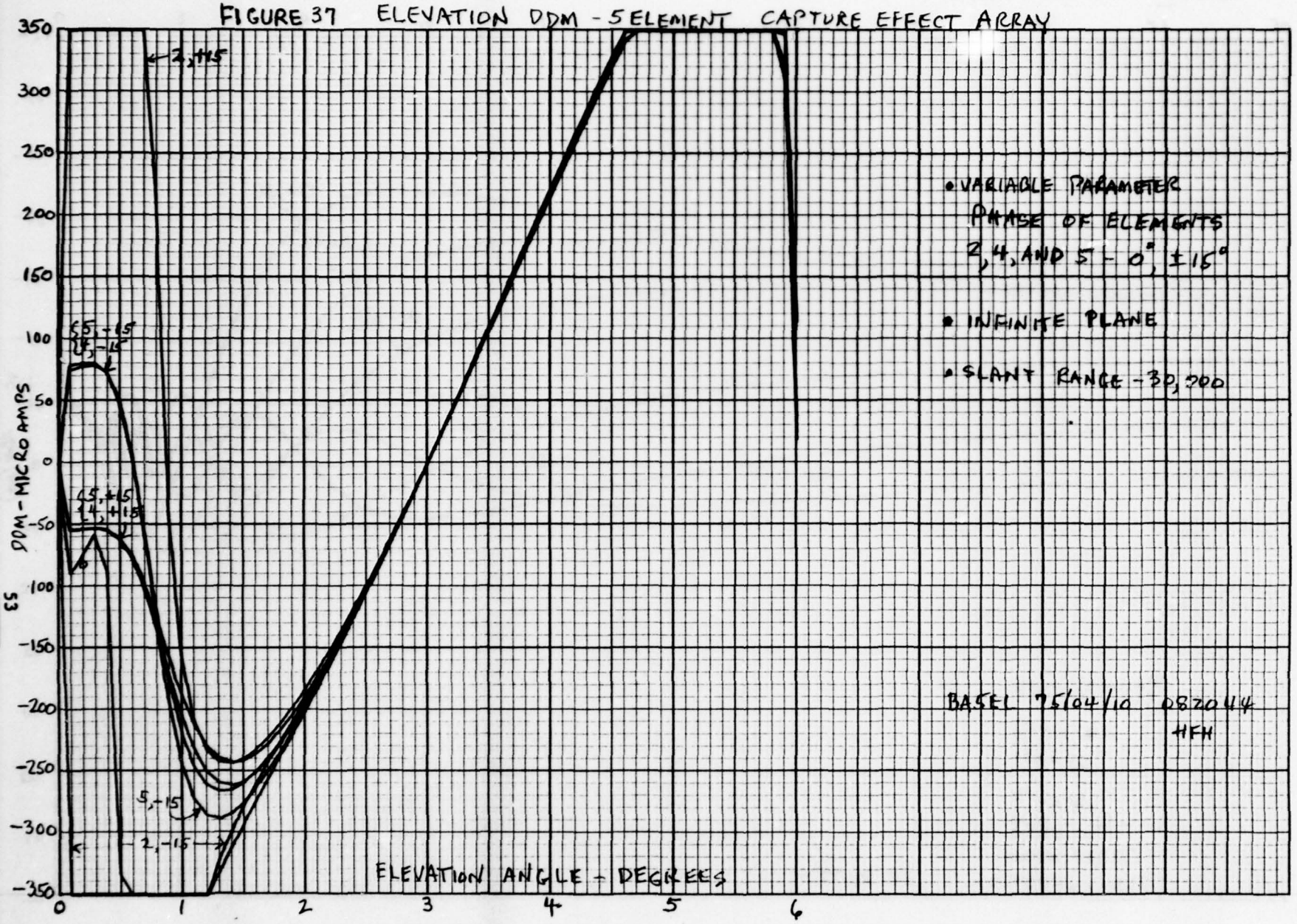

- VARIABLE PARAMETER PHASE OF ELEMENTS 2, 4, AND 5 - 0°, ±15°
- INFINITE PLANE
- SLANT RANGE - 30,000

BASEL 75/04/10 082044 HFH

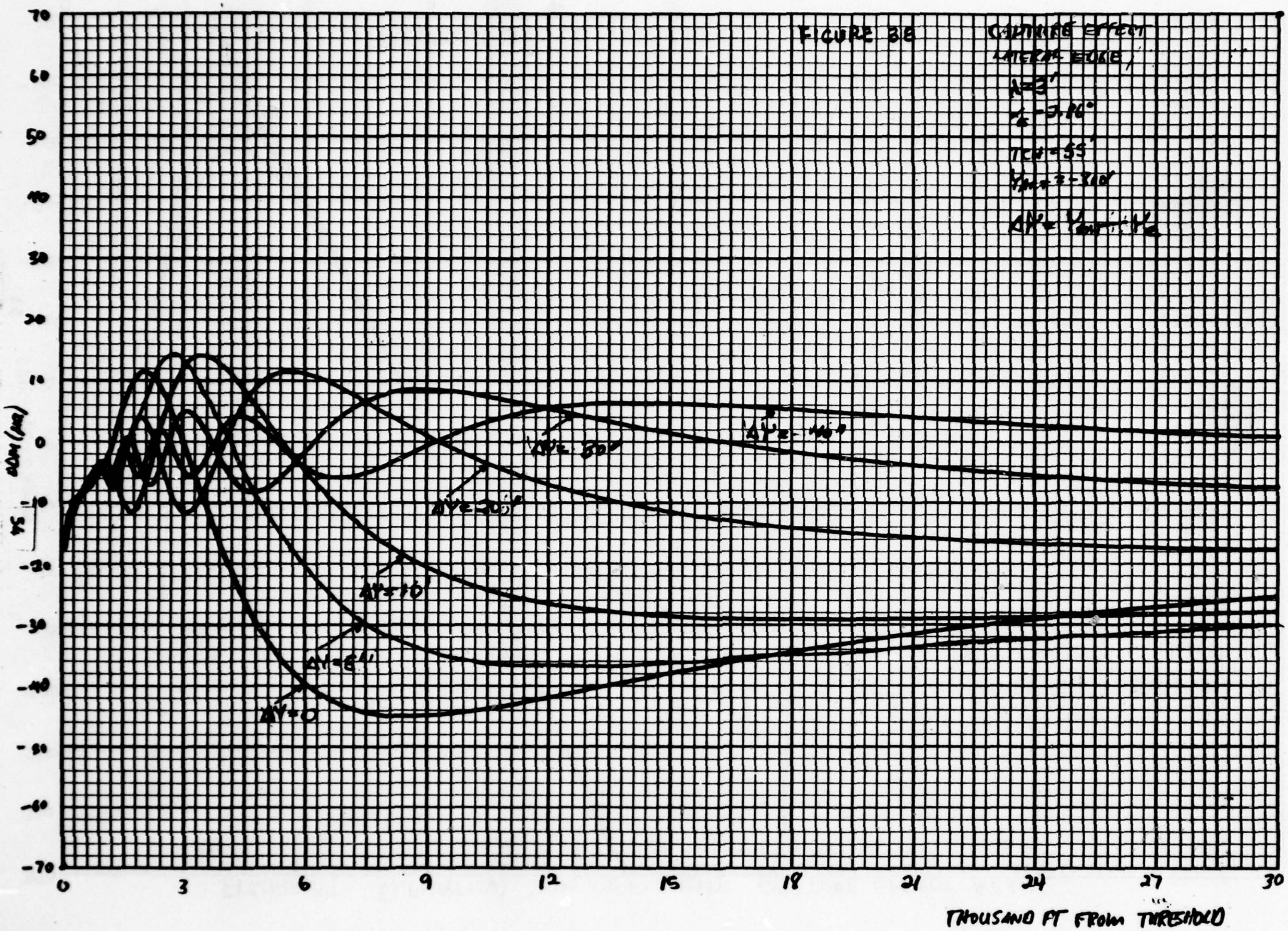
FIGURE 38
DDM (μa)
70
60
50
40
30
20
10
0
-10
-20
-30
-40
-50
-60
-70
0
3
6
9
12
15
18
21
24
27
30
THOUSAND FT FROM THRESHOLD

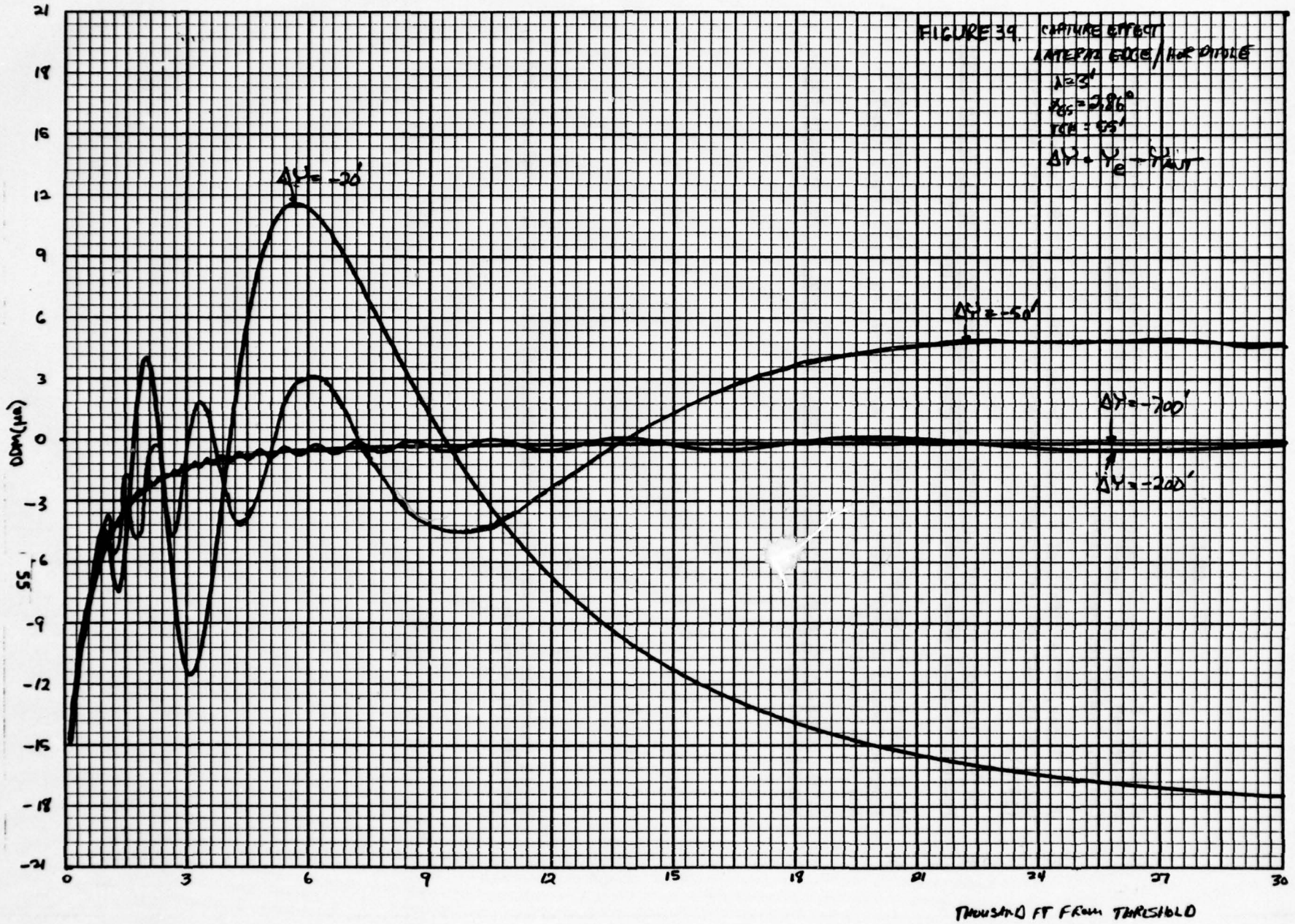
FIGURE 39. CAPTURE EFFECT
LATERAL EDGE / HOR DIPOLE
Δ=3'
ΔY = Y_E − Y_AUT
ΔY = -20'
ΔY = -50'
ΔY = -100'
ΔY = -200'
DDM(μa)
21
18
16
12
9
6
3
0
-3
-6
-9
-12
-15
-18
-21
0
3
6
9
12
15
18
21
24
27
30
THOUSAND FT FROM THRESHOLD

LIST OF REFERENCES

1. S. Morin, P. Newsom, D. Kahn and L. Jordan, "ILS Glide Slope Performance Prediction", Vol. A, Report No. FAA-RD-74-157.A, Transportation Systems Center, Cambridge, Mass. (1974).*

2. J. G. Lucas, "The Effect of a Limited Ground Plane on a 2.86 Degree M-Array Glide Path", Air Navigation Group, University of Sidney, Sidney, Australia (1972).

3. DOT/FAA Handbook No. 6750.6A, Installation Instructions for ILS Glide Slope. Federal Aviation Administration, Washington, D. C. (1969). *

4. R. W. Redlich, "Computed Performance of Glide Slope Arrays on Sites with Limited Ground Planes", IEEE Trans. on Aerospace and Elec. Sys., AES-7, No. 5, p. 854 (1971).

5. J. G. Lucas, A Microwave Model of an Instrument Landing System Glide Path. Unpublished report.

* These documents are available through National Technical Information Service, Springfield, Virginia 22151.

APPENDIX A : Image Type Glide Slope Systems and Guidance Signal (DDM) Derivation

Image type glide slope arrays consist of two or more horizontally polarized antenna elements above flat ground which combine with their images to form radiation patterns used as guidance signals by aircraft. Typically glide slope frequencies are allocated in a 2% band centered at 332 MHz. The radiated fields are amplitude modulated with 90 Hz and 150 Hz signals in such a manner that when the aircraft is on the glide slope path the combined fields produce an RF carrier in the receiver with equal modulation of the 90 and 150 Hz signals. Below glide path the 150 Hz modulation dominates while the 90 Hz dominates above. The receiver envelope detects the amplitude modulation, separates the 90 and 150 Hz signals by appropriate filtering, peak detects the separate signals, and then subtracts the resulting DC signals. The difference signal is called DDM (difference in depth of modulation) and is displayed visually for the pilot indicating that he is on course (zero DDM), should fly-up (negative signal) or fly-down (positive signal).

There are three image type glide slope arrays in use: the null reference, sideband reference and capture effect arrays. The operational and radiation pattern characteristics of these arrays are given in Reference 3 (pages 3 to 14). In all cases one type of radiation is directed along the glide path which consists of an RF carrier modulated with the 90 and 150 Hz signals. This radiation is referred to as the carrier plus sideband (CSB) signal. A sideband only radiation (SBO) is also generated which consists of the 90 Hz (phase opposite to CSB) and 150 Hz (phase same as CSB) sidebands with the carrier suppressed. This radiation has a null along the glide path. The SBO fields reverse phase as the null is crossed with the sum of the CSB and SBO fields producing the carrier modulation variation described previously.

The null reference array consists of two antennas with the lower element radiating the CSB field and the upper the SBO field. The sideband reference array also uses two antennas but they are closer to the ground than the null reference array which permits some reduction in terrain requirements for satisfactory operation. The CSB signal is radiated by the lower element while the SBO signal is radiated from both elements. The capture effect array employs three antennas where CSB is distributed to the two elements closest to the ground and SBO is sent to all three. The advantage of the capture effect array is that low angle radiation is suppressed so that the array can be used where irregularities preclude

operation with the other two arrays. In addition to the basic capture effect array pattern a clearance signal is also generated which is independent of the primary glide path guidance. Table A-1 illustrates the heights of the antennas for the various arrays in terms of the glide slope angle, α_{gs}, and the radiation wavelength, λ.

Element Number	Null Reference	Sideband Reference	Capture Effect
1	$h_1 = \lambda/(4 \sin \alpha_{gs})$	$h_1 = \lambda/(8 \sin \alpha_{gs})$	$h_1 = \lambda/(4 \sin \alpha_{gs})$
2	$h_2 = 2\ h_1$	$h_2 = 3\ h_1$	$h_2 = 2\ h_1$
3	----	----	$h_3 = 3\ h_1$

Table A-1. Antenna Heights in Terms of the Glide Slope Angle and Radiation Wavelength

In Table A-2 the relative amplitude and phase of the CSB and SBO excitation on the antennas of each array, as used in the calculations presented, is given.

At a given point in the glide slope space the field from each array antenna has an average amplitude which is inversely proportional to the distance from the element and a phase delay which is directly proportional to this distance. The physical field is described in terms of real quantities; however, it is useful to work with complex fields, keeping in mind that the physcial phenomena are represented by the real part of these complex fields.

Element Number	Null Ref. CSB	Null Ref. SBO	Sideband Ref. CSB	Sideband Ref. SBO	Capture Effect CSB	Capture Effect SBO
1	1	0	1	-1	1	-.5
2	0	1	0	1	-.5	1
3	-	-	-	-	0	-.5

Table A-2. Relative Antenna Excitation for CSB and SBO Signals

The current in an antenna radiating an amplitude modulated carrier may be represented mathematically as follows:

$$\begin{aligned} i &= I\,(1 + m\cos W_m t)\ \cos(W_o t + \phi) \\ &= \mathrm{Re}\ I\, e^{i\phi}\,(1 + m\cos W_m t)\, e^{iW_o t} \end{aligned} \tag{A.1}$$

where m is the modulation index, W_m is the modulation angular frequency, W_o is the carrier angular frequency and ϕ is the carrier phase angle. Let $\hat{i}$ be the complex current whose real part is i. Then

$$\hat{i} = \hat{I}\, e^{iW_o t} \tag{A.2}$$

where $\hat{I} = I\, e^{i\phi}\,(1 + m\cos W_m t)$ is the complex envelope of the current. The far field in front of the antenna may be represented by

$$\hat{e} = \hat{E}\, e^{iW_o t} \tag{A.3}$$

where $\hat{E}$ is the envelope $\hat{E} = \hat{A}\,(1 + m\cos W_m t)$ with $\hat{A}$ a field vector whose amplitude is inversely proportional to the distnace from the antenna and whose phase is directly proportional to this distance. It also contains the source amplitude and phase and constants relating antenna current to electric (magnetic) field.

As stated earlier, both the CSB and SBO fields are amplitude modulated with 90 and 150 Hz signals. Representing these frequencies by W_1 and W_2, the complex CSB field envelope and similarly that for the SBO may be represented

$$\hat{E}_c = \hat{A}_c\,(1 + m\,(\cos W_1 t + \cos W_2 t)) \tag{A.4a}$$

$$\hat{E}_s = \hat{A}_s m\,(\cos W_1 t - \cos W_2 t) \tag{A.4b}$$

where $\hat{A}_c$ and $\hat{A}_s$ are the sum of the field vectors from all antennas carrying CSB and SBO currents, respectively. The total complex field envelope at the aircraft is the sum of the envelopes of the CSB and SBO fields. The RF envelope detector in the aircraft receiver outputs a signal proportional to the amplitude of the total complex field envelope. Defining a normalized detector output, E_d, one has

$$\begin{aligned} E_d &= \left|(\hat{E}_c + \hat{E}_s)/\hat{A}_c\right| \\ &= \left|1 + m\,(1 + \hat{A}_s/\hat{A}_c)\cos W_1 t + m\,(1 - \hat{A}_s/\hat{A}_c)\cos W_2 t\right| \\ &= ((1 + E_R)^2 + E_Q^2)^{\frac{1}{2}} = (1 + 2E_R + E_R^2 + E_Q^2)^{\frac{1}{2}}, \end{aligned} \tag{A.5}$$

where $E_R = m\,(1 + \mathrm{Re}(\hat{A}_s/\hat{A}_c))\cos W_1 t + m\,(1 - \mathrm{Re}(\hat{A}_s/\hat{A}_c))\cos W_2 t$ and $E_Q = \mathrm{Im}\,(\hat{A}_s/\hat{A}_c)m(\cos W_1 t - \cos W_2 t)$.

Expanding (A.5) in a power series

$$E_d = 1 + \frac{2E_R + E_R^2 + E_Q^2}{2} + \frac{(2E_R + E_R^2 + E_Q^2)^2}{8} + \text{higher order terms.} \tag{A.6}$$

E_R contains undistorted 90 Hz and 150 Hz signals. E_R^2 and E_Q^2 contain harmonics and sum and difference of 90 and 150 Hz frequencies. The third and higher order terms contain higher order harmonics and cross product frequencies including some additional small amplitude 90 and 150 Hz signals. The 90 and 150 Hz filters following the envelope detector essentially pass only the 90 and 150 Hz components of (A.6). The contributions of third and higher terms to 90 and 150 Hz frequency are small compared to that of the second term. Thus the outputs of these two filters may be considered to come from the E_R of the second term of (A.6).

Following the filters the amplitudes of the 90 and 150 Hz signals are subtracted to obtain the DDM guidance signal. Thus

$$\text{DDM} = m\,(1 + \text{Re}\,(\hat{A}_s/\hat{A}_c)) - m(1 - \text{Re}\,(\hat{A}_s/\hat{A}_c)) \tag{A.7}$$

$$= 2m\,\text{Re}(\hat{A}_s/\hat{A}_c)$$

Referring to Equations (A.4a,b) it is seen that $\hat{A}_s$ and $\hat{A}_c$ are the complex field amplitudes of the SBO and CSB fields, respectively. Denoting $\hat{A}_s$ and $\hat{A}_c$ by SBO and CSB

$$\text{DDM} = 2m\,\text{Re}\left(\frac{\text{SBO}}{\text{CSB}}\right) \tag{A.8}$$

Glide slope systems are normalized so that at $\pm\ 0.35^\circ$ relative to the desired path angle the aircraft DDM indicator reads ± 75 microamps. Thus the normalized DDM satisfy

$$\text{DDM}\ (\mu a) = 75\ \frac{\text{Re}\left(\frac{\text{SBO}}{\text{CSB}}\right)}{\frac{1}{2}\left[\left|\text{Re}\left(\frac{\text{SBO}}{\text{CSB}}\right)\right|_{\theta_{gs}\,=\,.35^\circ} + \left|\text{Re}\left(\frac{\text{SBO}}{\text{CSB}}\right)\right|_{\theta_{gs}\,=\,-.35^\circ}\right]} \tag{A.9}$$

APPENDIX B

MATHEMATICAL MODEL USED TO CALCULATE FIELD OF A HORIZONTALLY POLARIZED ELECTRIC DIPOLE OVER A CONDUCTING HALF PLANE

The total field at point P (see Figure B-1) due to transmitting antenna T is the sum of the geometric optics field and the field due to diffraction by the edge of the half-plane. The points of interest lie largely in front of the dipole and the field variation due to azimuth pattern will be small and will be ignored in this analysis. This permits the use of a horizontally polarized point source in mathematical analysis.

The normalized geometric far fields are as follows:

$$E_y^{(g)} = \frac{e^{ikR}}{kR} - \frac{e^{ikR'}}{kR'} \qquad 0 \le \theta < \theta_1$$

$$= \frac{e^{ikR}}{kR} \qquad \theta_1 \le \theta \le \theta_2$$

$$= 0 \qquad \theta_2 < \theta < 2\pi.$$

where $k = 2\pi/\lambda$, λ = wavelength, R is distance from antenna to aircraft position P (Figure B-1), R' is distance from antenna image to P. θ, θ_1, and θ_2 are defined in Figures B-1 and B-2.

The diffracted field has been derived in closed form involving Frenel integrals, from fundamental electromagnetic theory:

$$E_y^{(d)} = \sqrt{\frac{2}{\pi}}\, e^{-i\pi/4} \left[-\mathrm{sgn}(A) \frac{e^{ikR}}{\sqrt{kR_1 k(R+R_1)}} F(|A|) + \mathrm{sgn}(A') \frac{e^{ikR'}}{\sqrt{kR_1 k(R'+R_1)}} F(|A'|) \right],$$

where

$$A = 2\sqrt{\frac{krr_0}{R+R_1}} \cos\tfrac{1}{2}(\theta - \theta_0),$$

$$A' = 2\sqrt{\frac{krr_0}{R'+R_1}} \cos\tfrac{1}{2}(\theta + \theta_0),$$

$$R_1^2 = (r + r_o)^2 + (Y - Y_o)^2 ,$$

$$F(a) = F_R(a) + i\, F_I(a) ,$$

$$F_R(a) = \sqrt{\frac{\pi}{2}} \times [\tfrac{1}{2} - C_2(a^2)] , \qquad C_2(a^2) = \frac{1}{\sqrt{2\pi}} \int_o^{a^2} \frac{\cos t}{\sqrt{t}}\, dt,$$

$$F_I(a) = \sqrt{\frac{\pi}{2}} \times [\tfrac{1}{2} - S_2(a^2)] , \qquad S_2(a^2) = \frac{1}{\sqrt{2\pi}} \int_o^{a^2} \frac{\sin t}{\sqrt{t}}\, dt.$$

Variables and constants used in the above equations are defined in Figure B-1.

FIGURE B-1 ILLUSTRATING COORDINATES FOR FIELD CALCULATION

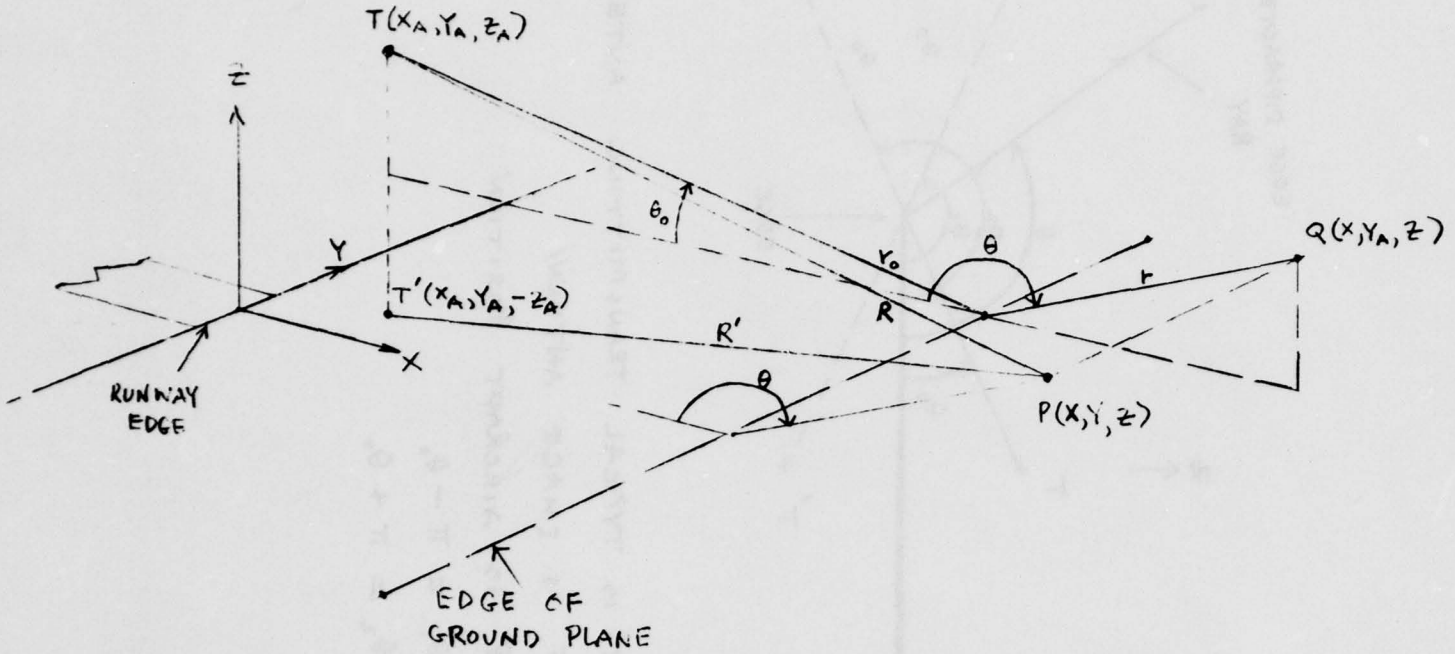

T IS A TYPICAL TRANSMITTING ANTENNA

T' IS THE IMAGE ANTENNA

P IS AIRCRAFT POSITION

FIGURE B-2 ILLUSTRATING θ COORDINATES

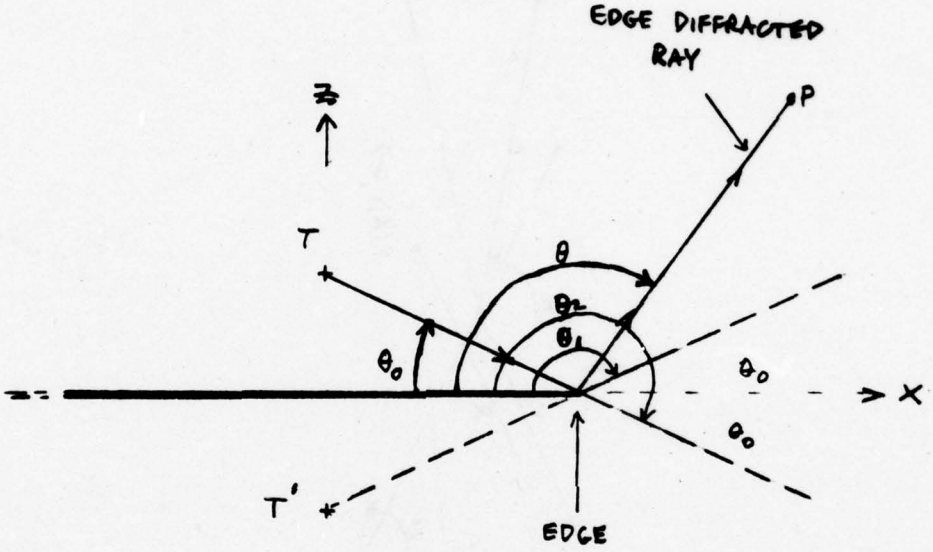

T IS TYPICAL TRANSMITTING ANTENNA

T' IS IMAGE ANTENNA

P IS AIRCRAFT POSITION

$\theta_1 = \pi - \theta_0$

$\theta_2 = \pi + \theta_0$

APPENDIX C

CORRELATION OF WESTINGHOUSE HALF-PLANE ANALYSIS WITH TRANSPORTATION SYSTEMS CENTER ANALYSIS

Some comparisons have been made of fly-in results reported by the Transportation Systems Center (TSC)[1] and those computed using the Westinghouse analytic method described in Appendicies B and E herein. The TSC method involves the numerical summation of fields due to ground current strips parallel to the ground plane edge, whereas the Westinghouse method is an analytic solution involving Fresnel integrals. The latter is believed to require much less computer time than the former.

Figure 2B* of the TSC report shows a null reference array fly-in over flat terrain where fields from ground current strips out to 5000 feet in front of the antenna were included. This condition would correspond to having the array over a half-plane extending to 5000 feet in front of the antenna. This case was computed using the Westinghouse analytic method and identical results were obtained. This is illustrated in Figure C-1 herein where the Westinghouse results were overplotted on the TSC curves. Fly-in curves for the Capture Effect array over half-planes also exhibit oscillations but they are small as in Figure 7 or they are not visible with path width DDM scales as in Figures 11 through 15.

A Capture Effect array fly-in was computed with the 1200 foot half-plane and 20 feet drop-off to a second half-plane as in the TSC report Figures 4 and 4F. The result is the curve labeled 20 in Figure C-2 herein. The curves are similar (excluding the flare) but different in detail, up to about 6000 feet from touchdown. The TSC case involved a second edge on the lower plane at 5000 feet from the antenna, but this edge would not cause oscillations until after about 6000 feet from touchdown as in Figure 2B* of the TSC report. Figure C-2 herein is believed to be a more accurate result because the edge shadow regions are illuminated by edge diffracted rays in the Westinghouse analysis whereas the TSC analysis includes only line-of-sight illumination of the lower surface. Figure C-2 includes fly-ins with 10 and 30 foot drop-offs also. The DDM characteristic is seen to be sensitive to the amount of the drop-off to the second plane.

* Figure 2B of the TSC draft report was used in the comparison. The corresponding figure in the TSC final report (Reference 1) is Figure 2A in which the threshold approach flare was removed by having the aircraft fly a hyperbolic approach.

FIGURE C-1

NULL REFERENCE ARRAY FLY-IN OVER 5000FT HALF PLANE

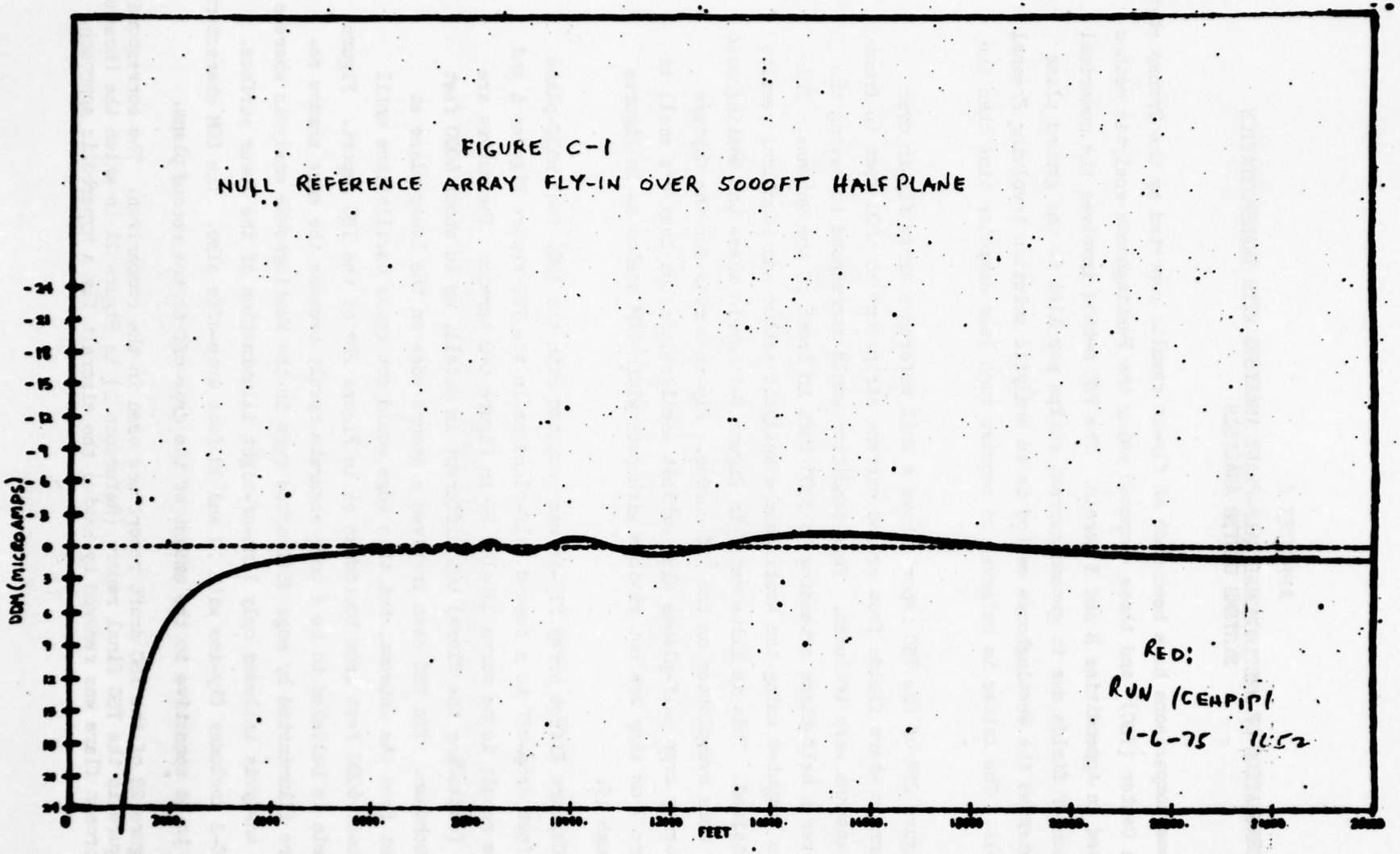

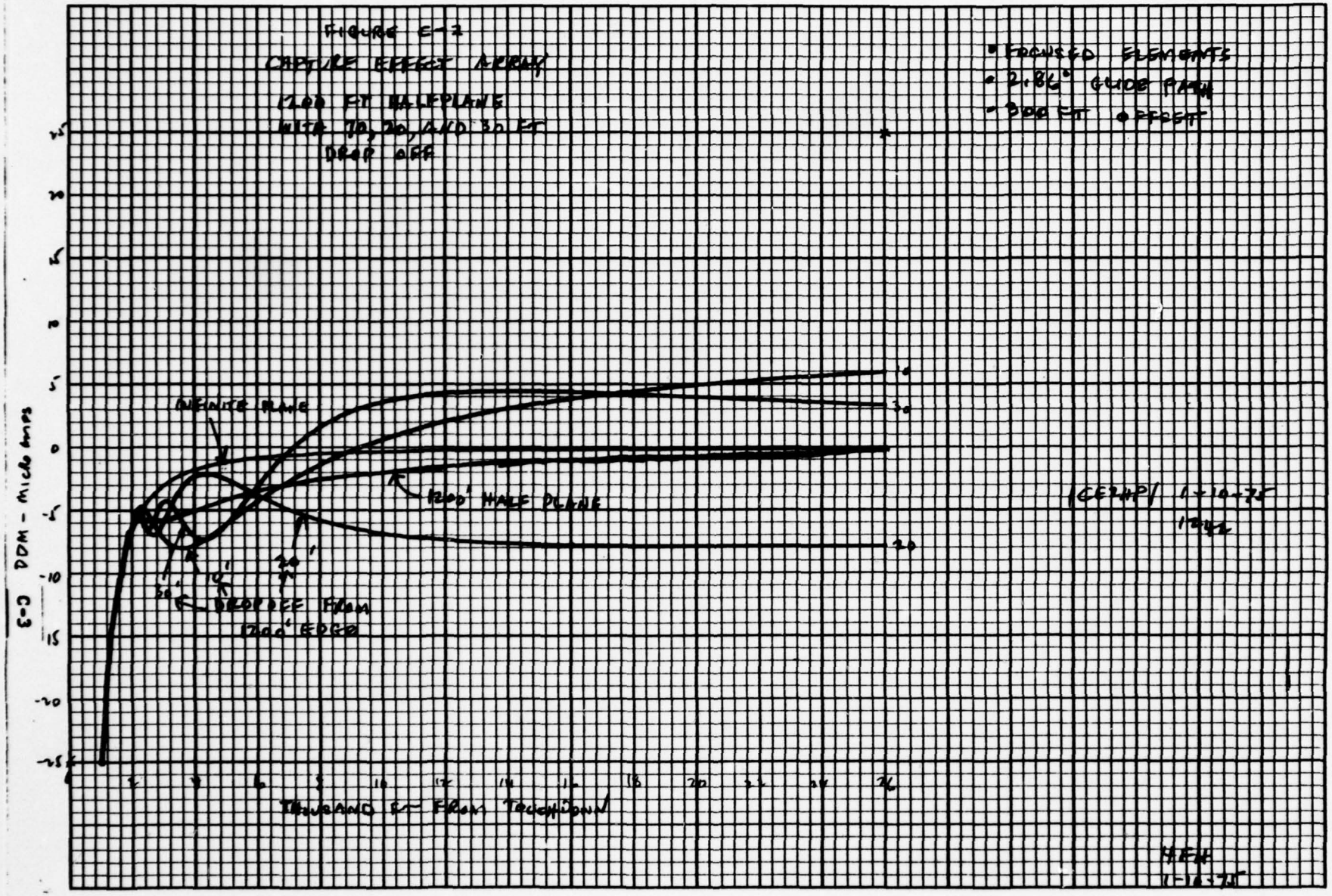
FIGURE C-2
CAPTURE EFFECT ARRAY
1200 FT HALFPLANE
WITH 10°, 20°, AND 30° FT
DROP OFF
■ FOCUSED ELEMENTS
• 2.8° GLIDE PATH
- 1000 FT OFFSET
DEFINITE PLANE
1200' HALF PLANE
30°
10°
20°
DROP OFF FROM
1200' EDGE
C-3 DDM - Microamps
THOUSAND FT FROM TOUCHDOWN

APPENDIX D

COMPARISON BETWEEN THEORY AND EXPERIMENT FOR THE CAPTURE EFFECT ARRAY OVER A SEMI-INFINITE GROUND PLANE

INTRODUCTION

The purpose of this section is to discuss the agreement between experiment and theory of measured signal levels for a capture effect antenna (M-array) illuminating a semi-infinite ground plane. From a practical viewpoint it is difficult to conduct an experiment in which only a half-plane contributes to the diffracted fields. An experiment by Lucas[2] was performed for the case of a semi-infinite ground plane over an infinite ground plane. The semi-infinite plane used by Lucas is only approximate since its transverse dimensions correspond to a plane of width 360 feet rather than being infinite.

The experimental set-up is depicted in Figure D-1 a,b. Lucas' model was constructed in the ratio of 1:30 to real life. Pattern information (SBO and CSB) as well as DDM crossover data were obtained for vertical scans above the 0^{o} reference point, which marks the level of the semi-infinite plane. Data is presented for the case of a semi-infinite plane of longitudinal widths 1785 feet, 1200 feet, 600 feet and 450 feet.

During the course of an experiment the receiver is positioned so that no direct reflected illumination occurs. Only direct radiation, diffracted radiation and reflected diffraction fields are allowed to reach the receiver. The receiver is carefully positioned using a laser beam and the antenna heights are critically adjusted (a sharp side-band null is obtainable at the glide slope angle). The approximate antenna heights are 5, 10, and 15 λ and the glide slope angle used was 2.86^{c}. A ground plane of 1785 feet was used while the amplitudes and phases of the system were adjusted. In effect this procedure yields a sharper null at the glide slope angle (SBO) than would occur if these adjustments were done at significantly larger distances.

The initial motivation for Lucas' experiment was to compare results with the half-plane calculations of Redlich[4]. In this regard it should be pointed out that Redlich's analysis assumes no second infinite plane (below the half-plane) which contributes reflected diffraction term. Clearly Redlich should expect agreement as the longitudinal width of the half-plane becomes large. Redlich performs his calculations for a two-dimensional model whereas, the current Westinghouse effort includes the full three-dimensional treatment. In the Westinghouse analysis the results of Appendix B have been used and applied in the manner outlined in Appendix E.

Due to the lack of exact detail in Lucas' discussion it was necessary to make several assumptions regarding the geometry of the experiment. The patterns obtained depended rather strongly on the following factors:

1. Exact longitudinal location of the receiving antenna
2. Exact height of semi-infinite plane above infinite plane
3. Offset of receiver from antenna
4. Focusing of antenna array elements

Lucas indicates for the 1785 and 1200 feet half-plane that no apparent change in the longitudinal location of the receiving antenna was made. This assumption was inferred from the fact that a change is noted for a 600 foot half-plane but not the 1200 foot. The requirement that no reflected direct rays illuminate the antenna dictates that the x-position (longitudinal) of the receiver must be at least 4400 feet from the antenna. For the 600 foot and 450 foot half-plane this position drops to 2600 feet (since again no change between these two sets of measurements is indicated).

The half-plane height above the infinite plane is given to be approximately 120 feet and this height was used for the 1785 foot, 1200 foot and 600 foot half-plane. It was additionally assumed that at an x-position of 4400 feet, the antenna and receiver were on a line perpendicular to the edge of the half-plane, thus, no offset or focusing was required. For the 600 foot half-plane an offset of 214.8 feet was used based on calculations assuming that the receiver moved in along a path intersecting the y-position of the antenna at 525 feet (reference Lucas[5] - see Figure D-1). Finally, the assumption was made that the antenna (for the 600 foot half-plane) was focused about the 525 foot offset.

In Figure D-2a and b the SBO and CSB signals, respectively, are illustrated for the 1785 feet ground plane. The insert in the upper left-hand corner depicts the results obtained by Lucas. As indicated above the SBO null at 2.86° is not quite as pronounced in the analytical results. In Figure D-2c the DDM crossover pattern is illustrated (also included are Lucas' results in the insert). As this figure indicates very good agreement exists between the experimental results and the analysis over the region where the signal is of interest (from $-150\,\mu a$ to $150\,\mu a$). Also plotted on this figure are the results for Redlich's calculation for an 1800 foot ground plane. The graph plotted is for the half-plane with no infinite sheet below. As a check on the validity of this plot the signals (DDM) with and without the half-plane located 120 feet above an infinite plane

were compared and no difference was found - except at very small angles where a slight oscillation in the DDM of the half-plane over the infinite plane could be discerned. Also, since the calculations are for a 1785 foot half-plane a comparison was made in the current analysis and no difference was found in the pattern due to the added 15 feet.

The Westinghouse calculations yield much closer agreement with experiment than do Redlich's analysis. It appears that the difference occurs because Redlich does the analysis for an infinite wire over a ground plane, whereas, the present analysis duplicates the situation examined by Lucas - a dipole over a plane. Also, Redlich's result represents a two-dimensional solution, whereas, the analysis presented is the full three-dimensional calculation. Comparison of these results with those of Redlich manifests itself in significantly lower DDM over the range $.4^{o}$ - 1.5^{o} while the CSB and SBO patterns show remarkable similarity. This latter fact indicates that the phases must differ from those of Redlich.

In Figures D-3 a and b again the SBO and CSB patterns are presented for the 1200 foot half-plane. Now the oscillation at smaller angles are readily apparent. The SBO null at 2.86^{c} is not as deep.

Figure D-3c illustrates the DDM crossover results for the present study as well as the experimental results of Lucas and Redlich's calculations. Again, there is quite good agreement between the Westinghouse calculations and the experimental data. The agreement becomes less for angles below 1.76^{o} (the angle at which the clearance signal would normally dominate). Redlich clearly has the wrong slope in his data.

Figures D-4 a, b and c present the 600 foot half-plane data. The oscillation in both SBO and CSB signals show remarkable similarity to those obtained by Lucas. Also, the oscillations in the DDM appear qualitatively similar but slightly out of phase. The DDM crossover results show good agreement above 1.76^{o}. Typically, one would expect Redlich's results to be poorer (as the figure indicates) since the ground currents near the edge of the half-plane are somewhat larger for the 600 foot half-plane as opposed to the 1200 foot and 1785 foot case. This reflects itself in changes in both the diffracted field and the reflected diffraction field (which Redlich fails to include).

Figures D-5 a, b, and c illustrate the 450 foot half-plane data. It is interesting to note that the sideband null occurs slightly below the glide slope

angle. The SBO pattern data from the analysis occurs slightly below the glide slope angle. The SBO pattern data from the analysis again duplicate the experimental curves remarkably. The DDM crossover plot shows somewhat less agreement in the range - 150 μa to 150 μa. This is due to the fact that the calculated pattern oscillations are slightly out of phase with those obtained experimentally. Redlich's results are also plotted and as previously observed show poorer agreement. Clearly, the effects of the reflected diffraction fields are becoming important.

Finally, in Figure D-6 the DDM crossover results are plotted for the 450 foot half-plane. For this plot attempts were made to obtain agreement in the region of small angles. This required a height of the half-plane above the infinite plane of 130 feet (instead of 120 feet) with focusing about the 525 foot offset. As the figure indicates poorer agreement exists in the region about 2.86^{c} (with this fit).

Discussion

The present calculation demonstrates very good agreement with the experimental data in the region between -150μa and 150μa of DDM. Below -150 μa the results are qualitatively in agreement; however, fail to quantitatively match. Several reasons would exist for the discrepancies in DDM:

1. Lateral diffraction and corner effects could become important for short half-planes in the experimental set-up.
2. In the small angle region the DDM experimental data could deteriorate due to the very low signal levels in the SBO and CSB signals.
3. The experimental conditions are not exactly duplicated in the analysis.
4. The analytical model deteriorates as the ground plane is shortened (very high ground currents near the diffracting edge).

In general there exists good qualitative agreement between the analysis and experimentally measured SBO and CSB patterns. The major deviation is the lack of a very sharp null (SBO) at the glide slope angle for the analysis. Comparisons with other theoretical analysis (Redlich) demonstrate much closer agreement with the experimental results than had previously existed.

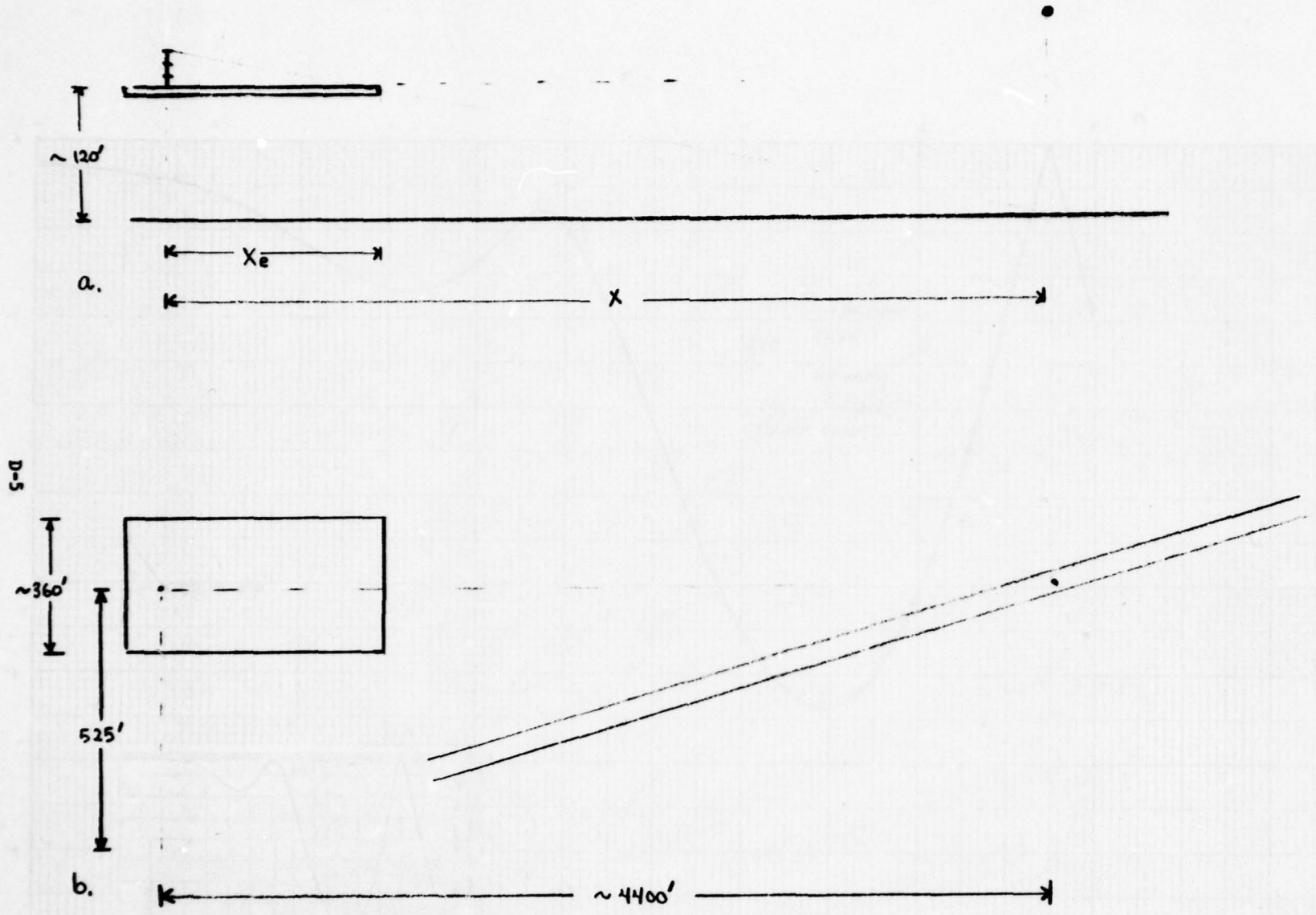

FIGURE D-1 GEOMETRY OF LUCAS EXPERIMENTS

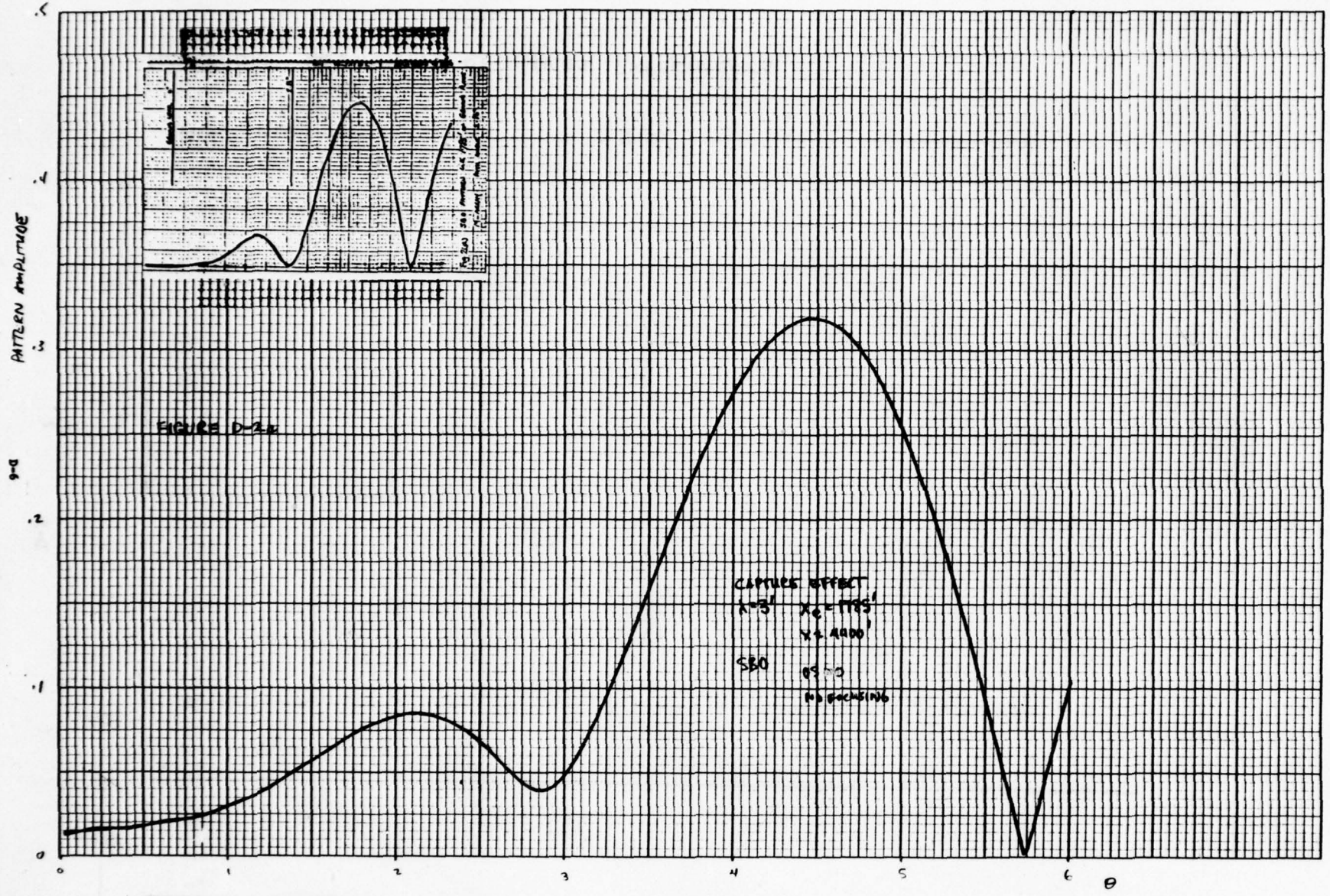

FIGURE D-12

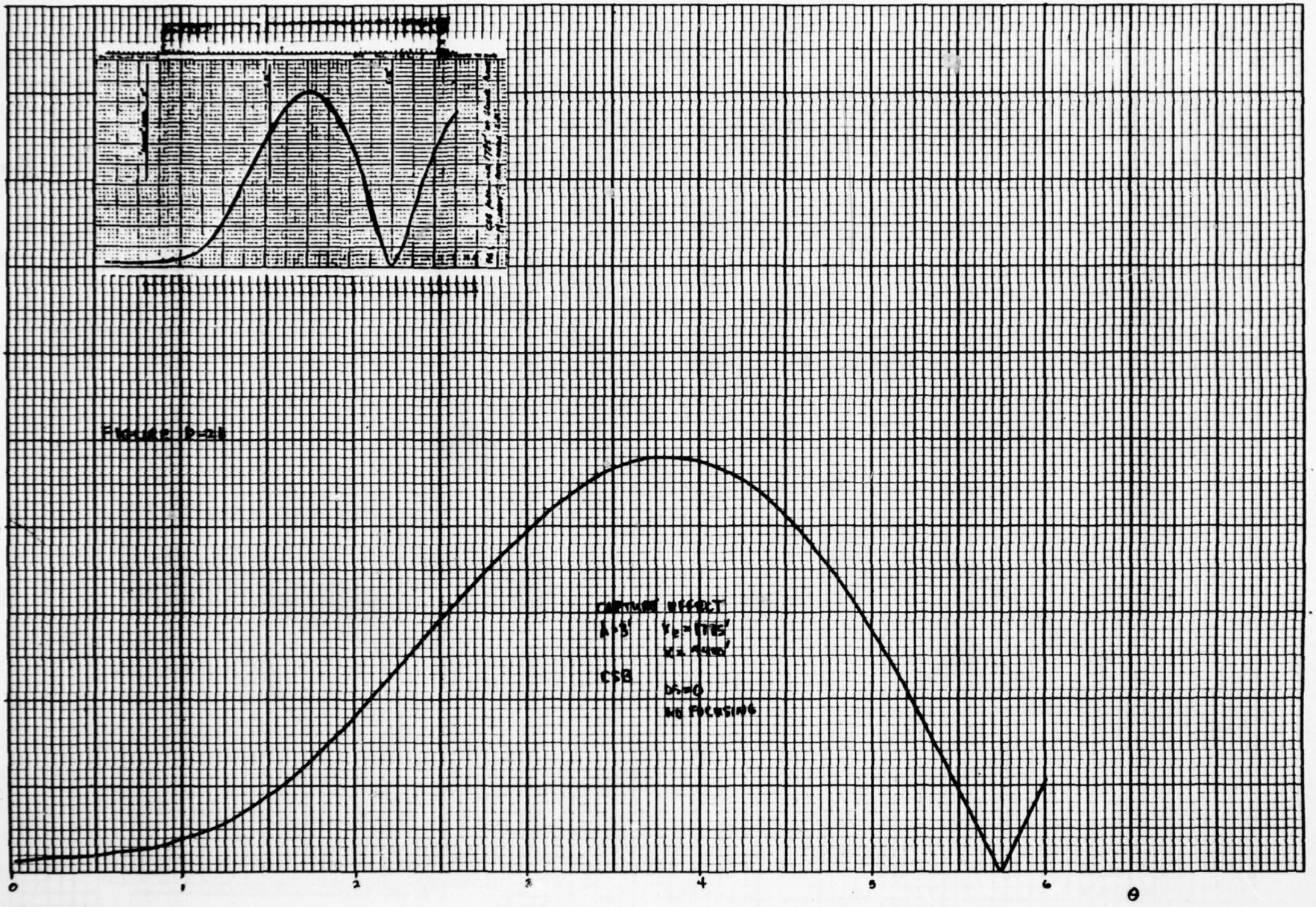
.5
.4
.3
.2
.1
0
1
2
3
4
5
6
θ
CARRIER EFFECT
A-B
CSB
No Focusing

FIGURE D-2C

CAPTURE EFFECT
$\lambda = 3'$ $X_c = 1795'$
$X = 11400'$
$H = \infty$

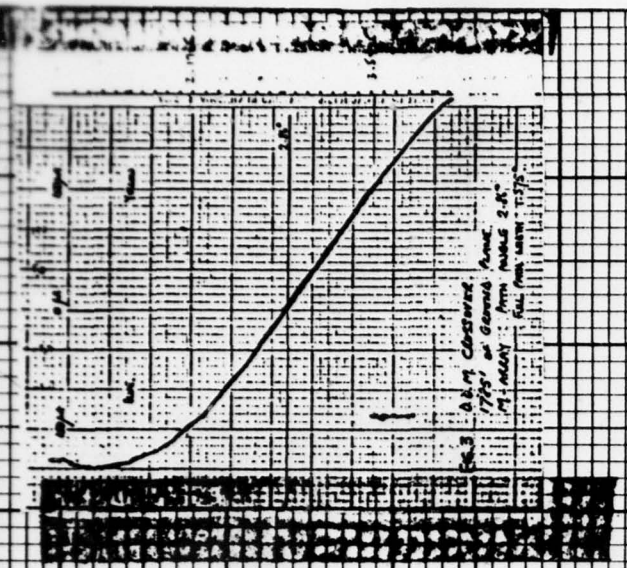

LUCAS
PRODUCT

$\Theta - D$

0
-100
-200
-300
-400
-500

0
1
2
3
4

$\Theta(0)$

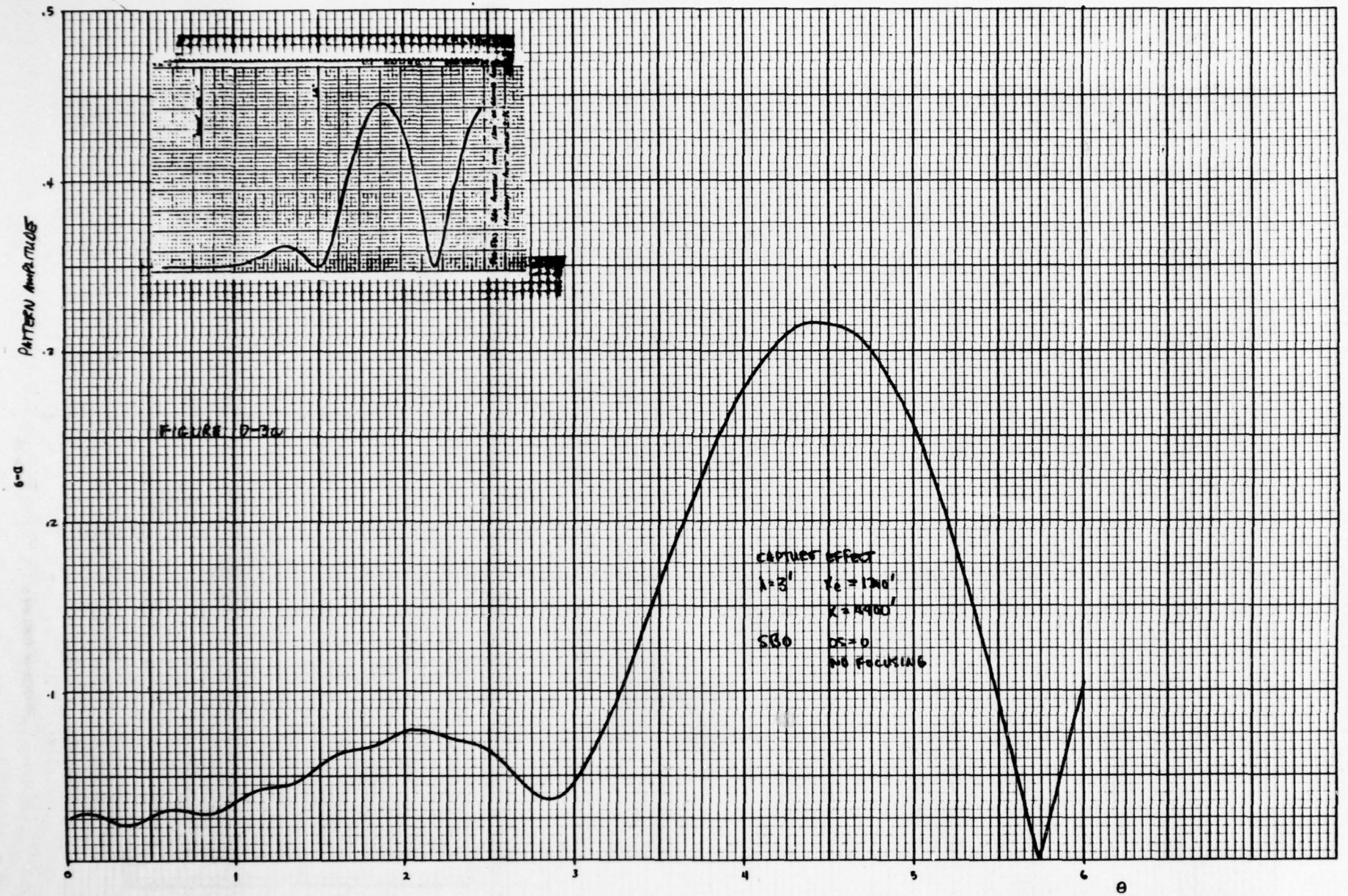
PATTERN AMPLITUDE
.5
.4
.3
.2
.1
0
1
2
3
4
5
6
θ
FIGURE D-3a
6-a
CAPTURE EFFECT
λ=3'
Ye = 1320'
K = 44400'
SBO
DS = 0
no FOCUSING

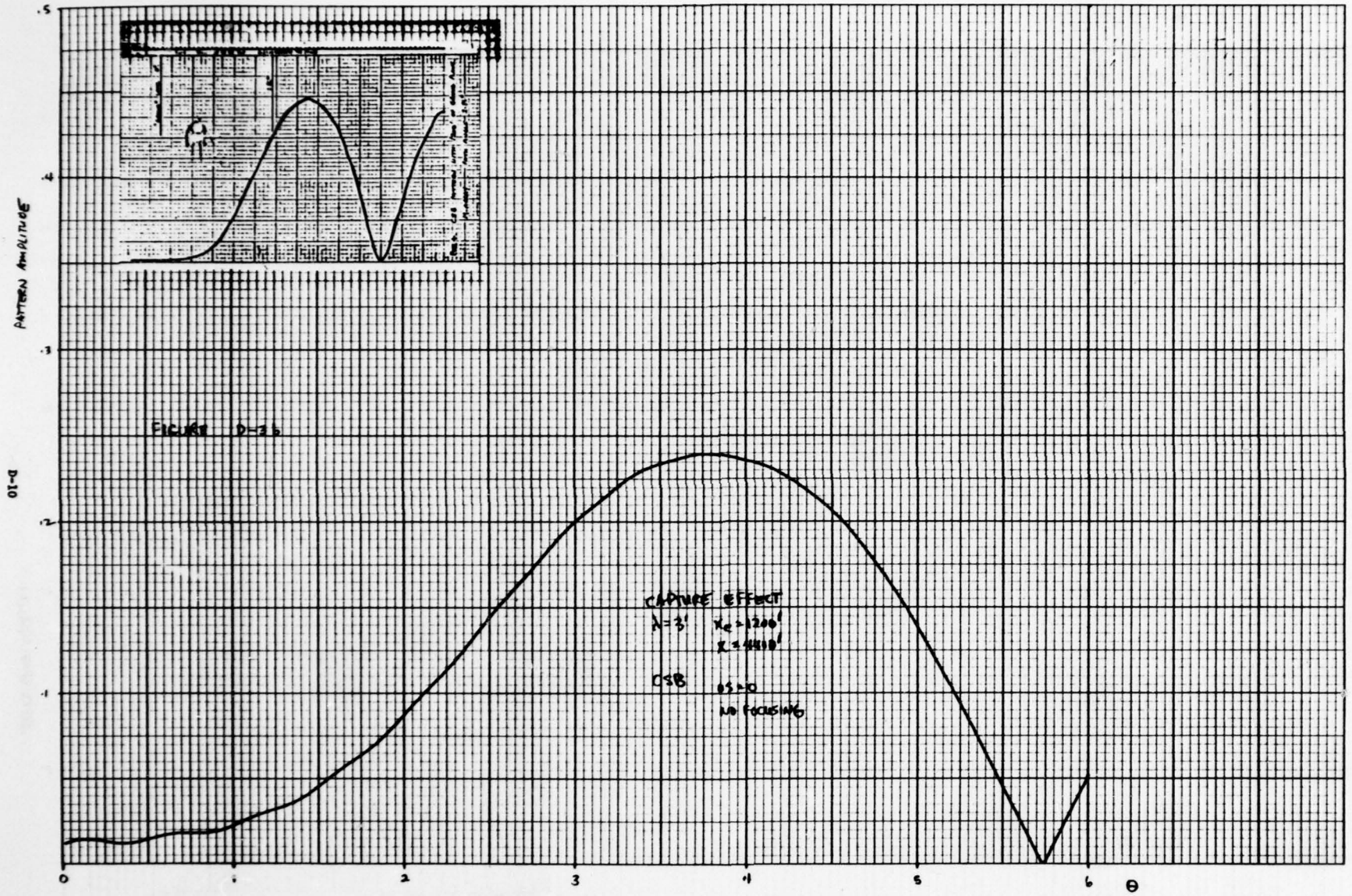
PATTERN AMPLITUDE
.5
.4
.3
.2
.1
0
1
2
3
4
5
6
θ
CAPTURE EFFECT
CSB
NO FOCUSING

FIGURE D-2b

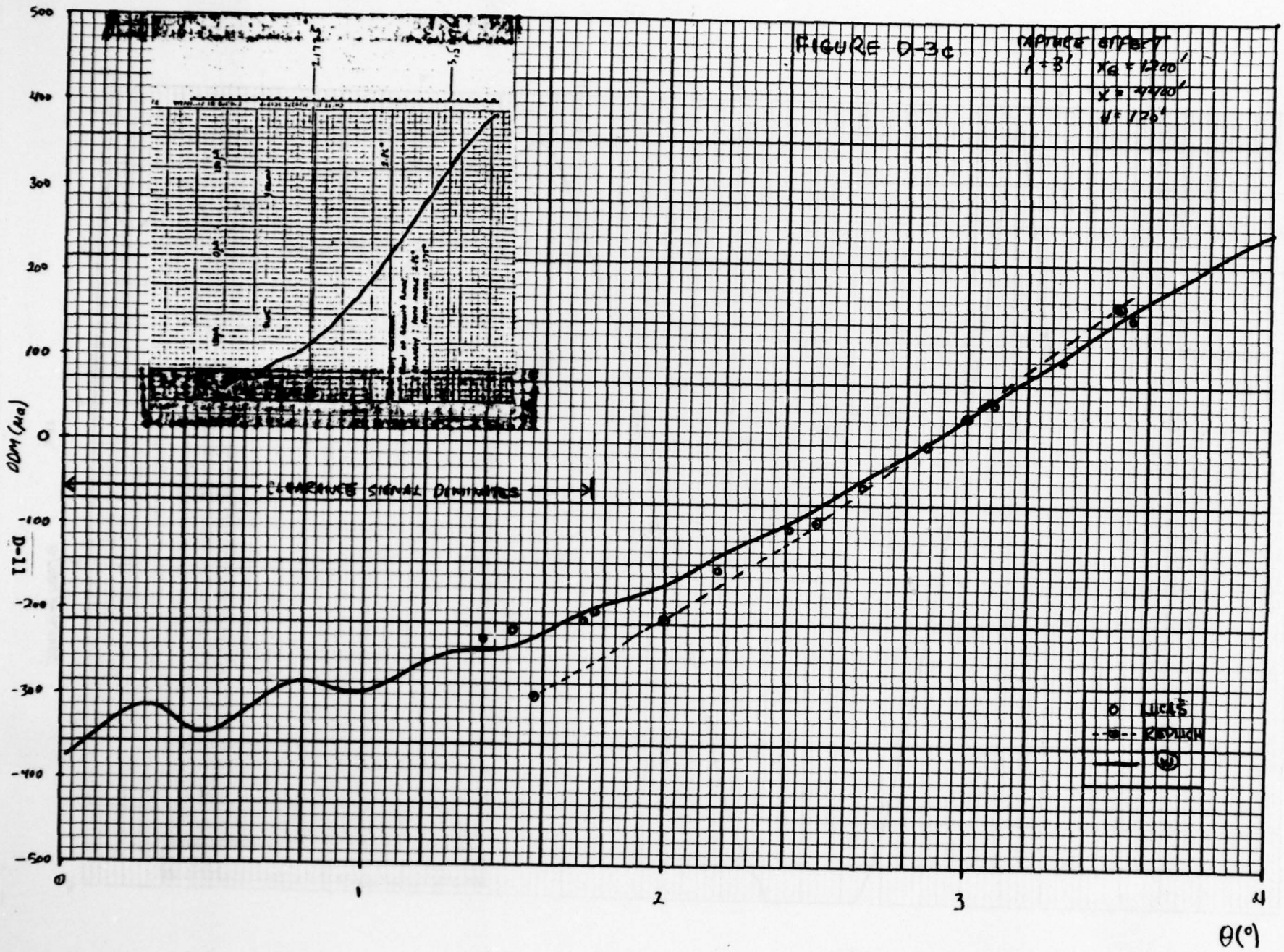
FIGURE D-3c
RAPTURE EFFECT
λ = 3'
X_0 = 12'00"
X = 47'40"
Y = 12'6"
RAPTURE SIGNAL DENIGRATES
LUCAS
ZAPRUCH
MD
ODM (μa)
θ(°)
500
400
300
200
100
0
-100
-200
-300
-400
-500
0
1
2
3
4

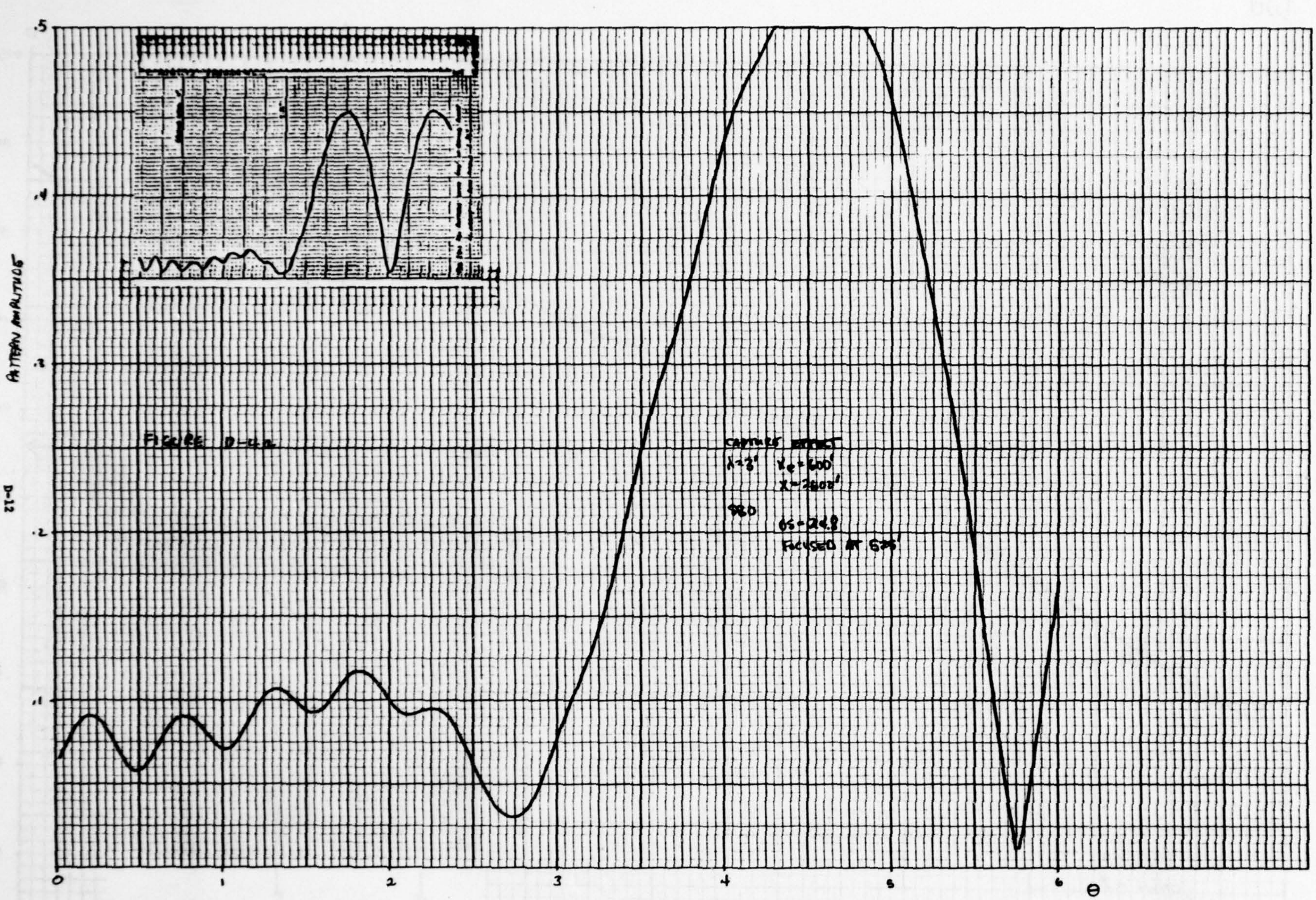
PATTERN AMPLITUDE
.5
.4
.3
.2
.1
0
1
2
3
4
5
6
θ
FIGURE D-4a
CAPTURE EFFECT
X=2800'
FOCUSED AT 625'

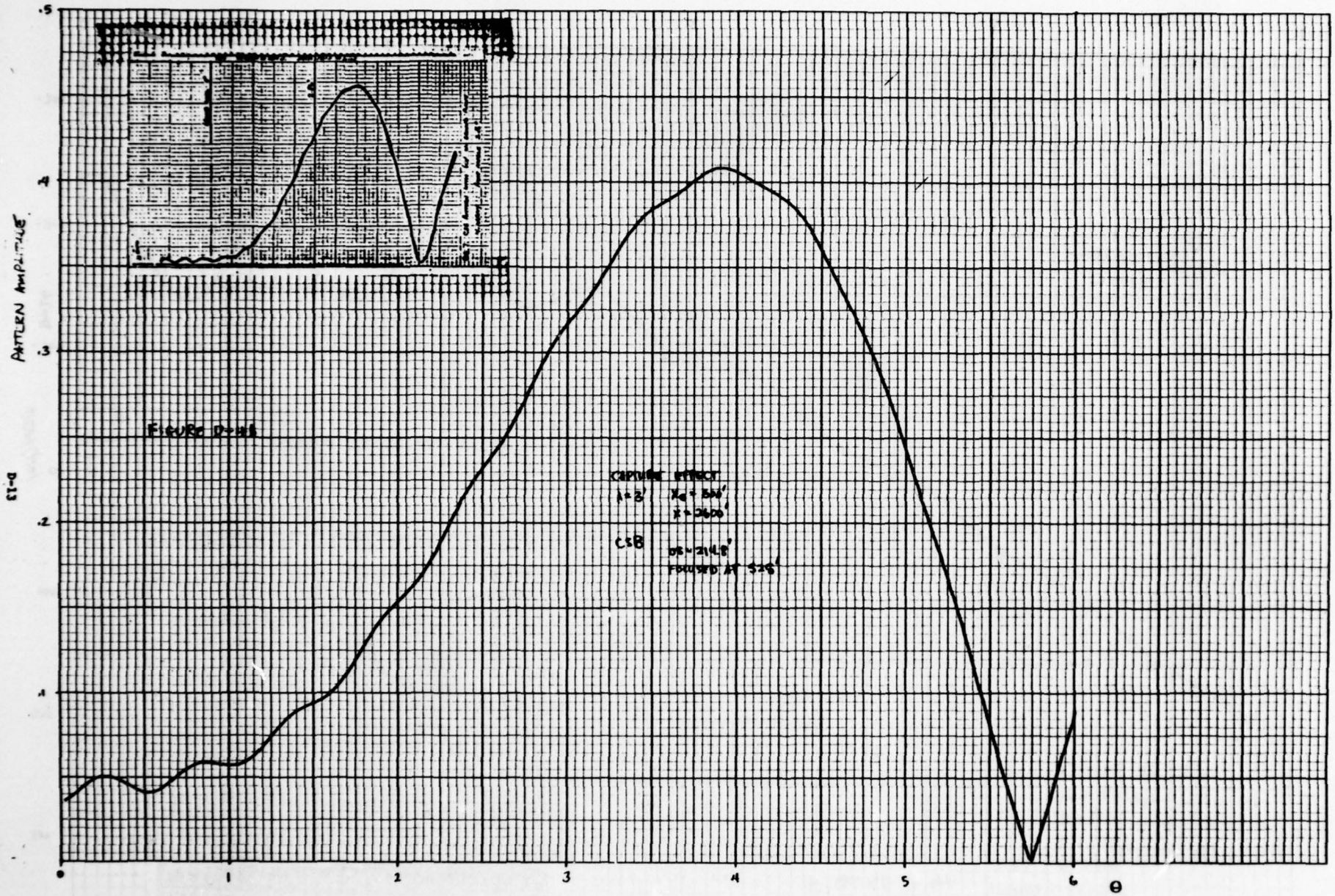
.5
.4
.3
.2
.1
0
1
2
3
4
5
6
θ
PATTERN AMPLITUDE
FIGURE D-13
CAPTURE EFFECT
CSB

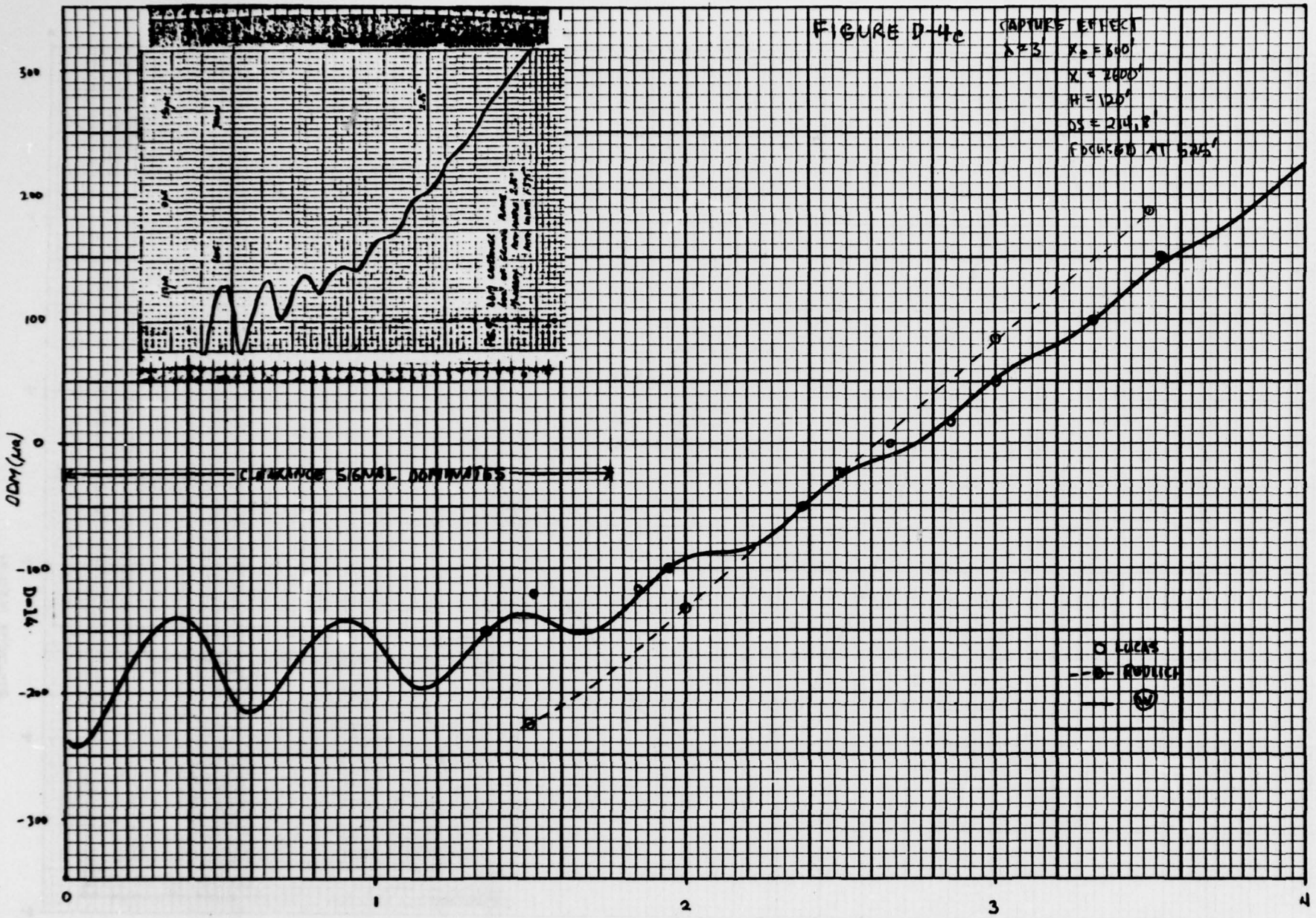
FIGURE D-4c
CAPTURE EFFECT
Δ=3'
X_0 = 300'
X = 2000'
H = 120'
DS = 214.8'
FOCUSED AT 525'
CLEARANCE SIGNAL DOMINATES
DDM (μa)
300
200
100
0
-100
-200
-300
0
1
2
3
4
LUCAS
RUDLICH
D-14

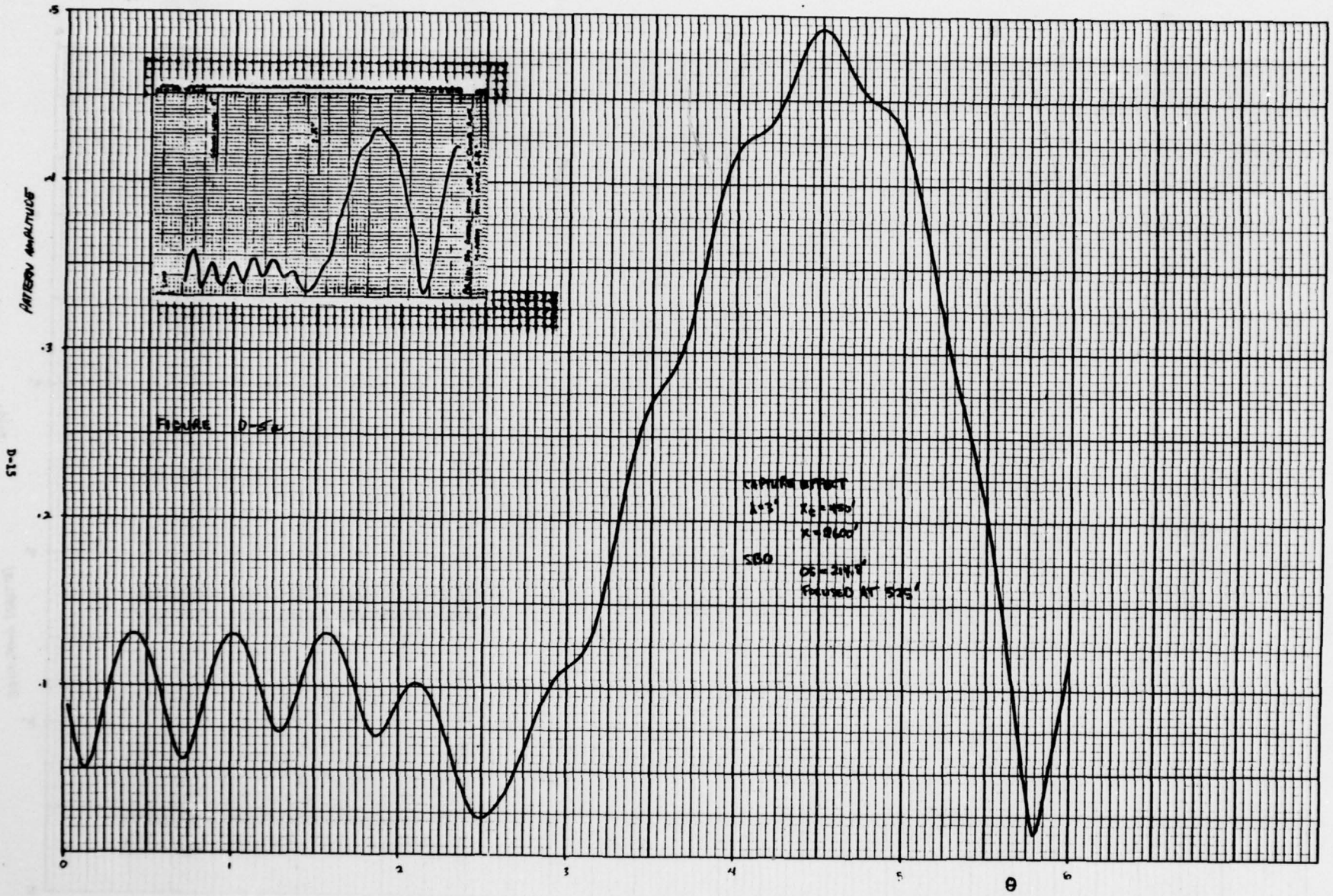
PATTERN AMPLITUDE
.5
.4
.3
.2
.1
0
1
2
3
4
5
6
θ
FIGURE D-8a
CAPTURE EFFECT
SBO

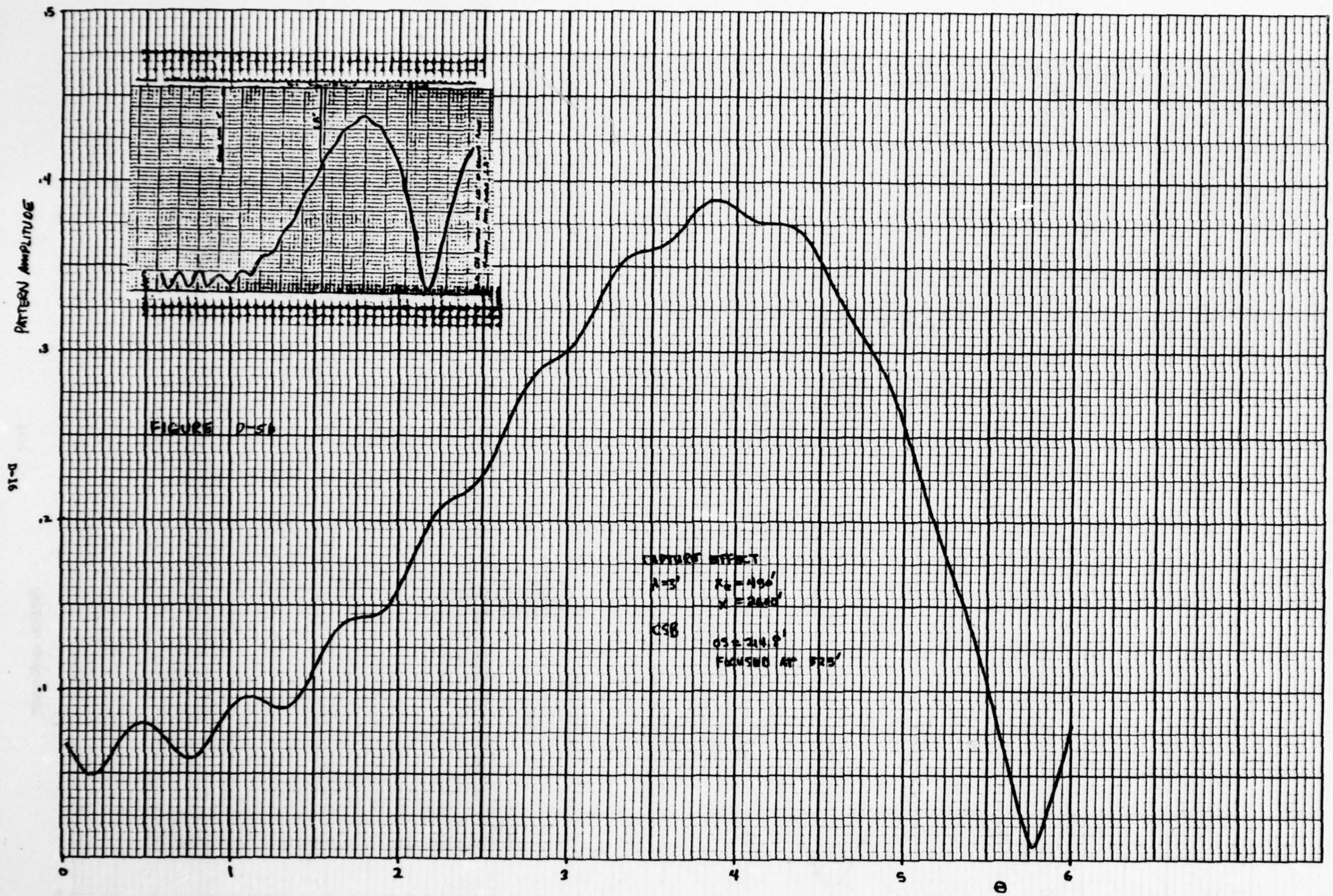
PATTERN AMPLITUDE
.5
.4
.3
.2
.1
0
1
2
3
4
5
θ
6
FIGURE D-56
CAPTURE EFFECT
A=3'
R_2=490'
X=2600'
CSB
05=214.8'
FOCUSED AT 525'

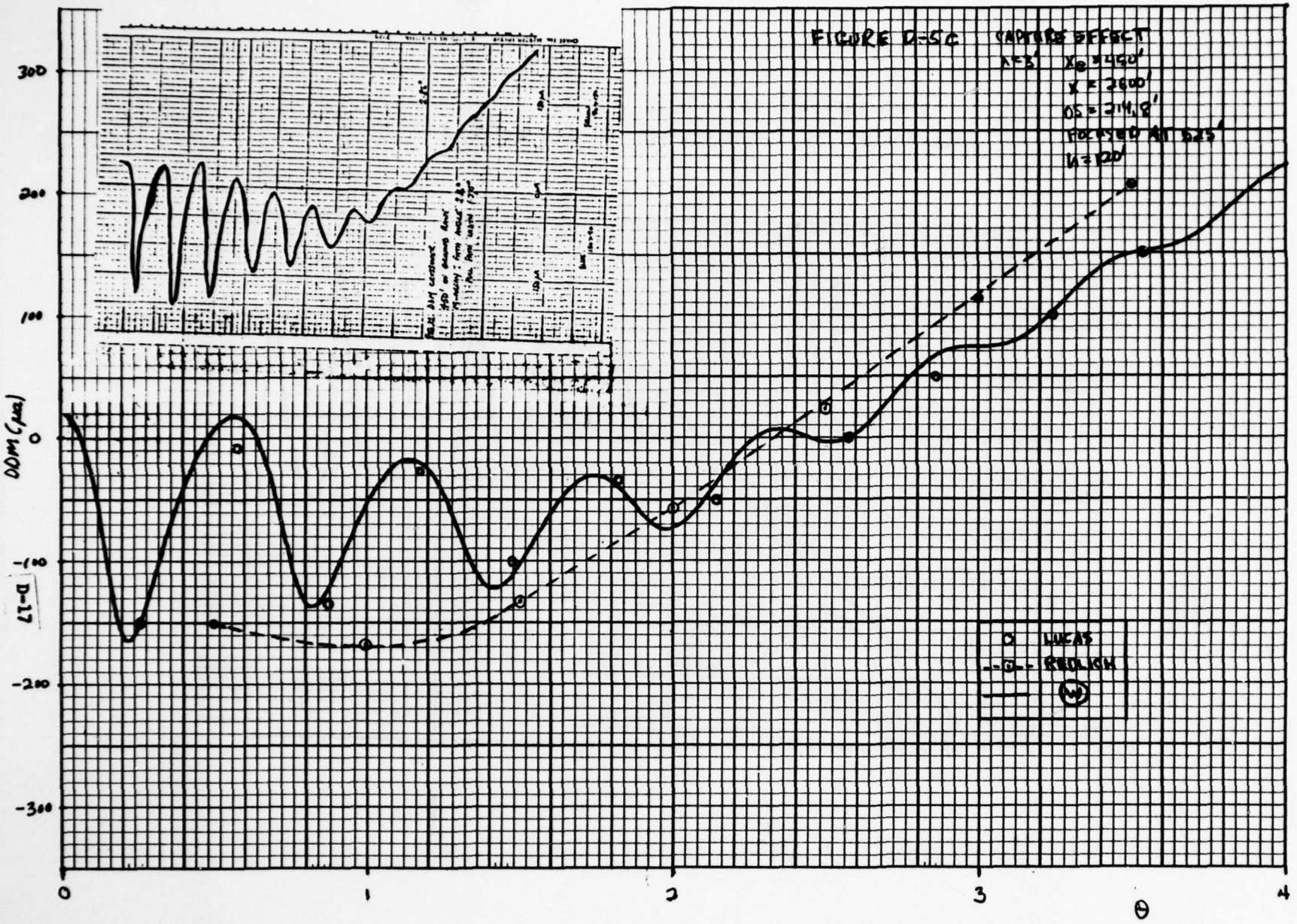
FIGURE D-5C CAPTURE EFFECT
A=3
X_B = 450'
X = 2600'
OS = 214.8'
FOCUSED AT 625'
W = 100'
LUCAS
REDLICH
DDM (μa)
300
200
100
0
-100
-200
-300
0
1
2
3
4
θ

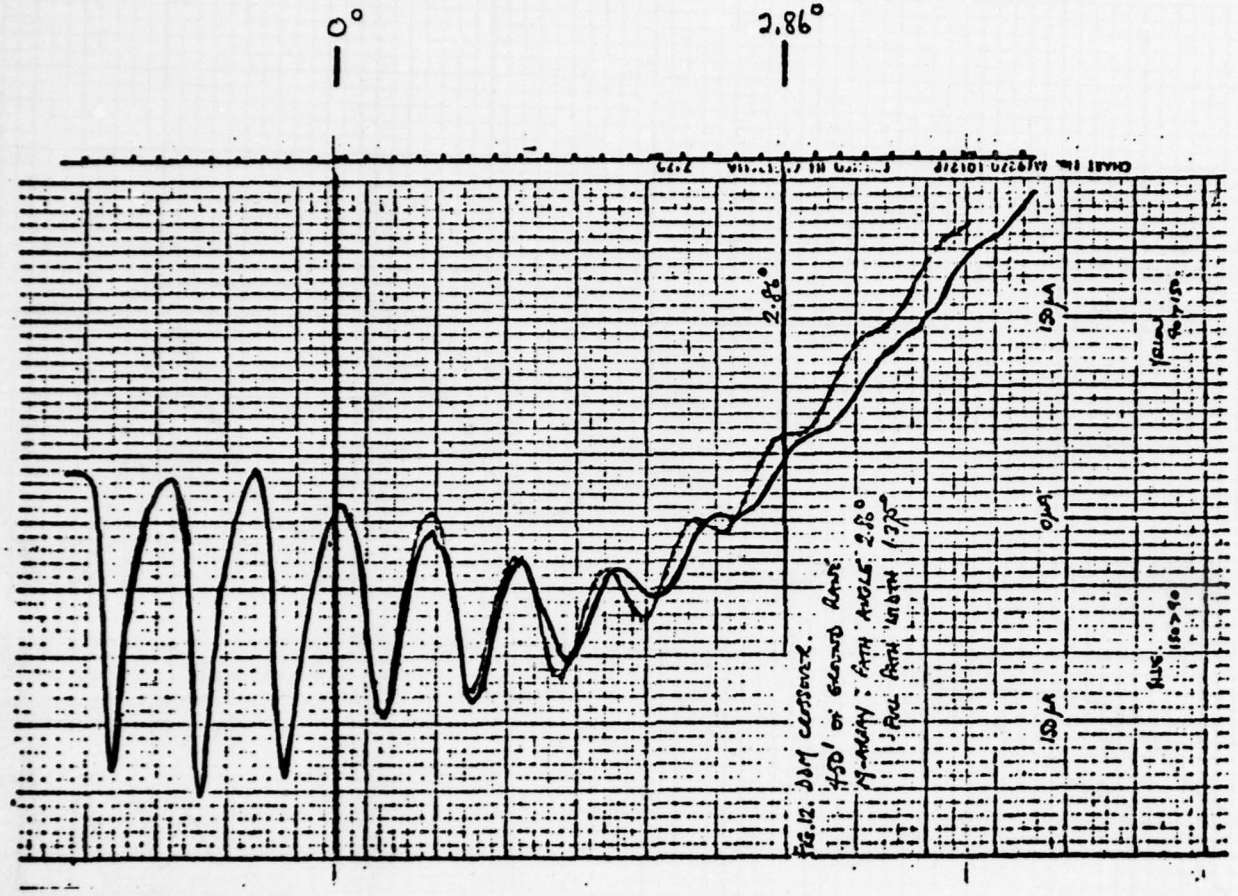

FIGURE D-6 COMPARISON OF CALCULATION AND LUCAS MEASUREMENT

APPENDIX E

ANALYSIS OF A SEMI-INFINITE GROUND PLANE OVER AN INFINITE GROUND PLANE

The behavior of diffraction from a semi-infinite ground plane has been examined in Appendix B. In order to include the effects of a ground plane below the half-plane it is useful to divide the diffraction problem into the four regions of Figure E.1. For convenience we indicate in Table E-1 the contributions as seen by the observer for each region.

FIELDS	REGION I	REGION II	REGION III	REGION IV
DIRECT	X	X	X	X
IMAGE	X	X		
DIFFRACTION	X	X	X	X
REFL. DIFF.		X	X	X
REFL.DIRECT				X

TABLE E-1 FIELD CONTRIBUTIONS BY REGION

θ denotes the angle between the half-plane and a vector from the half-plane edge to the observer, θ_c represents the angle between the half-plane and a vector from the half-plane edge to the antenna, x the position of the observer in the longitudinal direction, x_e the half-plane edge distance, h the height of the half-plane above the infinite plane, z the vertical height of the observer and r the length of the vector from the half-plane edge to the observer. In terms of these quantities, the four regions indicated above are defined by the following conditions:

REGION I : $\theta \le \pi/2$; $x \le x_e$

REGION II : $\frac{\pi}{2} < \theta \le \pi - \theta_c$; $x > x_e$

REGION III : $\pi - \theta_c < \theta \le \pi + \theta_c$; ① $x - x_e \le h\,|\tan\theta_c$, ② $x - x_e > h\,|\tan\theta_c$; $z > -2h + (x - x_e)\tan\theta_c$

REGION IV : $\pi - \theta_c < \theta \le \pi + \theta_c$; $x - x_e > h\,|\tan\theta_c$, $z < -2h + (x - x_e)\tan\theta_c$

There is, of course, a fresh region where $\theta > \pi + \theta_c$, however, this region corresponds to flying in under the half-plane and is eliminated by the restriction $z \ge 0$. The semi-infinite and infinite ground planes are assumed to lie in the x-y plane.

The direct, image and diffracted fields have been discussed in Appendix B. The reflected diffractions field has a very similar form to the diffracted field except the displacements are now determined by the image distances of the half-plane (see Figure E.1). This field is defined as follows:

$$E_D^r = -\sqrt{\frac{2}{\pi}}\, e^{-i\pi/4}\left[\operatorname{sgn}\tau_{R'}\, K\sqrt{R_1'(R'+R_1')}\, F(|\tau_{R'}|) + \operatorname{sgn}\tau_{S'}\, K\sqrt{R_1'(R'+S_1')}\, F(|\tau_{S'}|)\right]$$

where

$$\tau_{R'} = 2\sqrt{\frac{kr'r_c'}{R_1'+R'}}\cos\tfrac{1}{2}(\theta'-\theta_c') \quad , \quad \tau_{S'} = 2\sqrt{\frac{kr'r_c'}{R_1'+S'}}\cos\tfrac{1}{2}(\theta'+\theta_c')$$

$$r' = \sqrt{(x-x_e)^2 + (z+2h)^2} \quad , \quad r_c' = \sqrt{(x_e-x_c)^2 + z_c^2}$$

$$R' = \sqrt{(x-x_c)^2 + (y-y_c)^2 + (z+2h+z_c)^2}$$

$$S' = \sqrt{(x-x_c)^2 + (y-y_c)^2 + (z+2h-z_c)^2}$$

$$R_1' = \sqrt{(r'+r_c')^2 + (y-y_c)^2}$$

$$\theta' = \pi + \tan^{-1}\left[(z+2h)/(x-x_e)\right]$$

$$\theta_c' = \tan^{-1}\left[z_c/r_c'\right]$$

The reflected direct field satisfies

$$E_{I'}^q = \frac{e^{-ikR'}}{kR'}$$

where R' is defined as above.

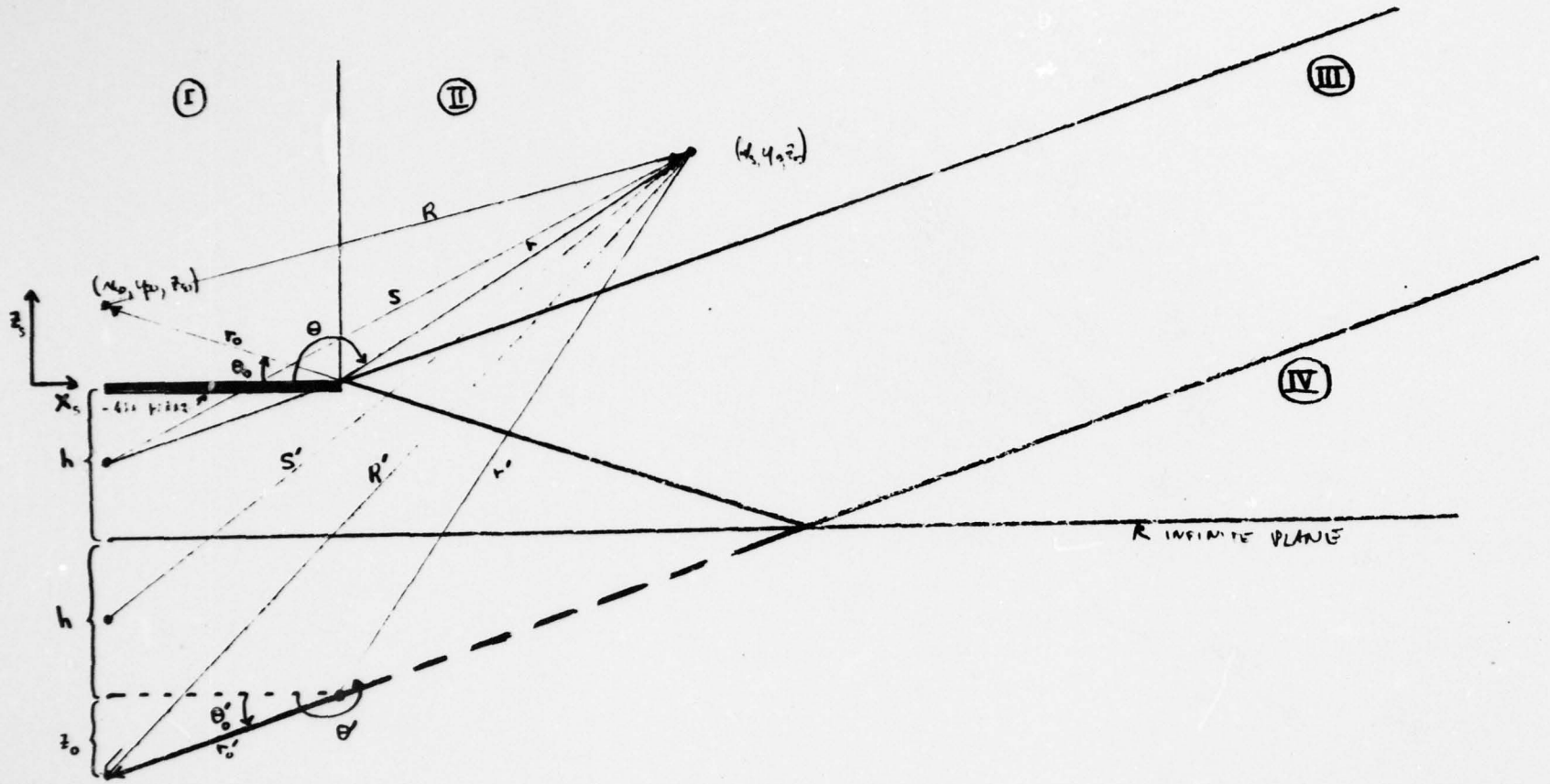

FIGURE E.1. GEOMETRY FOR HALFPLANE OVER INFINITE PLANE